WAVES OF COMMUNICATION: METABOLOMICS DESCRIBE THE NATURE AND ROLE OF WATERBORNE CUES IN THE MARINE ENVIRONMENT

A Dissertation
Presented to
The Academic Faculty

by

Remington X. Poulin

In Partial Fulfillment
of the Requirements for the Degree
Doctor of Philosophy in the
School of Chemistry and Biochemistry

Georgia Institute of Technology
December 2017

WAVES OF COMMUNICATION: METABOLOMICS DESCRIBE THE NATURE AND ROLE OF WATERBORNE CUES IN THE MARINE ENVIRONMENT

Approved by:

Dr. Julia Kubanek, Advisor
School of Biological Sciences
School of Chemistry and Biochemistry
Georgia Institute of Technology

Dr. Pamela Peralta-Yahya
School of Chemistry and Biochemistry
Georgia Institute of Technology

Dr. Facundo Fernández
School of Chemistry and Biochemistry
Georgia Institute of Technology

Dr. Marc Weissburg
School of Biological Sciences
Georgia Institute of Technology

Dr. Adegboyega Oyelere
School of Chemistry and Biochemistry
Georgia Institute of Technology

Date Approved: October 30th, 2017

“In the course of time I have learned to tramp about coral reefs, twenty to thirty feet under water, so unconcernedly that I can pay attention to particular definite things. But after all my silly fears have been allayed, even now, with eyes overflowing with surfeit of color, I am still almost inarticulate. We need a whole new vocabulary, new adjectives, adequately to describe the designs and colors of under sea.”
-William Beebe

ACKNOWLEDGEMENTS

I would like to start by thanking my family for years of support and encouragement. From our first visit to the aquarium to the Florida Sea Base and multiple dive trips to Mexico, they have always encouraged my interest in the ocean and its inhabitants. They must also be thanked for allowing me to keep countless fish tanks, reef tanks, and other animals while growing up that helped support my interest in marine biology. I must thank my amazing wife Cherry for helping me survive the last few years, for all of the late night dinners, help prepping figures, trips to Savannah to collect crabs, and the overall unpredictable life that graduate school causes. I also must thank my fur-baby Mikha for ensuring I made it to work and back safely each day, for providing on-demand cuddles when experiments didn't work, and for keeping me company during late night experiments and weekends when the lab was empty.

While at Georgia Tech, I have matured as an individual and as a scientist and neither would have been possible without the assistance of numerous individuals. First, I wish to thank my advisor, Julia Kubanek, for her unending support, insightful questioning, constructive edits, and for our many scientific discussions. She supported my interest in higher education and allowed me to shape both my thesis and my studies. I would like to thank my thesis committee members: Facundo Fernandez, Adegboyega Oyelere, Pamela Peralta-Yahya, and Marc Weissburg for feedback that improved my research. I would like to separately thank Marc Weissburg for his invaluable experience, expertise, and insights with invertebrates and ecological interactions as well as Mark Hay for allowing me to join him in the South Pacific and gain unique field experience.

Lastly, the work I have completed would not have been possible without the support of many lab mates, coworkers, and friends that I must thank. First, I must thank the many undergraduates that allowed me to mentor them in the laboratory, that supported me in my research, that trusted my scientific knowledge, and that afforded me an opportunity to apply my educational training in a hands-on setting. I would like to separately thank Kristy Syhapanha, Katie Martin, Katie Siegel, Megan Phillips, and David Brumley for not only supporting me in the laboratory, but also befriending me in life. Secondly, I must recognize other members of the Kubanek Lab, past and present including: Margi Teasedale, Drew Sieg, Kelsey Poulson-Ellestad, David Snare, Troy Alexander, Jessie Roy, Stina Jakobsson, Blair Lunceford, Korry Barnes, Serge Lavoie, Nazia Mojib, Sam Mascuch, Emily Brown, Anne Marie Sweeny-Jones, Bhuwan Chhetri, Zinka Bartolek, Elizabeth McMillan, and Nellie Ochs. I'd like to thank all my collaborators and coworkers in the Fernandez, Hay, and Weissburg labs for their support and help over the last five years from space in their labs, troubleshooting an instrument, to transporting live animals and helping extract crab urine. Lastly, I'd like to thank the many friends I have outside of GT that have listened to my terrible jokes, shared a drink with me, and helped make the long days a bit more fun. In closing, my time at Georgia Tech has been one of highs and lows, of career defining insights and scientific frustrations beyond imagination, none of which I would trade or abandon as all were necessary to get me to this point. I will remember my time at GT fondly and I will continue in science with the support and guidance of those I've met during my studies.

TABLE OF CONTENTS

LIST OF TABLES

LIST OF FIGURES

SUMMARY

Understanding how organisms interact with members of their own species (intraspecific interactions), with members of other species (interspecific interactions), or with their environment is a central theme of ecology. For these interactions to occur, individuals must be able to sense and recognize other organisms, nutrients, and resources. However, not all organisms sense others and their environments by similar mechanisms: some species rely on sight, sound, olfaction, or taste, whereas others utilize mechanosensory cues, magnetosensory cues, or gravitational cues. In the marine environment, waterborne olfactory cues released into the water column are commonly utilized since visual, auditory, and mechanosensory cues can be complicated by wave action and turbidity. Additionally, waterborne cues are important in competitive interactions among organisms. Despite decades of dedicated research, we still know little about the chemical nature of waterborne cues and physiological responses by individuals that detect the cues.

First, to better understand the chemical nature of waterborne cues in chemosensory detection, we investigated how the mud crab *Panopeus herbstii* detects its predator, the blue crab *Callinectes sapidus*, via waterborne cues (see Chapter 2) (1). Using a multi-platform metabolomics approach combining ^{1}H nuclear magnetic resonance (NMR) spectroscopy and mass spectrometry (MS), two compounds, trigonelline and homarine, were identified as the major constituents of the waterborne cue released in the urine of blue crabs that induces fear in mud crabs. We also found that mud crabs adjust their behavior depending on the diet of the blue crab, with exposure to urine from blue crabs fed mud

crabs leading crabs to exhibit a stronger fear response than exposure to urine from blue crabs fed oysters. This suggests that mud crabs exhibit differential risk perception. The concentrations of trigonelline and homarine were highest in blue crab urine associated with the greatest fear response and lowest in urine with the lowest perceived risk. More generally, this ability of prey to chemically detect predators and in turn avoid predation is vital to survival and is expected to have significant implications on community structure. This case study involving blue crabs and mud crabs is an example of non-consumptive effects of predators, i.e., predator-prey interactions that do not necessarily result in consumption of prey but that alter physiology or behavior of prey with cascading impacts on lower trophic levels. Thus, the waterborne cues identified in this study could have a large impact not only on blue crabs and mud crabs but also on populations of other organisms and on the entire estuarine community.

To better understand the role of waterborne cues in competition, we investigated the chemical basis of allelopathy, the release of compounds that negatively affect competitors, involving the red tide phytoplankton *Karenia brevis* (See Chapter 3) (2). *K. brevis* is a common inhabitant of Gulf of Mexico offshore and nearshore waters, frequently forming dense blooms of congregated cells, colloquially known as the red tide. *K. brevis* exudes unidentified allelopathic compounds that negatively affect competitors through sub-lethal effects. However, *K. brevis* allelopathy is variable among blocks and strains. We investigated the chemical nature of variable allelopathic potency of *K. brevis* against its competitor *Asterionellopsis glacialis*. Combining an *in vitro* laboratory-based assay to assess allelopathic potency and ^{1}H NMR spectroscopic profiling, we identified three distinct metabolic modalities of *K. brevis*: allelopathic, non-allelopathic, and stimulatory.

Each metabolic modality exhibited a distinct chemical fingerprint with compounds that were more abundant in the exuded metabolomes of the most allelopathic *K. brevis* blocks and strains possessing aromatic moieties, unsaturated lipid-derived moieties, or both functionalities. This variation has been previously underutilized in understanding chemically mediated interactions involving *K. brevis* and could serve as a model for other phytoplankton systems.

In addition to understanding the compounds serving as waterborne cues (see Chapter 2) (1) and allelopathy (see Chapter 3) (2), it is important to investigate the physiological and molecular consequences of allelopathy on competitors. The molecular underpinnings of chemosensory detection, or chemoreception, such as G protein-coupled receptors and ensuing signaling cascades, are the subject of considerable historic evaluation, while the metabolic responses by individuals responding to chemically mediated competition, such as allelopathy, are not well studied. We investigated alterations in the lipidomes of two competitors, *A. glacialis* and *Thalassiosira pseudonana*, in response to *K. brevis* allelopathy (see Chapter 4) (3). Using a multi-platform metabolomics approach (NMR and MS profiling), both competitors' lipidomes were found to be affected by allelopathy. However, the lipidome of *T. pseudonana* was significantly more disrupted than that of *A. glacialis.* Co-occurrence of *A. glacialis* and *K. brevis* in the Gulf of Mexico could have provided *A. glacialis* with the opportunity to evolve some partial resistance to allelopathy. Decreases in concentrations of lipids common to cell membranes and chloroplast membranes were detected when *T. pseudonana* was exposed to allelopathy. Perforations in the cell membrane observed via fluorescence microscopy were consistent

with the observed decreases in membrane-associated lipids. These findings suggest that allelopathy acts through membrane destabilization and the disruption of photosynthesis.

In summary, my dissertation research provides insights into the chemical nature of waterborne cues and their impacts on biological systems. Using complex multivariate modeling and multi-platform profiling techniques, the molecular nature of a waterborne cue mixture was characterized and the molecular responses of species sensitive to allelopathy were illuminated. Lastly, the current work reveals the challenges of identifying waterborne cues and provides a framework for investigating the chemical nature and importance of interactions mediated by waterborne cues.

CHAPTER 1. INTRODUCTION

One of the most fundamental aspects of ecology is understanding interactions among organisms and interactions between organisms and their environments (4). These interactions are dependent on mechanisms to detect other organisms via visual (5, 6), olfactory (7, 8), auditory (9, 10), mechanosensory (11, 12), or other specialized cues. In the marine environment, many organisms use chemical senses such as olfaction and taste, as wave action, turbidity, and darkness can complicate other detections mechanisms. However, despite significant evidence that chemosensation is widespread (7, 13-15), little is known of the ecologically important compounds being sensed in marine environments. In one of the few chemically described systems, di-$_{L}$-prolyl diketopiperazine (Figure 1.1) mediates the attraction of mates in the phytoplankton *Seminavis robusta* (16). In another example, the phytoplankton *Alexandrium minutum* responds to a specialized class of taurolipids called copepodamides (Figure 1.1) released by copepod predators, increasing production of defensive toxins by up to 20-fold (17).

Many of the waterborne cues responsible for mediating interactions among marine organisms are particularly difficult to characterize due to their chemical properties. Waterborne cues are often polar, labile, and found in relatively low concentrations in the water column (18). Bioassay-guided fractionation is time and resource intensive and does not favor waterborne cues. Additionally, the separation of multicomponent cues can lead to loss of bioactivity during compound isolation. The lack of appropriate methodologies to isolate and characterize waterborne cues has led to a dearth of knowledge regarding the chemical nature of signaling in marine systems.

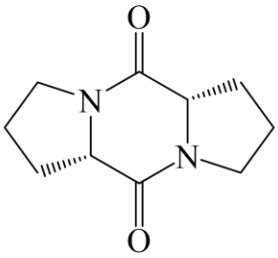

di-L-prolyl diketopiperazine

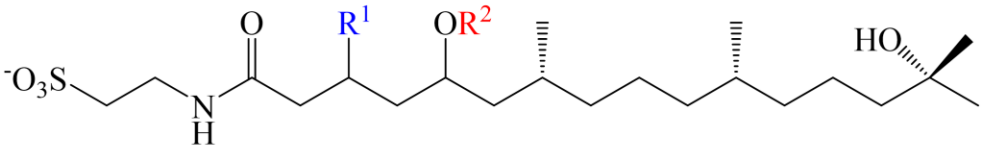

Copepodamide	R^1	R^2
A	$-CH_3$	Docosahexaenoic acid (DHA)
B	$-CH_3$	Eicosapentaenoic acid (EPA)
C	$-CH_3$	Stearidonic acid (SDA)
D	$=CH_2$	Docosahexaenoic acid (DHA)
E	$=CH_2$	Eicosapentaenoic acid (EPA)
F	$=CH_2$	Stearidonic acid (SDA)
G	$-CH_3$	H
H	$=CH_2$	H

Figure 1.1: Molecular structures of the previously identified waterborne cues: di-L-prolyl diketopiperazine and copepodamides A-H.

The intertidal zone is a particularly harsh environment that straddles the boundary between land and water. Intense abiotic stressors such as direct sunlight, fluctuating temperatures, and arid conditions when intertidal communities are exposed to the air have led to adaptive behaviors and physiological enhancements that reduce desiccation and predation (19-21). When submerged, organisms are subjected to a completely different set of stressors including predators that may not be relevant when exposed at low tide. One useful adaptation is for individuals to detect predators at a distance and avoid contact, thus preventing the need for additional costly investment in defense. In Southeastern U.S. estuarine oyster reefs, the mud crab *Panopeus herbstii* is known to cease foraging activities and hide from predatory blue crabs, *Callinectes sapidus*, in the interstitial spaces between oysters (22). Previous studies have suggested that detection is chemically mediated although neither the transmission source of the cue nor the compounds responsible for detection were identified (22). I hypothesized that small, primary metabolites released in the urine of blue crabs are perceived and utilized by mud crabs as a warning that a predator is nearby.

Alteration of behavior of prey in response to the detection of predators, also known as non-consumptive effects, is predicted to have large impacts on community structure, possibly more than the direct consumption of prey by predators (23). For example, the reintroduction of wolves in Yellowstone National Park is shown to have affected the movement, feeding habits, and reproduction of elk (24-26). Altered elk behavior allowed aspen, willow, and cottonwood populations to rebound near riverbanks which further allowed beavers and bison to reclaim lost habitat (27). Additional effects, such as increases in the populations of songbirds have also been attributed to cascading non-consumptive

effects of wolf reintroduction (28). Similarly to how the presence of wolves in Yellowstone altered the behavior of elk, the fear-inducing cue alters the behavior of mud crabs, suggesting that the fear-inducing cue could affect community structure and composition. This warrants additional investigation into the chemical nature of the cue in the field as well as the ecological impact on the community.

Chemical cues are also important in mediating competitive interactions. Allelopathy, the release of compounds that negatively affect competitors, is a common feature among bloom-forming phytoplankton hypothesized to play a role in bloom dynamics (29). Despite a long history of researchers investigating the potent neurotoxins that bloom-forming phytoplankton exude (30-32) and their disastrous effects on marine life (33, 34), little is known of the compounds responsible for allelopathy. Perhaps surprisingly, the neurotoxins that threaten human health and cause wildlife mortality are not typically allelopathic towards other phytoplankton. Additionally, little is known of the metabolic responses of phytoplankton exposed to allelopathy or the mechanisms of action of allelopathic compounds.

The red tide dinoflagellate, *Karenia brevis*, is common to the Gulf of Mexico and has been shown to utilize allelopathy as a form of interference competition. Previous research into the chemical nature of allelopathy has revealed that *K. brevis* allelopathy has species-dependent effects on competitors and is sub-lethal (35, 36) with allelopathic exposure leading to compromised osmoregulation, decreased photosynthesis, and increased oxidative stress in the competitor *Thalassiosira pseudonana* (37). Additionally, bioassay-guided fraction identified that bioactive fraction containing allelopathic compounds exhibited spectral characteristics of aromatic and fatty-acid derived moieties

but that complete characterization was not possible due to degradation (38). I hypothesized that *K. brevis* exudes variable concentrations of allelopathic compounds that correlate with allelopathic potency and that this variation could be used to classify *K. brevis* into distinct fingerprints, or chemical profiles. A more thorough understanding of the chemical nature of allelopathy and the effects on competitor physiology allows for further investigation into the mechanism of action of allelopathy and into the role of specific compounds in bloom dynamics.

In this dissertation, I examine the chemical nature of waterborne cues utilizing metabolomics and multivariate statistical modeling. I first describe a multicomponent fear-inducing cue that is utilized by prey to detect their predators in a Southeastern U.S. estuarine oyster reef. I then detail the chemical distinctions between allelopathic, non-allelopathic, and stimulatory *Karenia brevis* via spectroscopic fingerprinting. I follow by describing the catastrophic metabolic consequences of allelopathic exposure in two competing phytoplankton species. I conclude with future directions regarding the identification and characterization of waterborne cues.

CHAPTER 2. CHEMICAL ENCONDING OF RISK PERCEPTION AND PREDATOR DETECTION AMONG ESTUARINE INVERTEBRATES (1)

2.1 Abstract

An effective strategy for prey to survive in habitats rich in predators is to avoid being noticed. Thus, prey may be selected to recognize predators and adjust their behavior which can impact numerous community-wide interactions. Many animals in murky and turbulent aquatic environments rely on waterborne chemical cues. Previous research showed that the mud crab, *Panopeus herbstii*, recognizes the predatory blue crab, *Callinectus sapidus*, via a cue in blue crab urine. This cue is strongest if blue crabs recently preyed upon mud crabs. Subsequently, mud crabs reduce their foraging activity, reducing predation by blue crabs. Using nuclear magnetic resonance spectroscopy- and mass spectrometry-based metabolomics, chemical variation in urine from blue crabs fed different diets was related to prey behavior. We further identified the urinary metabolites trigonelline and homarine as components of the cue that mud crabs use to detect blue crabs, with concentrations of each metabolite dependent on blue crab diet. At concentrations found naturally in blue crab urine, trigonelline and homarine alone, as well as in a mixture, alerted mud crabs to the presence of blue crabs leading to decreased foraging by mud crabs. Risk perception by waterborne cues has been widely observed by ecologists, but the molecular nature of these cues has never been identified. Metabolomics provides an opportunity to study waterborne cues where other approaches have historically failed,

allowing for the advancement of our understanding of the chemical nature of a wide range of ecological interactions.

2.2 Introduction

Gathering and interpreting information from the environment is imperative to organisms' ability to recognize food, mates, predators, and appropriate habitat. Many aquatic species rely on chemical cues (39-41) in the marine environment where auditory, visual, and mechanosensory mechanisms are often compromised. Significant efforts have been made to understand chemical defenses and feeding deterrents (42-45) as many have potential medicinal applications (46-48), however waterborne cues remain almost completely unidentified.

The ability to sense and recognize predators remotely is particularly important for organisms because it allows for the production of behavioral, morphological, or life-historical adjustments to minimize predation (49). Although significant evidence exists for widespread chemical detection of predators and alarm cues among conspecifics in the marine environment (50-52), little is known about the molecular nature of the cues involved. These cues are of particular importance as they routinely produce ecologically significant non-consumptive effects, that is, altered species interactions beyond the effects of lost prey due to consumption due to changes in the morphology, behavior, or life-history of prey (23). Non-consumptive effects have been demonstrated in aquatic (21, 53, 54) and terrestrial environments (55), and are suggested to have even greater capacity to structure many communities than the direct effects of consuming prey (23). Due to the lack of a molecular understanding of these cue systems, little is known about how cues disperse in

aquatic systems, the receptors that mediate chemoreception and recognition of these cues, and the specificity to these cues, necessitating further research.

One explanation for the lack of characterized waterborne cues is that purification methodologies for highly water-soluble compounds have been unsatisfactory, especially when working with seawater samples that contain substantial quantities of inorganic salts. Standard sampling methods for airborne chemical cues such as headspace analysis for volatile insect pheromones (56) are unavailable for non-volatile waterborne cues. Many waterborne cues are present in very low concentrations, unstable to handling in the laboratory, and produced by organisms that either are not abundant or not readily cultivated in the laboratory. It may be difficult to identify in which tissues of an organism these cues are produced or stored, and when this is possible the signaling molecules may occur as part of a complex mixture with many other, irrelevant metabolites.

Traditionally, chemists have applied a process of bioassay-guided fractionation to purify and then characterize biologically active compounds. However, this multi-step approach often leads to decomposition of labile cues and exclusion of multicomponent cues, while simultaneously requiring substantial quantities of the chemical cue mixture for biological testing after each chemical separation step (38). Recent advances in nuclear magnetic resonance (NMR) spectroscopy and mass spectrometry (MS) metabolomics allow for fast, efficient, and cost-effective profiling of complex mixtures containing waterborne cues, whose chemical variation can be leveraged to correlate the presence or abundance of particular compounds within the mixture with biological potency of the mixture. Recently, a novel microalgal mate attraction pheromone was identified using MS-based metabolomics despite pheromone concentrations in the nanomolar range (16).

Previous research showed that the mud crab, *Panopeus herbstii,* detects its predator, the blue crab, *Callinectus sapidus,* using unknown metabolites released in the urine of blue crabs (57). Mud crabs distinguished urine from blue crabs fed different diets and reacted differently to urine from blue crabs fed mud crabs vs. other prey. Using NMR- and MS-based metabolomics, we aimed to leverage the chemical variation in urine from blue crabs fed different diets to identify the component(s) of the cue mixture that mud crabs use to recognize blue crabs. This study provides a roadmap to identify complex waterborne cues that can be used to further our understanding of chemically mediated interactions in the marine environment.

2.3 Materials and Methods

Animal Maintenance and Sample Collection

Blue crabs, *Callinectes sapidus,* were collected from the tributaries and rivers around Wassaw Sound, Savannah, GA, and either kept in a seawater flow-through system at the Skidaway Institute of Oceanography (SkIO) or transported to the Georgia Institute of Technology (GT), Atlanta, GA. The seawater flow-through system at SkIO housed animals in 2000 L tanks at ambient temperature with running seawater. Crabs at GT were held in a 4000 L recirculating system of artificial seawater (Instant Ocean™) formulated to maintain salinity between 25-30 ppt at 21-22 °C. The system contained a particulate bacterial biofilter, protein skimmer, and carbon filter. Animals were kept under a 12:12 light:dark cycle and water quality was checked and adjusted weekly to maintain levels recommended for marine invertebrates. Urine was collected from intermolt crabs, 10-15 cm carapace width from spine to spine. Animals were starved (36-48 h) prior to urine

collection to ensure urine was not contaminated with metabolites from their previous diet. Crabs were fed 7-12 g/day of either locally collected crushed mud crabs, *Panopeus herbstii,* or freshly shucked oysters, *Crassostrea virginica*, natural constituents of blue crab diets and members of the Wassaw Sound intertidal community (37). The diets mimicked *ad libitum* amounts for each prey type; 7 g oyster flesh and 12 g crushed mud crab (the difference accounting for the crab carapace that was not consumed). Blue crabs were housed in tanks with other members of the same diet treatment (20-24 crabs per treatment; groups of 4-6) and removed from the experiment if the full amount of food provided was not consumed daily. Blue crabs were maintained on their respective diet for a minimum of 5 days prior to urine collection.

Urine was collected from blue crabs via catheter twice weekly, by gentle suction (<35kPa) via a 22-gauge needle inserted into each nephropore of a blue crab. Urine contaminated with haemolymph or particulate matter was rejected. Urine from blue crabs of each diet treatment was collected approximately every other day, pooled, filtered by 0.22 µm Teflon syringe filter, and stored at -20 ˚C at GT. A total of 12 unique urine samples (each from 2-6 different crabs) per diet treatment were collected. Urine collected at SkIO as transported to GT frozen and stored at -20 ˚C. Urine was either assayed or profiled within 2 weeks of collection.

Behavioral Assay

The mud crab behavioral assay was performed following the previously reported protocol (57). In short, mud crabs collected from oyster reefs at low tide in the area surrounding Wassaw Sound were transported to GT where they were housed in a 380 L

recirculating artificial seawater system similar to that used for blue crabs. Mud crabs were fed an *ad libitum* shrimp diet 2-3 times weekly. Four mud crabs, 20-25 mm carapace width, were placed in 40 L aquaria with 2.0 L of freshly prepared artificial seawater of salinity (25-30 ppt) equal to the holding tanks. No more than three crabs of a single sex were maintained in each enclosure to average potential effects of sex on mud crab foraging. Crabs acclimated to their enclosure for 2 h, after which raw shrimp (3.8-4.2 g) cut into 6-10 pieces was added along with urine, cue solution, or artificial seawater as control (see below for specific details of treatments) and the water was agitated to ensure equal mixing. Mud crabs were allowed to eat undisturbed for 4 h, after which the remaining shrimp was collected and weighed to determine mass loss due to consumption. The amount of food consumed as a proportion of the total provided was analyzed using one-way analysis of variance with a Tukey post-hoc test using PRISM version 10.0.

Urine and cue treatments consisted of: 5.0 mL of urine added to a tank for a final concentration of 2.5 mL/L, or, 5.0 mL of a synthetic cue mixture solubilized in artificial seawater and formulated for a final concentration equal to that of the average concentration in blue crab urine across all urine samples. Negative controls consisted of 5.0 mL artificial seawater. Previous studies indicated that a mass loss control was unnecessary as shrimp mass change was negligible due to water loss/gain.[15] Potency of urine/cue treatment was determined following:

$$\text{Urine potency} = 1 - \left(\frac{\text{amount eaten by crabs exposed to urine or cue treatment}}{\text{amount eaten by crabs exposed to control}}\right) * 100$$

NMR sample preparation and data collection

Urine samples were prepared for ^{1}H NMR metabolomics by adding an antibacterial buffer solution and internal standard in deuterated water. Urine samples collected at SkIO were formulated from 345 µL urine, 115 µL buffer solution (0.4 M sodium phosphate pH 7.0, 0.5 % w/v sodium azide), and 40 µL internal standard 3-(trimethylsilyl)propionic-2,2,3,3-d_4 acid (TMSP) in D_2O (99.9% atom D_2O; Sigma-Aldrich), whereas urine samples collected at GT were formulated from 138 µL urine, 46µL buffer solution, and 16 µL of TMSP in D_2O. A Bruker Avance 500 MHz NMR spectrometer equipped with a 5 mm broadband direct detection probe in conjunction with a water suppression excitation-sculpting gradient pulse program (relaxation delay of 1 s and spectral width of 6.5 kHz) was used to acquire 256 scans per urine sample (37).

NMR spectroscopic data processing and analysis

^{1}H NMR spectra were processed in MATLAB, version 8.1.0.604, using NMRLab (58). Spectra were manually phased, baseline corrected, aligned, and the following regions excluded to remove contaminants from statistical analysis: TMSP (-0.5 to 0.5 ppm), water (4.6-5.2 ppm), residual methanol (3.2-3.4 ppm), and excess area (9.0-12.4 ppm) that contained no spectroscopic features. Spectroscopic features were clustered into 0.005 ppm bins, probabilistic quotient normalized (59) to remove dilution bias, and generalized log (glog) transformed to avoid bias towards high-concentration metabolites without affecting between-sample variation. Glog optimization values, λ, were generated from five technical replicates that consisted of equal parts from a single bulk urine sample using the methods above (60). For urine samples from SkIO, $\lambda = 2.9359 \times 10^{-7}$ and for urine samples at GT

$\lambda = 8.2585x10^{-9}$. Principal component analysis (PCA) and partial least squares discriminant analysis (PLSDA) were used to visualize differences in urine metabolite profiles from urine collected at SkIO (MATLAB and PLS_Toolbox, version 7.9.1). The PCA and PLSDA models were generated from data that was mean centered and cross-validated using Venetian blinds with eight data splits (n = 12 per treatment), and the loadings of the 1st principal component of the PCA model were used to identify spectroscopic features of significance in differentiating urine samples from blue crabs fed different diets.

A partial least squares regression (PLS-R) model was generated using the above spectroscopic preprocessing, matrix preprocessing, and relative potency values (determined in behavioral bioassay below) for a set of seven urine samples collect at GT, four from blue carbs fed mud crabs and three from blue crabs fed oysters. The loadings of the regression vector in addition to the variable importance parameter were used to identify spectroscopic features that increased in area under the curve with an increase in urine potency in the bioassay.

Identification of metabolites from NMR spectroscopic data

The NMR profiling database Chenomix was initially used to assign structures to metabolites with spectroscopic features present in the ^{1}H NMR spectra of blue crab urine. However, because blue crab urine is chemically complex with many overlapping signals, ^{1}H NMR spectroscopy was not sufficient to fully characterize metabolites. From a representative blue crab urine sample correlation spectroscopy (COSY), total correlated spectroscopy (TOCSY), heteronuclear single quantum coherence spectroscopy (HSQC), and heteronuclear multiple bond correlation spectroscopy (HMBC) were acquired using a

500 MHz Avance NMR spectrophotometer as above with a 5 mm indirect detection probe. The loadings from the PCA and PLS-R models pinpointed protons that distinguished urine from blue crabs fed different diets and for identifying the components of the fear inducing cue respectively. The COSY, TOCSY, HSQC, and HMBC data were used to connect multiple protons associated with the same metabolite (or to identify that no additional protons were associated). Concentrations of proposed metabolites were determined by comparing the integrated areas of non-overlapping proton signals to that of the internal standard of known concentration. Commercially available synthetic standards of each proposed metabolite were formulated to match the concentration of the proposed metabolite in blue crab urine as determined above, and subjected to low resolution mass spectrometry. A Waters Micromass ZQ2000 mass spectrometer was tuned (capillary voltage, cone voltage, extractor voltage, RF lens voltage, source temperature, desolvation temperature, desolvation gas flow, cone gas flow mass resolution, and ion energy) to each synthetic standard to obtain the best ionization and mass signal possible for each metabolite. Once tuned to a standard, a representative urine sample and the synthetic standard were compared by high performance liquid chromatography with a Waters 2495 pump equipped with a Phenomenex Luna C18 silica reversed phase column, using retention time, peak shape, and peak integration observed by a Waters 2996 photodiode array detector. If the two samples were sufficiently similar, low resolution mass spectrometry fragmentation data were collected and compared between the synthetic standard and the representative sample of blue crab urine using an Agilent 1100 HPLC with Phenomenex Gemini C18 silica reversed phase column coupled to a Micromass

Quattro mass spectrometer using electrospray ionization in both positive and negative mode.

UPLC-MS sample preparation and data collection

Urine samples from four blue crabs fed each diet (collected at GT) were thawed on ice, and protein were precipitated by the addition of methanol in a 5:1 volume ratio to 50 µL of urine. Samples were vortex-mixed for 30 s and centrifuged at 21,100 g for 5 min. After centrifugation, supernatant was transferred to an auto-sample vial with snap-on cap and placed in sample manager which was held at 4 °C. Samples were run in randomized order. The mass spectrometer was mass calibrated before analysis; a sample preparation blank was analyzed jointly with the samples.

UPLC-MS was performed using an Ultimate3000 (ThermoFisher Scientific), fitted with a Waters ACQUITY UPLC BEH HILIC column (2.1 x 75 mm, 1.7 µm particle size), coupled to a high-resolution accurate mass Q Exactive HF mass spectrometry system (ThermoFisher Scientific). The Q Exactive HF is a hybrid quadrupole-orbitrap instrument with a typical resolving power of 240,000 FWHM at m/*z* 200 and mass accuracy of <1 ppm. The heated electrospray ionization (HESI) source was operated at a capillary temperature of 275 ºC, a spray voltage of 3.5 kV, and sheath, auxiliary, and sweep gas flows of 48, 11, and 2, respectively. The instrument acquired data in the 70-1050 *m/z* range in positive and negative ionization modes. Data acquisition and processing were carried out using Xcalibur V4.0 (ThermoFisher Scientific) and Compound Discoverer V2.1 (ThermoFisher Scientific), respectively. The chromatographic method for sample analysis involved elution with 95:5 10 mM ammonium acetate with ~0.014% ammonium

hydroxide: acetonitrile (mobile phase A) and acetonitrile with ~0.014% ammonium hydroxide (mobile phase B) using the following gradient program: 0 min 5% A; 3 min 63% A; 7 min 63% A; 7.1 min 5% A; 9.9 min 5%. The flow rate was set at 0.30 mL min^{-1} for 0-7.1 min; increased to 0.5 mL min^{-1} from 7.1-7,2 min; 7.2-9.5 min at 0.5 mL min^{-1}; and decreased to 0.30 mL min^{-1} from 9.5 – 10.0 min. Optima (ThermoFisher Scientific) LC-MS grade water and acetonitrile was used to prepare all mobile phase components. Ammonium acetate (Sigma) molecular biology grade and ammonium hydroxide 28-30% solution (Fisher Chemical) were additives to the mobile phases. The column temperature was set to 50 °C, and the injection volume was 2 µL.

UPLC-MS/MS experiments were performed by acquiring mass spectra in a data dependent acquisition fashion. Full MS were collected with a resolution of 120,000 and the top 10 dd-MS^2 were collected at a resolution of 30,000 and an isolation window of 0.4 *m/z*. Stepped normalized collision energies of 10, 30, and 50 fragmented selected precursors in the HCD cell prior to combination of ion for analysis in the orbitrap. Dynamic exclusion was set at 10 s and ions with charges greater than 2 were omitted.

MS data processing and analysis

Data from two urine samples, one from each diet, were removed as outliers due to either overly low and high average signal intensity. The remaining data files were aligned with an adaptive curve and metabolic features (retention time (R_t), *m/z* pairs) were detected after removal of isotopes and adducts in Compound Discoverer. Background peaks were removed from the dataset using a sample blank. Fill gaps and normalization by constant sum was applied to the data. Select features with a fold change greater or equal to 2 in urine

from blue crabs fed mud crabs when compared to urine from blue crabs fed oysters and relative standard deviation of less than 30 were used to build an un-supervised principal component analysis (PCA) model with leave-one-out cross-validation using MATLAB R2012b (Version 8.0.0.783 The MathWorks, Inc.) and the PLS Toolbox (v.6.71, Eigenvector Research, Inc.). Data were preprocessed by auto-scaling the features' peak areas across the samples.

Identification of metabolites from MS data

Compound identification was carried out for the selected 28 unique discriminant features (Table 2.3). During data processing, elemental formulas were generated based on the mass accuracy and together with available MS^2 spectra potential hits were compiled based on searches against publicly-available databases: ChemSpider, the human metabolome database (HMDB), KEGG database, and MzCloud. In silico fragmentation of potential structural matches were calculated and scored against experimental data using Compound Discoverer. When available, metabolite standards were analyzed to support identification. Identification of metabolites was pursued per established criteria (61). See Table 2.1 for fragmentation data for all significant discriminant features.

Isolation and characterization of homarine (14)

Blue crab urine was initially separated using a Waters 1525 pump coupled to a Waters 2487 dual wavelength detector with a Vydac C18 silica column (5 µm, 10 x 250 mm). Chromatography was completed following a 5 min hold at 2 % aqueous methanol followed by a gradient from 2 % to 75 % aqueous methanol, at 3 mL/min. The fraction containing the metabolite of interest as detected by ^{1}H NMR spectroscopy was further

purified using a Tosoh Biosciences amide 80 (5 µm, 4.6 x 250 mm) column with an isocratic elution of 15% aqueous acetonitrile over 20 min at 1 mL/min. MS data were collected using a high resolution accurate mass Q Exactive HF mass spectrometry system (ThermoFisher Scientific). NMR spectroscopic data were acquired as described above.

Identification of blue crab urine cue constituents

Trigonelline (**1**) and trimethylamine (**8**) were purchased commercially whereas homarine (**14**) was synthesized (see below). All three compounds – commercial (**1**) and (**8**) and synthesized (**14) –** were tested alone and in combination in the behavioral assay to assess their roles in the fear-inducing cue. Urine assayed was collected from crabs housed at GT. A one-way ANOVA with Tukey post-hoc test was run to test statistical significance of foraging suppression.

Synthesis of homarine (14)

Homarine (**14**) was synthesized following a slightly modified protocol previously reported (62), as described below, from methyl picolinate:

Synthesis of methyl picolinate

A picolinic acid (1.02 g, 8.3 mmol) solution in methanol (10 mL) was cooled to 0 °C, and concentrated sulfuric acid (2.5 mL) was added dropwise. The reaction mixture was refluxed under agitation for 4 h, after which a saturated potassium carbonate solution (10 mL) was added. Solvents were removed *in vacuo* and the solid residue was suspended in chloroform and water. The organic layer was washed with water until neutral, dried with anhydrous magnesium sulfate, and the solvent was removed by rotary evaporation. The

crude oily product was characterized using ^{1}H NMR spectroscopy and used for in the next step without further purification. ^{1}H NMR (500 MHz, $CDCl_3$): δ 8.76 (ddd, J = 4.8, 1.8, 0.9 Hz, 1H), 8.15 (dt, J = 7.9, 1.1 Hz, 1H), 7.86 (td, J = 7.8, 1.8 Hz, 1H), 7.49 (ddd, J = 7.7, 4.7, 1.2 Hz, 1H), 4.02 (s, 3H).

Synthesis of homarine (**14**)

The crude methyl picolinate product was dissolved in toluene (3 mL) and dimethyl sulfate (5 mL, 53 mmol) was slowly added. The reaction mixture was agitated at room temperature for 16 h, then brought to boil for 1 h. The solvent and excess reagent were removed *in vacuo* after the reaction was complete. The product was suspended in 10% aqueous hydrochloric acid (10 mL) and refluxed for 4 h. The reaction mixture was neutralized with saturated potassium carbonate, and the final product was extracted with *n*-butanol. The organic layer was dried with anhydrous magnesium sulfate and evaporated *in vacuo*. The oil was freeze-dried overnight after which crystals were recovered. Pure homarine (**14**) was obtained in an unoptimized yield of 0.9 % starting from picolinic acid. ^{1}H NMR (500 MHz, DMSO-d_6): δ 9.14 (br d, J = 6.1 Hz, 1H), 8.71 (td, J = 7.9, 1.4 Hz, 1H), 8.49 (dd, J = 7.9, 1.6 Hz, 1H), 8.25 (ddd, J = 7.8, 6.1, 1.7 Hz, 1H), 4.49 (s, 3H). ^{13}C NMR (125 MHz, DMSO-d_6): δ 161.3, 148.8, 146.6, 144.4, 129.6, 129.2, 48.3. High resolution mass spectrometric (HRMS) data collected on a Waters Xevo QTOF instrument equipped with a Waters Aquity C18 silica BEH reserved-phase column. HRMS (ESI) *m/z*: $[M+H]^+$ Calculated for $C_7H_8NO_2$ 138.0554; found 138.0566.

Geometry optimization of trigonelline (1) and homarine (14)

Three-dimensional structures of trigonelline, homarine, picolinic acid, and *o*-toluic acid were drawn and submitted to Gaussian '09 (63) for geometrical optimization at the B3LYP/6-31++G** level of theory. Thereafter, the resulting geometries were subjected to vibrational and thermochemical calculations at the same level of theory, and the vibration frequencies were verified to ensure that all were positive and real. The structures were represented using PyMol (64).

2.4 Results

Mud crabs perceive risk via concentration differences in predator urinary metabolites

When we employed ^{1}H NMR-based metabolomics comparing the chemical profiles of urine from blue crabs fed mud crabs vs. oysters, principal component analysis (PCA) revealed a single principal component, accounting for 19.5 % of the total variation among urine samples, which differentiated urine of blue crabs fed the two diets (Figure 2.1A). An orthogonalized partial least squares discriminant analysis (oPLS-DA) model also differentiated urine from blue crabs fed these two diets; however the first latent variable only accounted for 10.4% of the total chemical variation (Figure 2.2). A complementary MS-based PCA model similarly distinguished urine from blue crabs fed different diets using a single principal component, accounting for 89.3% of the total variation among samples (Figure 2.1B).

Analysis of the NMR-based PCA loadings (Figure 2.3) which highlighted spectral features that were more abundant in urine from blue crabs fed one diet versus the other, along with two-dimensional NMR spectroscopic data of blue crab urine (Table 2.1; Figure 2.4, Figure 2.5, Figure 2.6) which determined the connectivity of atoms within

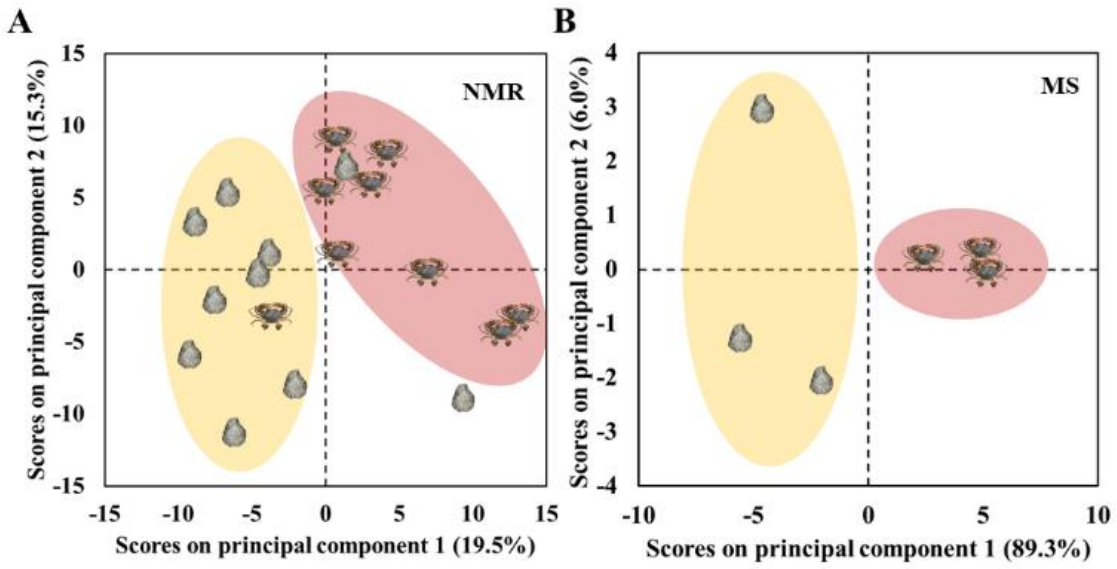

Figure 2.1: Blue crab diet affects urine metabolite profile. Principal component analysis (PCA) of metabolomics data from A) ^{1}H nuclear magnetic resonance (NMR) spectra and B) mass spectrometry (MS) differentiate urine of blue crabs fed mud crabs and from urine of blue crabs fed oysters along the first principal component (variance captured along PC1 is stated in parentheses, P = 0.0074 for NMR, P = 0.0003 for MS). Crab symbols represent data from urine from blue crabs fed mud crabs (N = 10 for NMR, N = 3 for MS); oyster symbols represent data from urine from blue crabs fed oysters (N = 9 for NMR, N = 3 for MS).

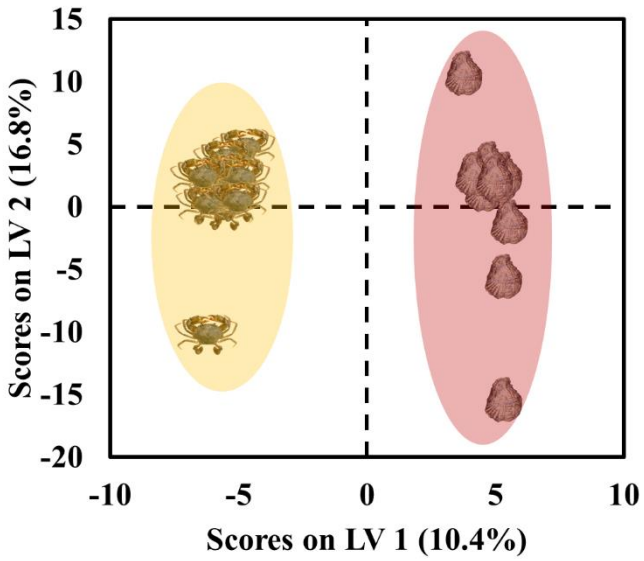

Figure 2.2: Diet of blue crab is represented in chemical profile of urine. Orthogonalized partial least squares discriminant analysis (OPSL-DA) scores for ^{1}H NMR spectra differentiates urine of blue crabs fed mud crabs and from urine of blue crabs fed oysters along the first latent variable using 10.45% of the total detected chemical variation within urine. Maroon circles represent data from urine from blue crabs fed mud crabs (N = 9); yellow circles represent data from urine from blue crabs fed oysters (N = 10).

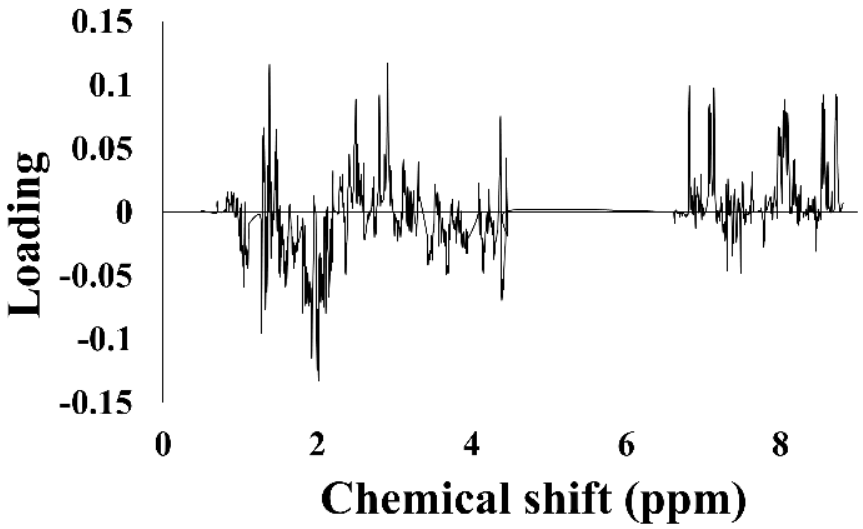

Figure 2.3: PCA loadings for ^{1}H NMR metabolomics highlight blue crab urinary metabolites whose concentrations are diet dependent. Spectroscopic features with positive loadings are associated with metabolites exhibiting increased concentration in urine from blue crabs fed mud crabs; spectroscopic features with negative loadings are associated with metabolites of an increased concentration in urine from blue crabs fed oysters (See Figure 2.1 for PCA scores plot).

Table 2.1: Spectrometric techniques used for identifying blue crab urine metabolites. MS data consisted of multiple reaction monitoring including mass transitions optimized with commercial standards prior to analysis. NMR data consisted of ^{1}H and two-dimensional approaches listed.

Compound	Molecular Ion (*m/z*)	Transition detected (*m/z*)	NMR method
Trigonelline (**1**)	138.0	94.0, 78.0	COSY, HSQC, HMBC
Pyrimidine (**2**)	81.0	54.0	HSQC, HMBC
Lactate (**3**)	89.0	45.0	COSY, HSQC, HMBC
Carnitine (**4**)	162.0	103.0, 60.0	HSQC, HMBC
Choline (**5**)	103.9	60.0, 45.0	COSY, HSQC, HMBC
Threonine (**6**)	119.8	74.0	COSY, HSQC, HMBC
Creatinine (**7**)	113.8	44.0	HMBC
Trimethylamine (**8**)	59.8	45.0	HSQC, HMBC
Methyl glutarate (**9**)	161.2	102.1	COSY, HSQC, HMBC
Acetate (**10**)	60.0	Fragments too small for detection	
Creatine (**11**)	131.8	90.0	HSQC
N-**3**-methylhistidine (**12**)	169.9	124.0	HSQC, HMBC
Alanine (**13**)	89.9	44.0	COSY, HSQC, HMBC

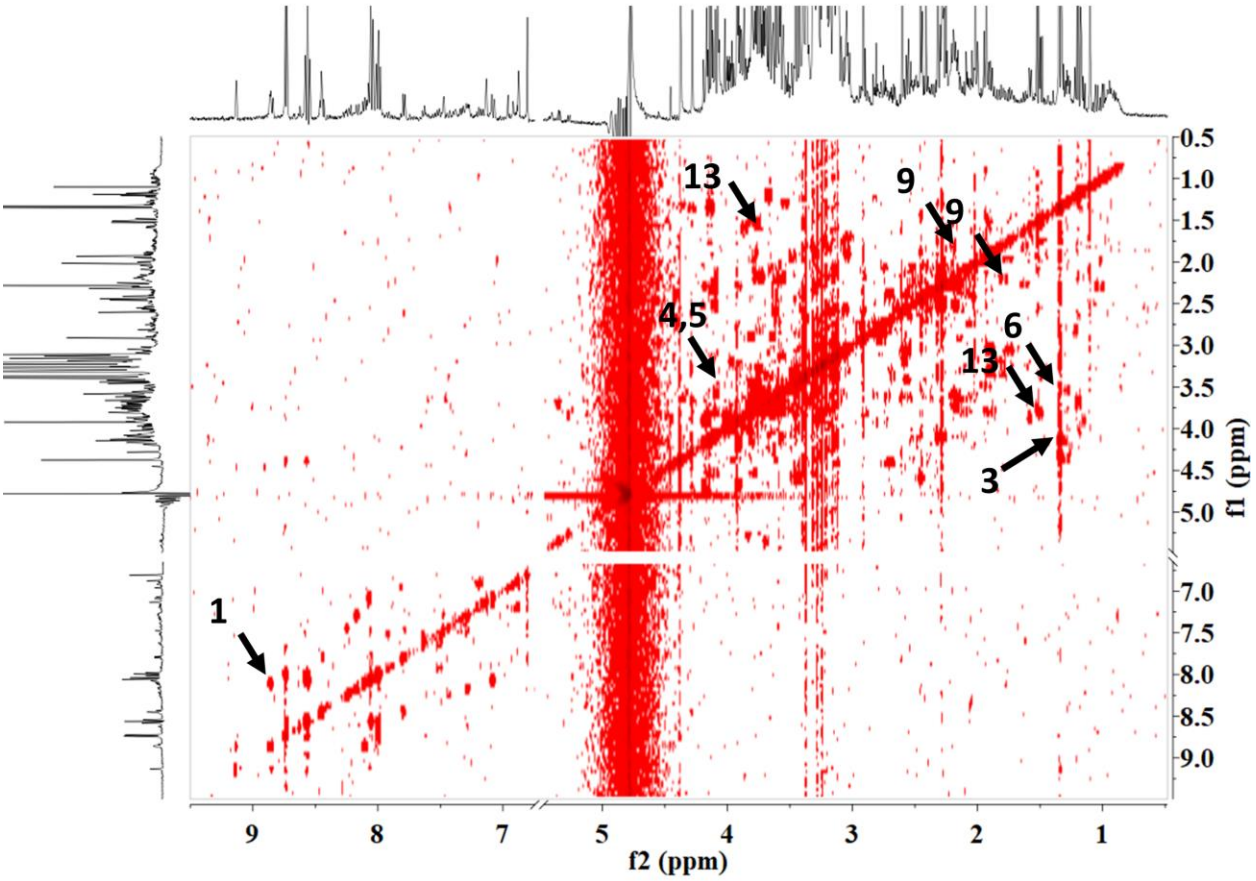

Figure 2.4: Correlation spectroscopy (COSY) spectrum of blue crab urine annotated with compound numbers indicating critical correlations for trigonelline (**1**), lactate (**3**), carnitine (**4**), choline (**5**), threonine (**6**), methyl glutarate (**9**), and alanine (**13**).

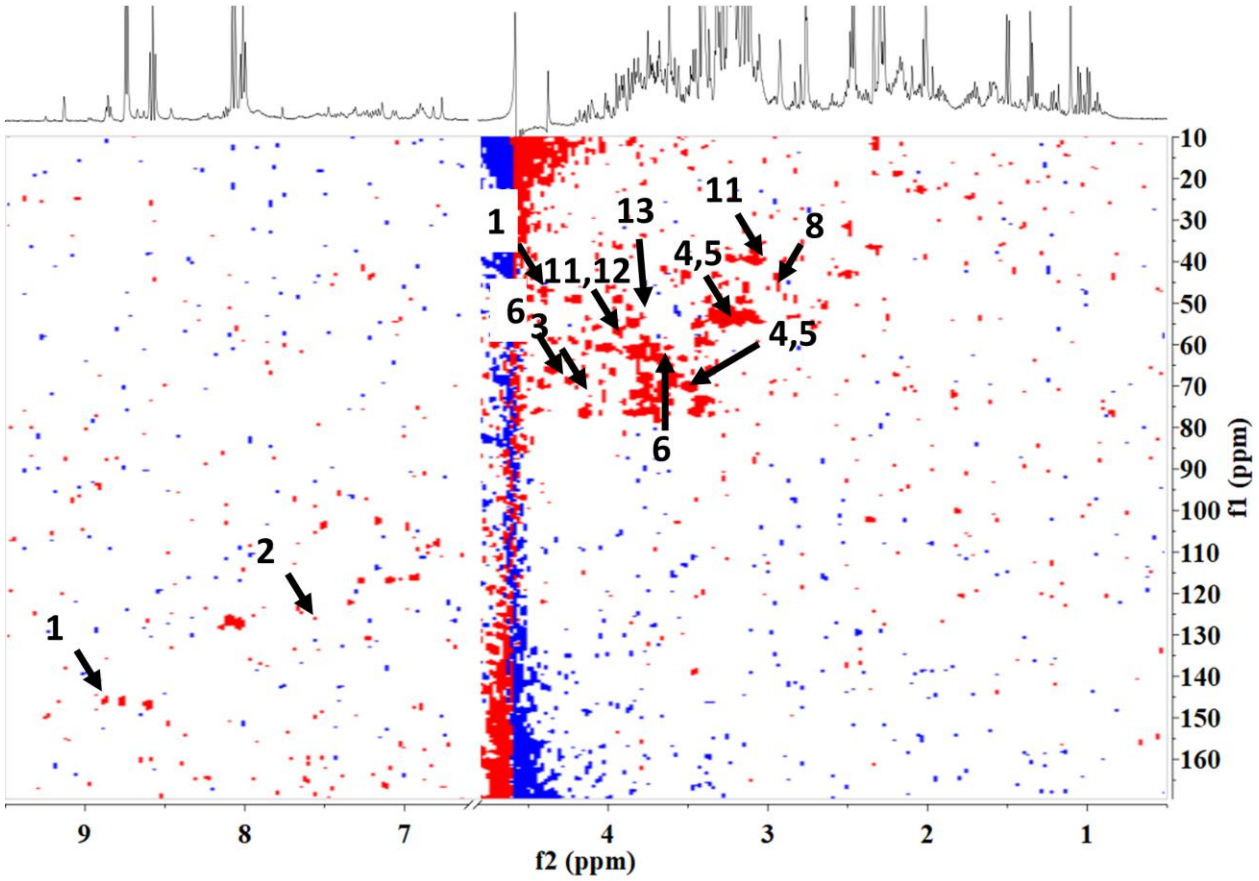

Figure 2.5: Heteronuclear single quantum coherence (HSQC) spectrum of blue crab urine annotated with compound numbers indicating critical chemical shifts for trigonelline (**1**), pyrimidine (**2**), lactate (**3**), carnitine (**4**), choline (**5**), threonine (**6**), trimethylamine (**8**), creatine (**11**), *N*-methylhistidine (**12**), and alanine (**13**).

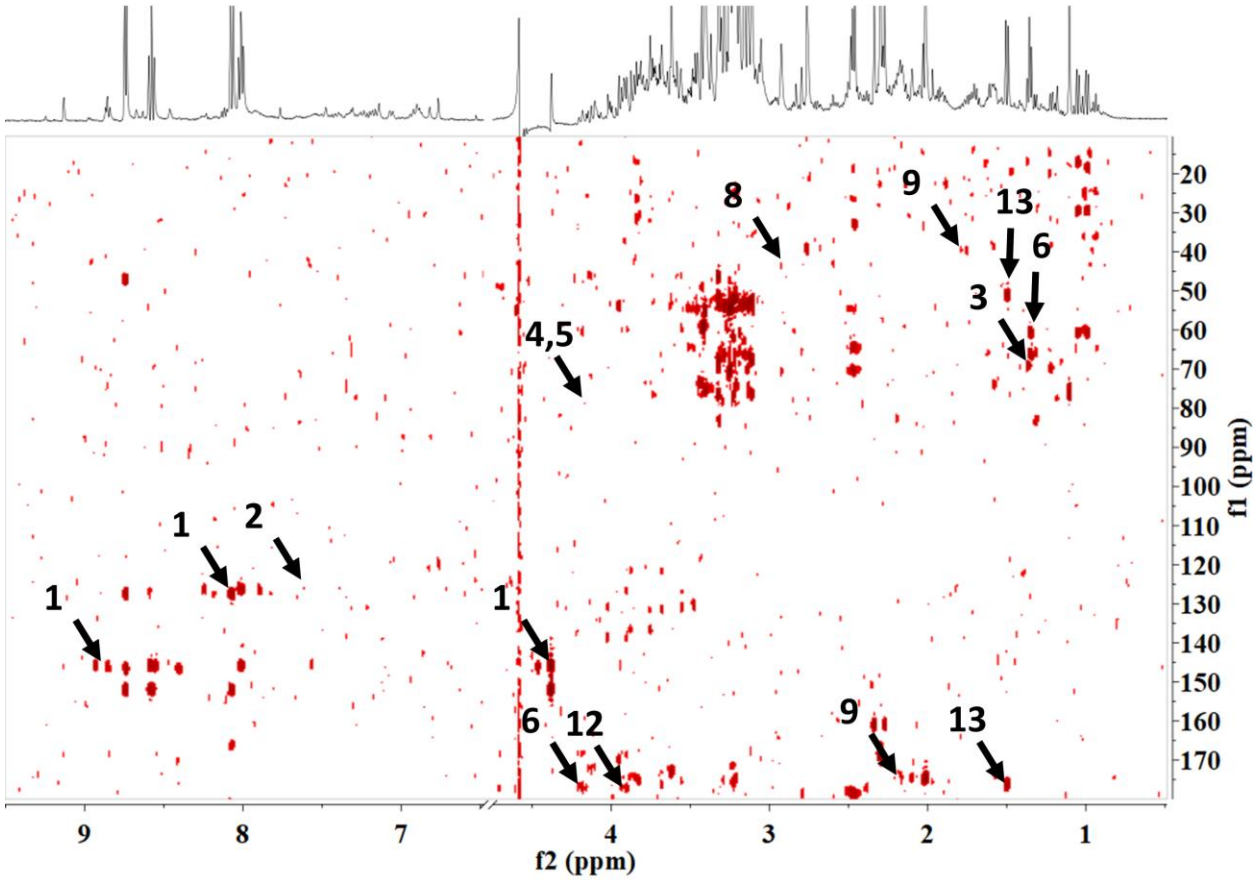

Figure 2.6: Heteronuclear multiple bond correlation (HMBC) spectrum of blue crab urine annotated with compound numbers indicating critical chemical shifts for trigonelline (**1**), pyrimidine (**2**), lactate (**3**), carnitine (**4**), choline (**5**), threonine (**6**), trimethylamine (**8**), methyl glutarate (**9**), *N*-methylhistidine (**12**), and alanine (**13**).

each molecule, led to the putative identification of a subset of urinary metabolites, 13 in total, that we hypothesized mud crabs use to differentiate among predators that impose different degrees of risk (Table 2.2). Mass spectrometric data confirmed these identifications (Table 2.1, Figure 2.7). Thus, whereas individual metabolites pinpointed via PCA were not purified from blue crab urine, their structures were confidently assigned, as components of a complex urine matrix, by a combination of NMR and MS approaches. Analysis of the MS-based PCA model highlighted 28 unique metabolites of the 661 total detected metabolites (Table 2.3, Table 2.4, Table 2.5) whose concentrations were enhanced in the urine of blue crabs fed mud crabs, which act as a discriminating panel to differentiate between urine from blue crabs fed different diets. Carnitine (**4**) was identified through both NMR- and MS-based metabolomics analyses as more abundant when blue crabs ate mud crabs, but most relevant molecules were revealed through statistical modeling by only one of the approaches, highlighting the complementary nature of the two techniques. Additionally, acetylcholine and propionylcarnitine were identified via MS profiling while choline and carnitine were identified via NMR spectroscopic profiling, further accentuating useful complementarity of the two spectroscopic techniques.

Different diets did not lead to different *identities* of metabolites in blue crab urine relevant to prey behavior, but rather resulted in altered *concentrations* of the same metabolites perceived by prey via exposure to urine (Figure 2.8). Variable concentrations of individual metabolites were evident from the differential integration of common ^{1}H NMR spectroscopic features (Figure 2.8B inset). These metabolites included those involved in amino acid metabolism, niacin metabolism, energy metabolism, energy

Table 2.2: Metabolites identified from blue crab urine by NMR spectroscopy-based PCA model. Relative concentrations were averaged from N = 9 urine samples for each diet type.

Metabolite	Concentration in urine of blue crabs fed mud crabs	
	Absolute (μM)	Relative to urine of blue crabs fed oysters
Trigonelline (1)	90	1.8×
Pyrimidine (2)	72	1.6×
Lactate (3)	250	1.3×
Carnitine (4)	160	1.2×
Choline (5)	110	1.2×
Threonine (6)	160	1.1×
Creatinine (7)	62	1.0×
Trimethylamine (8)	-[a]	-[a]
Methyl glutarate (9)	-[a]	-[a]
Acetate (10)	-[a]	-[a]
Creatine (11)	-[a]	-[a]
N-Methylhistidine (12)	99	0.75×
Alanine (13)	180	0.50×

[a] – Concentration could not be determined due to NMR spectral overlap of diagnostic protons.

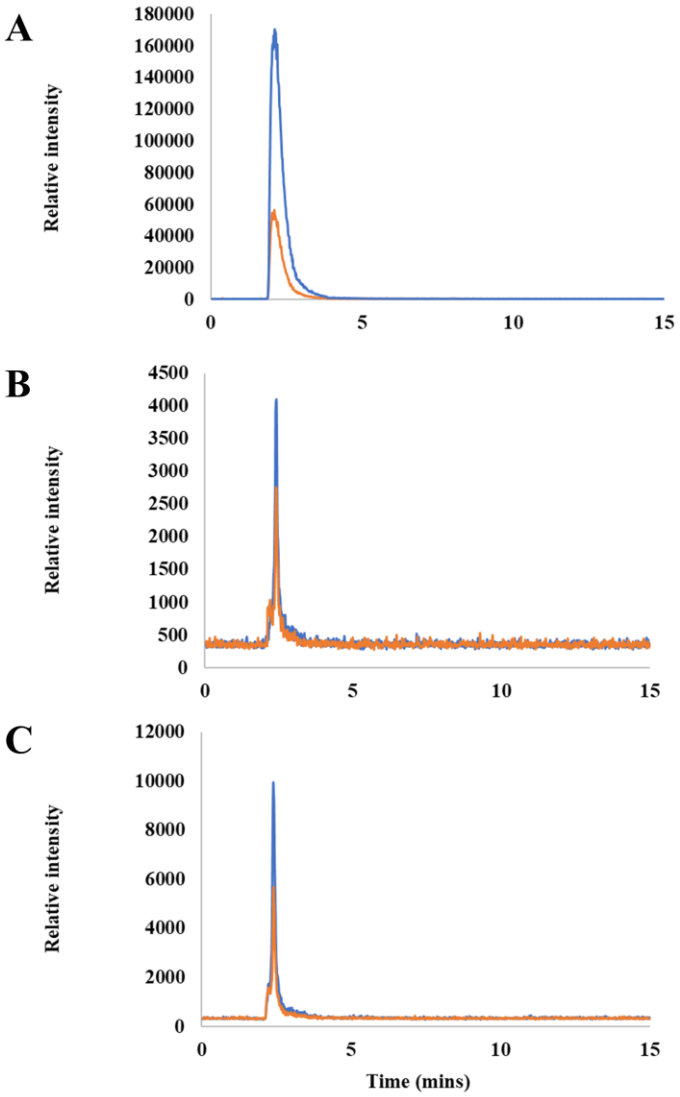

Figure 2.7: Multiple reaction monitoring LC/MS confirmation of trigonelline (**1**) in blue crab urine. Mass transitions of 138 amu to 94 amu (blue) and 138 amu to 78 amu (orange) were optimized using a commercially available standard of **1**. A) Commercial standard of **1** at 1 mg/mL, B) blue crab urine, and C) blue crab urine spiked with an equivalent amount of **1** which resulted in an approximate doubling of the peak associated with **1**, as predicted.

Table 2.3: Tentative identification of 28 unique metabolites detected via MS metabolomics whose concentrations were greater in urine from blue crabs fed mud crabs than urine from blue crabs fed oyster. Mass, retention time, ion type, theoretical mass, mass error, and elemental formula provided. Metabolites were matched to standards, literature spectra, or were at least consistent with potential molecular structure fitting the following requirements for each confidence level: 1) elemental formula, retention time, and MS/MS spectrum of standard matched to feature; 2) MS/MS spectrum consistent with literature spectra and fragmentation ions observed consistent with proposed structure; 3) putative compound class based on chromatographic elution window; and 4) unknown compounds. CAS# is provided where applicable.

Compound Number	**Average *m/z***	**Average Retention Time (min)**	**Ion Type**	**Ion Theoretical *m/z***	**Mass Error (PPM)**	**Elemental Formula**	**Tentative Metabolite Identification [CAS#] [ID level]**
19	146.1175	4.54	$[M+H]^{+1}$	146.1176	-0.7	$C_7H_{15}NO_2$	acetylcholine [51-84-3] [1]
34	162.1123	4.13	$[M+H]^{+1}$	162.1125	-1.2	$C_7H_{15}NO_3$	carnitine[541-15-1] [1]
40	76.0764	4.43	$[M+H]^{+1}$	76.0757	9.2	C_3H_9NO	1-aminopropan-2-ol [78-96-6] [2]
95	218.1387	4.04	$[M+H]^{+1}$	218.1387	0.0	$C_{10}H_{19}NO_4$	propionylcarnitine [NA] [2]
98	144.1384	5.42	$[M+H]^{+1}$	144.1383	0.7	$C_8H_{17}NO$	[NA] [4]
166	141.1387	5.34	$[M+H]^{+1}$	141.1386	0.7	$C_8H_{16}N_2$	[NA] [4]
172	222.0986	1.64	$[M+H]^{+1}$	222.0986	0.0	$C_9H_{11}N_5O_2$	6-acetyl-2-amino-1,7,8,9-tetrahydro-4H-pyrimido[4,5-b][1,4]diazepin-4-one [80003-63-0] [2]
174	377.1455	1.66	$[M+H]^{+1}$	377.1456	-0.3	$C_{17}H_{20}N_4O_6$	riboflavin [83-88-5] [2]; lyxoflavin [13123-37-0] [2]
176	285.0982	1.16	$[M+H]^{+1}$	285.0969	4.5	$C_{13}H_{16}O_7$	[NA] [4]
200	192.0516	1.36	$[M+H]^{+1}$	192.0516	0.0	$C_7H_5N_5O_2$	2-amino-4-hydroxypteridine-6-caraldehyde [721-30-1] [2]
215	120.1022	4.83	$[M+H]^{+1}$	120.1019	2.5	$C_5H_{13}NO_2$	[NA] [4]
223	198.0795	3.07	$[M+H]^{+1}$	198.0795	0.0	$C_6H_{15}NO_4S$	[NA] [4]
255	329.0811	1.71	$[M+H]^{+1}$	329.0809	0.6	$C_6H_{16}N_8O_4S_2$	[NA] [4]
262	238.0938	2.19	$[M+H]^{+1}$	238.0935	1.3	$C_9H_{11}N_5O_3$	biopterin [22150-76-1] [2]
307	144.1384	4.45	$[M+H]^{+1}$	144.1383	0.7	$C_8H_{17}NO$	[NA] [4]
348	226.0933	1.68	$[M+H]^{+1}$	226.0935	-0.9	$C_8H_{11}N_5O_3$	acyclovir [59277-89-3] [2]

Table 2.3 continued							
369	477.1721	1.71	$[M+H]^{+1}$	477.1713	-1.7	$C_{14}H_{33}N_6O_6PS_2$	[NA] [4]
388	375.1444	1.68	$[M+H]^{+1}$	375.1458	-3.7	$C_{13}H_{24}N_6O_3P_2$	[NA] [4]
393	184.0460	1.71	$[M+H]^{+1}$	184.0460	0.0	$C_5H_{13}NO_2S_2$	[NA] [4]
402	327.0680	1.80	$[M+H]^{+1}$	327.0675	1.5	$C_{12}H_{15}N_4O_3PS$	[NA] [4]
490	210.0439	0.91	$[M-H]^{-1}$	210.0442	-1.4	$C_6H_{13}NO_5S$	[NA] [4]
522	244.0651	0.95	$[M-H]^{-1}$	244.0649	0.8	$C_{10}H_{15}NO_4S$	[NA] [4]
532	162.0189	1.02	$[M-H]^{-1}$	162.0197	-4.9	$C_8H_5NO_3$	[NA] [4]
543	237.0630	1.12	$[M-H]^{-1}$	237.0629	0.4	$C_9H_{10}N_4O_4$	[NA] [4]
544	223.0392	1.13	$[M-H]^{-1}$	223.0394	-0.9	$C_6H_{12}N_2O_5S$	[NA] [4]
564	190.0365	1.30	$[M-H]^{-1}$	190.0370	-2.6	$C_7H_5N_5O_2$	[NA] [4]
596	157.9910	1.86	$[M-H]^{-1}$	157.9917	-4.4	$C_5H_5NO_3S$	[NA] [4]
603	236.0788	2.16	$[M-H]^{-1}$	236.0789	-0.4	$C_9H_{11}N_5O_3$	biopterin [22150-76-1] [2]
626	142.0501	3.14	$[M-H]^{-1}$	142.0510	-6.3	$C_6H_8NO_3$	[NA] [4]

Table 2.4: Detailed Tandem MS characteristics of the significant metabolites as determined by PCA. Fragment ions detected using a stepped normalized collision energy of 10, 30, and 50 eV are listed with selected precursor ions underlined. Ions in bold are those matched to standard spectra or literature spectra. Fragments were matched to standards, literature spectra, or were at least consistent with potential molecular structure fitting the following requirements for each confidence level: 1) elemental formula, retention time, and MS/MS spectrum of standard matched to feature; 2) MS/MS spectrum consistent with literature spectra and fragmentation ions observed consistent with proposed structure; 3) putative compound class based on chromatographic elution window; and 4) unknown compounds.

Feature ID	m/z of Fragment Ions Observed in MS/MS Experiments	Confidence Level	Match Details (Source)	Ionization method
19	146.1361, **146.1176**,146.0929, 129.1104, 87.1005, **87.0447**, 86.0970, 73.0485, 72.0451, 70.0740, **60.0817**, 58.0660	1	consistent with standard	
34	**162.1124**, 130.0863, 115.0630, **103.0395**, **102.0918**, 86.0970, **85.0291**, **75.0448,** 74.0973, 73.0893, 71.0292, 71.0136, 61.0293, **60.0816**, 59.0738, 59.0500, 58.0660, 57.0344, 56.0504	1	consistent with standard	positive
40	**76.0764**, **59.0738**, **58.0660**	2	consistent with spectrum (MzCloud)	positive
95	**218.1388**, **160.0971**, **159.0652**, **144.1021**, 99.0446, **85.0291**, **60.0817**	2	consistent with spectrum (MzCloud)	positive
98	144.1384, [*144.1020*], 139.0272, 98.0968, 98.0606, 85.0655, [*84.0815*], 67.0551, 60.0817, [*58.0660*], 57.0708, 57.0344	4	*[Interfering compound stachydrine]*	positive
166	141.0659, 138.8299, 107.9576, 100.5644, 97.8813, 97.0765, 81.7610, 76.9697, 76.6570, 75.4184, 65.6036, 57.2105, 54.8734	4		positive
172	**222.0987**, **205.0723**, **204.0881**, **177.0773**, 165.9701, **161.0821**, 159.0667, 138.2688, 132.0560, 130.4666, 119.0691, 115.9056, 110.0605, 109.4668, 84.5712, 76.5170, 71.3243, 68.9697, 59.6849, 51.8696	2	Consistent with in silico model (Mz Cloud)	positive
174	**377.1458**, **243.0878**, **172.0872**, 99.0447, **69.0342**, 57.0345	2	Consistent with in silico model (Mz Cloud)	positive
176	285.0983, 260.1032, 214.0977, 186.1028	4		positive
200	193.0357, 192.1597, 192.1380, **192.0516**, 188.9129, 185.0593, 174.1494, **149.0460**, **147.0302**, 98.0972, 66.0972, 66.7425, 56.4709	2	Consistent with in silico model (Mz Cloud)	positive
215	120.1022, 120.0559, 102.0918, 60.0816, 59.0739, 58.0660	4		positive
223	198.1599, 198.0795, 175.2923, 109.3497, 100.0763, 91.0548, 60.0817, 60.0800, 59.0739, 58.0660, 57.0345	4		positive
255	329.0811, 217.0625, 176.0353	4		positive
262	**238.0934**, **220.0826**, **194.0673**, **192.0883**, **178.0726**, **177.0649**	2	consistent with spectrum (MzCloud)	positive
307	144.1384, [*144.1020*], 139.0272, 98.0968, 98.0606, 85.0655, [*84.0815*], 97.0551, 60.0817, [*58.0660*], 57.0708, 57.0344	4	*[Interfering compound stachydrine]*	positive

Table 2.4 continued

348	226.1799, 226.1221, **226.0932**, 195.0751, **194.0674**, 180.1742, 166.0723, 163.1477, **141.0772**, 133.2471, 125.0459, **124.0508**, 114.5799, 101.9819, 99.5021, 95.0861, 91.0548, 81.0707, 72.1257, 50.4029	2	Consistent with in silico model (Mz Cloud)	positive
369	351.9716, 307.0989, 244.5152, 206.7861, 193.5730, 184.7968, 177.0741, 163.0505, 154.0533, 145.6610, 126.1556, 117.0741, 103.1398, 102.1094, 99.6238, 90.1905, 85.0477, 79.0730, 71.9434, 53.4041	4		positive
388	365.4666, 359.2511, 344.3310, 262.1635, 222.0987, 218.9116, 204.0881, 162.1907, 161.0811, 154.0533, 139.1276, 137.6107, 127.9275, 93.0815, 87.0389, 83.0149, 73.1141, 65.2577, 61.9992, 51.3429	4		positive
393	184.1700, 184.0462, 156.6481, 118.1686, 116.3248, 114.9496, 113.6535, 102.0919, 85.09197, 81.8920, 1.5119, 63.9509, 61.8697, 59.0739, 58.0661	4		positive
402	327.0679, 174.0221, 154.0533, 98.9847, 89.0603	4		positive
490	218.7906, 210.0431, 210.0318, 196.7856, 178.0362, 167.0561, 166.0166, 151.0248, 140.4884, 138.0258, 136.2590, 135.0299, 124.0060, 106.9794, 95.8013, 80.9637, 80.9298, 79.9558, 78.5550, 77.2331	4		negative
522	244.0649, 244.0280, 231.8818, 217.5685, 184.8859, 184.2925, 169.5757, 164.1073, 164.0709, 140.8959, 124.0067, 115.4720, 108.0207, 101.0348, 98.3682, 83.6366, 79.9562, 76.8413	4		negative
532	169.6786, 162.0297, 162.0184, 161.9124, 154.0088, 144.2172, 134.0234, 118.0285, 115.9194, 90.0335, 80.5210, 70.2573, 69.5410, 66.6257, 65.9971, 52.7061	4		negative
543	237.0630, 193.0363, 192.0280, 191.0204, 163.0255, 150.0299, 123.0192, 122.0350	4		negative
544	223.0390, 206.0124, 179.0172, 151.0220, 124.0063, 115.0503, 106.9798, 98.0236, 97.0396, 80.9639, 79.9561, 65.9972	4		negative
564	190.0364, 190.0146, 162.0185, 152.0880, 148.0141, 147.0302, 130.9299, 119.0353, 92.0242	4		negative
596	157.9907, 94.0285, 79.9560	4		negative
603	236.0958, **236.0786**, 225.2259, 205.8749, **192.0520**, 191.8226, 190.0365, 179.3277, 175.0134, 171.4098, **162.0415**, **147.0299**, 133.6492, **122.0348**, 107.5690, 79.9562, 66.1005, 62.6208, 56.3433, 53.4817	2	consistent with spectrum (MzCloud)	negative
626	159.06521, 142.0499, 142.0398, 99.9245, 60.0159	4		negative

Table 2.5: List of all compounds detected via UPLC-MS analysis. Molecular weight was determined using Compound Discoverer 2.1. The ionization polarity and retention time (RT) is listed for each compound.

Compound Number	Ionization Mode	Molecular Weight (g/mol)	RT (min)	Compound Number	Ionization Mode	Molecular Weight (g/mol)	RT (min)
1	positive	143.0945	3.83	**42**	positive	227.1884	0.87
2	positive	127.9463	4.37	**43**	positive	233.9105	4.35
3	positive	129.1518	3.20	**44**	positive	157.1467	3.65
4	positive	137.0475	3.41	**45**	positive	217.0408	1.17
5	positive	161.1050	4.26	**46**	positive	195.1007	3.41
6	positive	103.9854	4.37	**47**	positive	167.9388	4.37
7	positive	153.0458	1.70	**48**	positive	161.1050	3.88
8	positive	179.0945	4.53	**49**	positive	164.0436	3.42
9	positive	142.0742	4.00	**50**	positive	136.0385	1.72
10	positive	130.1107	4.65	**51**	positive	305.1740	1.93
11	positive	143.0945	4.31	**52**	positive	267.9911	4.37
12	positive	113.0843	4.72	**53**	positive	175.1208	3.93
13	positive	159.0894	3.77	**54**	positive	147.0895	3.70
14	positive	128.0587	3.93	**55**	positive	549.6216	3.01
15	positive	217.0408	1.25	**56**	positive	172.1325	4.49
16	positive	183.0565	2.35	**57**	positive	136.0385	1.63
17	positive	131.0947	3.81	**58**	positive	129.0904	5.10
18	positive	137.0475	3.81	**59**	positive	154.0742	4.29
19	positive	145.1102	4.54	**60**	positive	120.0577	1.24
20	positive	185.9881	4.36	**61**	positive	267.9911	4.31
21	positive	145.1102	4.26	**62**	positive	201.1477	3.83
22	positive	82.0538	3.22	**63**	positive	126.0431	3.65
23	positive	337.3341	0.87	**64**	positive	145.0115	4.36
24	positive	159.1259	4.62	**65**	positive	203.1158	4.13
25	positive	161.1050	3.70	**66**	positive	306.0917	1.66
26	positive	156.0899	4.09	**67**	positive	165.0790	4.55
27	positive	251.9211	4.38	**68**	positive	175.1208	4.45
28	positive	144.1263	4.57	**69**	positive	159.1259	3.66
29	positive	173.0146	1.88	**70**	positive	243.1833	1.55
30	positive	161.1050	4.16	**71**	positive	273.9030	4.36
31	positive	117.0792	3.91	**72**	positive	205.0374	1.79
32	positive	158.0691	3.90	**73**	positive	140.0585	3.76
33	positive	99.0689	4.59	**74**	positive	137.0475	3.56
34	positive	161.1050	4.13	**75**	positive	175.1208	4.15
35	positive	225.1727	0.87	**76**	positive	103.1002	4.67
36	positive	188.1161	4.00	**77**	positive	245.1627	3.89
37	positive	210.1618	0.88	**78**	positive	365.0749	2.27
38	positive	211.9286	4.38	**79**	positive	123.0356	2.12
39	positive	225.9805	4.37	**80**	positive	708.0654	0.92
40	positive	75.0692	4.43	**81**	positive	249.9418	4.37
41	positive	208.1461	0.87	**82**	positive	108.0326	3.65
83	positive	189.1000	3.94	**126**	positive	175.1209	4.34
84	positive	243.1833	0.87	**127**	positive	353.3291	0.88
85	positive	226.1566	0.87	**128**	positive	111.0436	2.62
86	positive	161.1417	5.43	**129**	positive	175.0279	1.69
87	positive	157.1103	3.81	**130**	positive	143.1311	4.82
88	positive	177.9975	3.90	**131**	positive	103.1002	2.36
89	positive	131.0947	4.33	**132**	positive	191.1158	4.15
90	positive	304.2959	3.34	**133**	positive	373.9556	4.38
91	positive	173.1053	4.06	**134**	positive	396.1686	1.07
92	positive	115.1001	4.68	**135**	positive	343.2208	1.55
93	positive	295.9110	4.37	**136**	positive	126.0908	4.98
94	positive	205.0375	0.95	**137**	positive	445.2890	1.42
95	positive	217.1315	4.04	**138**	positive	231.1472	3.96
96	positive	230.0360	0.92	**139**	positive	331.3239	3.32
97	positive	170.0725	1.70	**140**	positive	93.0584	3.41
98	positive	143.1312	5.45	**141**	positive	180.1513	0.87
99	positive	291.9524	4.37	**142**	positive	399.8961	4.37
100	positive	195.0566	2.77	**143**	positive	282.1680	1.42
101	positive	258.0674	1.12	**144**	positive	365.0749	1.88

Table 2.5 continued							
102	positive	190.1356	0.87	**145**	positive	115.1001	4.56
103	positive	150.1369	4.44	**146**	positive	213.1728	0.88
104	positive	205.0374	1.04	**147**	positive	187.1322	4.65
105	positive	143.9202	4.44	**148**	positive	219.1108	4.09
106	positive	293.9317	4.38	**149**	positive	387.2469	1.67
107	positive	217.0408	1.09	**150**	positive	205.0373	0.88
108	positive	211.0990	1.69	**151**	positive	367.0902	0.94
109	positive	120.0577	1.16	**152**	positive	401.8754	4.36
110	positive	227.1883	1.00	**153**	positive	240.1474	4.25
111	positive	714.0562	0.92	**154**	positive	225.1726	1.56
112	positive	315.9138	4.37	**155**	positive	125.0148	2.84
113	positive	161.1417	4.82	**156**	positive	194.1155	1.22
114	positive	712.0594	0.90	**157**	positive	238.1416	1.29
115	positive	401.2628	1.36	**158**	positive	96.0692	3.20
116	positive	317.8930	4.30	**159**	positive	260.1373	4.33
117	positive	159.0894	3.67	**160**	positive	349.9943	4.38
118	positive	159.0894	4.07	**161**	positive	369.3240	0.88
119	positive	339.8750	4.37	**162**	positive	355.9062	4.37
120	positive	209.9493	4.38	**163**	positive	357.2363	1.26
121	positive	379.8934	4.38	**164**	positive	443.0494	0.92
122	positive	263.1635	4.02	**165**	positive	140.1314	5.36
123	positive	111.0436	2.14	**166**	positive	225.0750	2.13
124	positive	159.0894	3.56	**167**	positive	205.0701	3.31
125	positive	375.9350	4.38	**168**	positive	189.0825	3.92
169	positive	217.1427	3.77	**212**	positive	115.1001	4.34
170	positive	331.9450	4.37	**213**	positive	172.0849	3.95
171	positive	221.0913	1.64	**214**	positive	119.0950	4.83
172	positive	129.0427	3.99	**215**	positive	197.0723	1.94
173	positive	376.1384	1.66	**216**	positive	288.0780	1.45
174	positive	219.1583	3.69	**217**	positive	189.0425	1.44
175	positive	284.0910	1.16	**218**	positive	431.2735	1.82
176	positive	173.1416	3.53	**219**	positive	337.0428	0.93
177	positive	423.8574	4.35	**220**	positive	119.0949	4.55
178	positive	232.1424	2.36	**221**	positive	193.0600	1.52
179	positive	114.0796	4.74	**222**	positive	197.0722	3.07
180	positive	351.3135	0.88	**223**	positive	138.0430	1.59
181	positive	187.1209	3.95	**224**	positive	377.9142	4.39
182	positive	215.1636	4.87	**225**	positive	274.1893	3.82
183	positive	463.8760	4.38	**226**	positive	475.2997	1.94
184	positive	363.2272	1.96	**227**	positive	431.9976	4.38
185	positive	197.1779	0.87	**228**	positive	163.0859	4.05
186	positive	157.0739	3.53	**229**	positive	143.9775	4.39
187	positive	119.0950	4.68	**230**	positive	253.9755	4.38
188	positive	165.0651	2.44	**231**	positive	276.1475	2.83
189	positive	183.0872	4.27	**232**	positive	334.2718	0.89
190	positive	169.1103	4.33	**233**	positive	199.1571	0.88
191	positive	496.0526	0.92	**234**	positive	159.0532	1.26
192	positive	299.1945	1.34	**235**	positive	151.0494	1.88
193	positive	299.1944	1.43	**236**	positive	297.1075	1.87
194	positive	313.2100	1.19	**237**	positive	192.1514	0.88
195	positive	183.1261	4.55	**238**	positive	367.0903	1.88
196	positive	379.8675	4.36	**239**	positive	171.1260	4.59
197	positive	207.1259	3.47	**240**	positive	194.9968	1.88
198	positive	489.3152	1.57	**241**	positive	200.0144	1.26
199	positive	191.0443	1.34	**242**	positive	113.0480	1.85
200	positive	131.0696	3.89	**243**	positive	286.1564	2.35
201	positive	288.0780	1.55	**244**	positive	155.0252	2.50
202	positive	157.1103	4.45	**245**	positive	78.0142	1.34
203	positive	137.0841	1.28	**246**	positive	150.0542	1.53
204	positive	367.0903	2.86	**247**	positive	224.0466	1.16
205	positive	82.0537	3.93	**248**	positive	131.1060	4.74
206	positive	457.9381	4.38	**249**	positive	167.0616	3.25
207	positive	245.9967	4.30	**250**	positive	189.1000	4.08
208	positive	191.0980	3.53	**251**	positive	246.1693	4.00
209	positive	201.1002	4.09	**252**	positive	157.1103	3.71
210	positive	203.1159	4.01	**253**	positive	479.9202	4.36
211	positive	256.1060	2.03	**254**	positive	328.0738	1.71
255	positive	166.0411	3.42	**298**	positive	154.0742	3.77
256	positive	455.9588	4.38	**299**	positive	78.0147	1.34

Table 2.5 continued							
257	positive	282.0965	1.55	**300**	positive	191.0018	1.71
258	positive	485.8580	4.35	**301**	positive	228.0747	3.49
259	positive	183.0565	1.94	**302**	positive	177.0557	3.73
260	positive	716.0534	0.92	**303**	positive	181.1103	4.36
261	positive	237.0864	2.19	**304**	positive	211.9650	4.40
262	positive	169.0409	2.50	**305**	positive	257.1013	2.15
263	positive	289.0843	1.71	**306**	positive	143.1311	4.45
264	positive	207.0201	1.17	**307**	positive	503.8813	4.38
265	positive	437.9095	4.37	**308**	positive	207.0167	1.04
266	positive	189.1477	3.81	**309**	positive	569.8402	4.37
267	positive	175.1321	3.91	**310**	positive	241.1097	2.36
268	positive	238.0702	1.12	**311**	positive	151.0633	3.87
269	positive	461.8965	4.37	**312**	positive	181.0601	1.97
270	positive	549.6216	0.91	**313**	positive	93.0585	4.85
271	positive	241.2039	0.88	**314**	positive	533.3417	1.67
272	positive	445.8394	4.37	**315**	positive	207.0930	4.14
273	positive	140.0585	3.51	**316**	positive	200.0621	4.10
274	positive	241.0408	1.26	**317**	positive	162.1407	0.88
275	positive	309.3029	0.88	**318**	positive	169.0599	1.13
276	positive	215.1520	0.88	**319**	positive	77.9492	4.45
277	positive	259.1324	2.22	**320**	positive	104.0354	4.37
278	positive	243.0165	3.50	**321**	positive	201.1479	4.60
279	positive	171.9725	4.39	**322**	positive	367.3085	0.88
280	positive	184.1213	4.55	**323**	positive	266.1993	3.42
281	positive	117.1157	4.51	**324**	positive	168.9786	2.86
282	positive	161.0688	3.58	**325**	positive	173.1165	4.13
283	positive	229.2407	3.36	**326**	positive	159.8942	4.46
284	positive	261.8807	3.59	**327**	positive	187.1209	4.14
285	positive	113.0593	2.78	**328**	positive	215.1521	1.85
286	positive	260.1737	3.80	**329**	positive	100.0723	4.60
287	positive	205.1427	3.70	**330**	positive	197.1165	4.33
288	positive	327.9998	4.32	**331**	positive	245.1012	3.48
289	positive	395.3246	0.89	**332**	positive	228.1476	4.18
290	positive	257.2719	3.37	**333**	positive	249.8846	4.44
291	positive	97.0646	4.52	**334**	positive	255.1682	1.30
292	positive	211.0957	3.60	**335**	positive	358.0834	1.77
293	positive	135.0545	2.32	**336**	positive	229.9693	2.77
294	positive	159.1259	4.44	**337**	positive	247.1533	3.94
295	positive	290.2455	0.88	**338**	positive	216.1224	4.04
296	positive	101.1209	0.90	**339**	positive	233.1740	3.93
297	positive	233.0326	2.65	**340**	positive	240.1143	1.70
341	positive	241.1676	0.87	**384**	positive	173.1053	4.23
342	positive	120.0326	1.60	**385**	positive	235.0479	0.94
343	positive	100.0642	4.48	**386**	positive	101.0846	4.53
344	positive	271.2145	0.87	**387**	positive	374.1371	1.68
345	positive	481.1201	1.71	**388**	positive	216.1112	4.03
346	positive	519.9126	4.38	**389**	positive	464.9191	3.50
347	positive	225.0861	1.68	**390**	positive	277.9367	4.38
348	positive	197.1414	0.89	**391**	positive	125.0591	3.12
349	positive	219.1583	3.88	**392**	positive	183.0387	1.71
350	positive	189.0425	0.95	**393**	positive	514.0009	4.38
351	positive	537.9620	4.38	**394**	positive	191.1308	0.89
352	positive	187.1209	3.73	**395**	positive	276.1685	3.77
353	positive	288.1797	3.32	**396**	positive	383.3034	0.88
354	positive	527.8425	4.37	**397**	positive	325.2979	0.89
355	positive	459.9172	4.38	**398**	positive	183.1261	4.41
356	positive	153.0651	2.31	**399**	positive	192.1264	3.61
357	positive	231.1108	1.46	**400**	positive	145.1102	3.71
358	positive	107.0410	3.74	**401**	positive	326.0606	1.80
359	positive	211.0705	1.24	**402**	positive	187.1209	4.45
360	positive	141.0792	4.03	**403**	positive	413.9482	4.36
361	positive	495.9512	4.37	**404**	positive	174.1006	4.14
362	positive	203.0985	4.15	**405**	positive	108.0942	0.88
363	positive	207.9313	4.42	**406**	positive	169.0409	1.77
364	positive	561.9231	4.38	**407**	positive	155.0329	0.96
365	positive	183.9128	4.44	**408**	positive	169.1465	0.87
366	positive	439.3509	0.89	**409**	positive	134.0402	4.26
367	positive	197.1414	1.86	**410**	positive	289.8771	4.44
368	positive	476.1646	1.71	**411**	positive	159.1007	4.10

Table 2.5 continued							
369	positive	208.1699	0.88	**412**	positive	454.2218	1.06
370	positive	507.8398	4.36	**413**	positive	200.0584	0.94
371	positive	199.1571	1.01	**414**	positive	167.0616	3.57
372	positive	174.1407	0.87	**415**	positive	149.0702	3.60
373	positive	253.2039	0.87	**416**	positive	198.0387	0.96
374	positive	216.1223	3.91	**417**	positive	381.0698	1.69
375	positive	179.0806	1.85	**418**	positive	122.0482	1.22
376	positive	229.1792	4.04	**419**	positive	265.1316	3.87
377	positive	183.1260	4.17	**420**	positive	181.0773	3.20
378	positive	214.0737	3.54	**421**	positive	146.0402	4.10
379	positive	213.1727	1.00	**422**	positive	209.1417	4.12
380	positive	200.1274	3.99	**423**	positive	151.0633	4.35
381	positive	461.8706	4.37	**424**	positive	201.1478	4.87
382	positive	483.8787	4.38	**425**	positive	163.1210	4.58
383	positive	255.2196	0.88	**426**	positive	215.1634	3.81
427	positive	265.9158	4.43	**470**	positive	283.9652	4.43
428	positive	156.0899	3.90	**471**	positive	146.1094	0.88
429	positive	93.0578	3.41	**472**	positive	189.1366	4.22
430	positive	186.1006	4.16	**473**	positive	201.9621	4.43
431	positive	155.0948	4.18	**474**	positive	130.0783	0.88
432	positive	439.3509	1.01	**475**	positive	120.0940	0.87
433	positive	230.1267	3.31	**476**	positive	280.1422	3.81
434	positive	323.2822	0.89	**477**	positive	245.0721	1.04
435	positive	342.2884	3.38	**478**	positive	211.1934	0.88
436	positive	119.9592	4.44	**479**	negative	243.0566	0.84
437	positive	99.0325	3.93	**480**	negative	259.0517	0.85
438	positive	483.3773	0.89	**481**	negative	243.1835	0.86
439	positive	571.1663	1.27	**482**	negative	373.3119	0.86
440	positive	179.0527	3.74	**483**	negative	93.9342	0.86
441	positive	223.0879	3.58	**484**	negative	405.3019	0.87
442	positive	118.0533	3.41	**485**	negative	437.2917	0.87
443	positive	117.0580	0.88	**486**	negative	421.2970	0.87
444	positive	331.8878	4.43	**487**	negative	320.2489	0.88
445	positive	174.0640	3.81	**488**	negative	367.0910	0.89
446	positive	90.0475	0.88	**489**	negative	143.9793	0.89
447	positive	171.1260	4.50	**490**	negative	211.0512	0.91
448	positive	231.1585	4.09	**491**	negative	198.0384	0.91
449	positive	205.1137	4.31	**492**	negative	125.9977	0.91
450	positive	241.9547	4.43	**493**	negative	118.0256	0.91
451	positive	154.0742	3.63	**494**	negative	197.0354	0.91
452	positive	202.0953	3.38	**495**	negative	265.0591	0.91
453	positive	197.0549	0.94	**496**	negative	129.0416	0.91
454	positive	140.1313	4.43	**497**	negative	225.0498	0.91
455	positive	217.1426	4.14	**498**	negative	167.0245	0.92
456	positive	300.2049	3.82	**499**	negative	217.9883	0.92
457	positive	252.0873	3.41	**500**	negative	230.0361	0.92
458	positive	224.1273	3.35	**501**	negative	183.0197	0.92
459	positive	274.1640	3.33	**502**	negative	232.0042	0.92
460	positive	217.1791	3.65	**503**	negative	224.0465	0.92
461	positive	134.1095	0.88	**504**	negative	156.0084	0.92
462	positive	219.1107	3.94	**505**	negative	189.0422	0.92
463	positive	120.0816	4.54	**506**	negative	161.0469	0.92
464	positive	106.0786	0.87	**507**	negative	184.0226	0.92
465	positive	248.1737	3.80	**508**	negative	284.9948	0.92
466	positive	194.0693	4.20	**509**	negative	131.8956	0.92
467	positive	144.1263	4.11	**510**	negative	260.0471	0.93
468	positive	179.0947	3.57	**511**	negative	216.0567	0.93
469	positive	148.1251	0.88	**512**	negative	205.0372	0.93
513	negative	180.0277	0.93	**556**	negative	137.0830	1.25
514	negative	197.0544	0.93	**557**	negative	470.0593	1.25
515	negative	235.0481	0.93	**558**	negative	456.0646	1.25
516	negative	367.0911	0.93	**559**	negative	158.0431	1.25
517	negative	140.0325	0.94	**560**	negative	302.0188	1.26
518	negative	183.0386	0.94	**561**	negative	115.0370	1.27
519	negative	120.9823	0.94	**562**	negative	155.0435	1.30
520	negative	168.0197	0.94	**563**	negative	122.0357	1.30
521	negative	93.9342	0.95	**564**	negative	191.0438	1.30
522	negative	245.0723	0.95	**565**	negative	197.0544	1.32
523	negative	138.8982	0.95	**566**	negative	189.0420	1.38

Table 2.5 continued							
524	negative	123.9820	0.97	**567**	negative	145.0518	1.38
525	negative	320.2489	1.00	**568**	negative	282.0968	1.46
526	negative	112.0150	1.00	**569**	negative	193.0595	1.50
527	negative	268.0733	1.01	**570**	negative	243.1835	1.51
528	negative	223.0115	1.02	**571**	negative	288.0784	1.54
529	negative	270.9825	1.02	**572**	negative	138.0420	1.54
530	negative	205.0372	1.02	**573**	negative	115.0259	1.55
531	negative	284.9948	1.02	**574**	negative	216.0397	1.57
532	negative	163.0262	1.02	**575**	negative	127.0082	1.57
533	negative	207.0165	1.03	**576**	negative	102.0306	1.62
534	negative	245.0723	1.03	**577**	negative	221.0911	1.65
535	negative	367.0912	1.04	**578**	negative	230.0326	1.66
536	negative	215.0652	1.04	**579**	negative	130.0256	1.67
537	negative	142.4961	1.04	**580**	negative	189.0221	1.67
538	negative	214.0241	1.06	**581**	negative	213.0668	1.67
539	negative	292.0719	1.06	**582**	negative	139.0293	1.69
540	negative	240.9979	1.07	**583**	negative	153.0455	1.69
541	negative	183.0386	1.07	**584**	negative	479.2386	1.69
542	negative	140.0325	1.07	**585**	negative	196.0513	1.69
543	negative	238.0702	1.12	**586**	negative	136.0375	1.73
544	negative	224.0465	1.13	**587**	negative	99.0309	1.73
545	negative	217.0406	1.15	**588**	negative	169.0401	1.73
546	negative	374.0624	1.16	**589**	negative	216.0566	1.75
547	negative	168.0197	1.18	**590**	negative	161.0469	1.75
548	negative	254.0575	1.20	**591**	negative	205.0372	1.76
549	negative	180.0277	1.20	**592**	negative	118.0619	1.81
550	negative	211.0702	1.20	**593**	negative	215.1519	1.83
551	negative	217.0405	1.22	**594**	negative	341.1512	1.84
552	negative	275.0000	1.23	**595**	negative	116.0464	1.85
553	negative	188.0540	1.23	**596**	negative	158.9982	1.86
554	negative	219.0363	1.24	**597**	negative	173.0140	1.86
555	negative	140.9909	1.25	**598**	negative	365.0756	1.88
599	negative	367.0912	1.90	**631**	negative	237.8909	3.48
600	negative	368.1702	1.91	**632**	negative	80.9634	3.48
601	negative	183.0559	1.93	**633**	negative	315.8721	3.48
602	negative	104.0462	2.14	**634**	negative	177.9235	3.48
603	negative	237.0860	2.16	**635**	negative	175.9440	3.48
604	negative	120.9824	2.22	**636**	negative	179.9572	3.48
605	negative	365.0756	2.24	**637**	negative	277.8497	3.48
606	negative	123.9820	2.24	**638**	negative	97.9662	3.48
607	negative	243.0777	2.34	**639**	negative	97.9671	3.48
608	negative	226.0622	2.34	**640**	negative	195.9341	3.48
609	negative	169.0402	2.34	**641**	negative	99.9703	3.48
610	negative	207.0892	2.36	**642**	negative	99.9619	3.49
611	negative	153.0451	2.38	**643**	negative	217.9164	3.49
612	negative	165.0643	2.43	**644**	negative	260.8469	3.49
613	negative	183.0559	2.47	**645**	negative	180.8892	3.49
614	negative	169.0402	2.50	**646**	negative	197.8921	3.51
615	negative	172.0729	2.53	**647**	negative	337.8666	3.51
616	negative	155.0244	2.55	**648**	negative	175.9440	3.57
617	negative	172.0729	2.63	**649**	negative	153.9928	3.61
618	negative	233.0324	2.65	**650**	negative	175.0475	3.62
619	negative	90.0306	2.67	**651**	negative	126.0420	3.65
620	negative	154.0023	2.68	**652**	negative	219.1106	3.77
621	negative	181.0403	2.76	**653**	negative	146.0683	3.81
622	negative	123.9820	2.77	**654**	negative	243.0470	3.90
623	negative	125.0137	2.83	**655**	negative	158.0684	3.90
624	negative	210.9561	2.84	**656**	negative	128.0576	3.92
625	negative	367.0911	2.85	**657**	negative	142.0733	3.99
626	negative	143.0574	3.14	**658**	negative	147.9723	6.15
627	negative	129.0416	3.21	**659**	negative	293.8445	8.46
628	negative	102.0306	3.23	**660**	negative	317.7868	8.59
629	negative	186.1364	3.30	**661**	negative	235.8272	8.70
630	negative	158.1048	3.38				

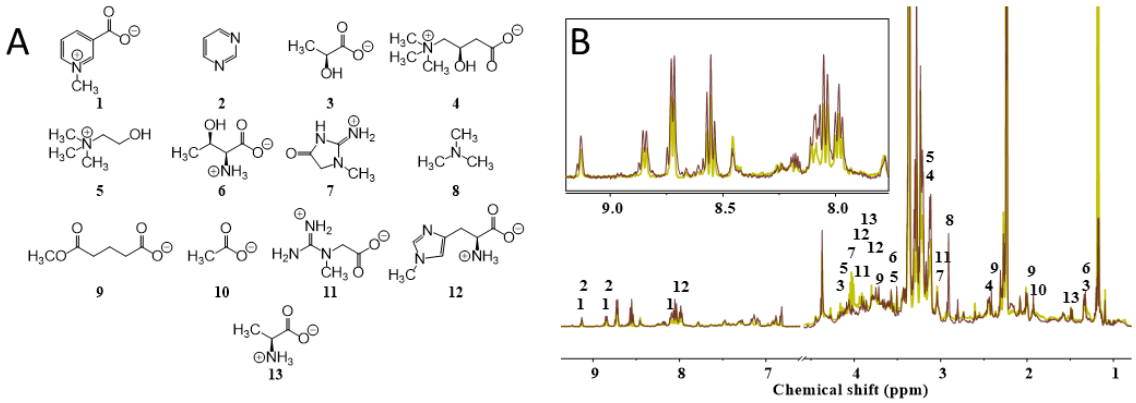

Figure 2.8: Blue crab diet affects concentration of specific urinary metabolites. (*A*) Compounds identified by ^{1}H NMR metabolomics PCA model that distinguish urine of blue crabs fed mud crab vs. oyster diets. Annotated metabolites consisted of: trigonelline (**1**); pyrimidine (**2**); lactate (**3**); carnitine (**4**); choline (**5**); threonine (**6**); creatinine (**7**); trimethylamine (**8**); methyl glutarate (**9**); acetate (**10**); creatine (**11**); *N*-methylhistidine (**12**); alanine (**13**). (*B*) Overlay of ^{1}H NMR spectra of urine from blue crabs fed mud crabs (brown) oyster (yellow) averaged across 12 urine samples for each diet. Peak intensity was normalized to an internal standard whose concentration was identical in all samples. Numbers above ^{1}H NMR signals in (B) refer to numbered compounds in (A). Only protons used to calculate concentration of metabolites are labeled. Inset is expansion of downfield region of overlaid ^{1}H NMR spectra.

shuttling, and choline metabolism (65) (Table 2.2, Table 2.3). Collectively, these data predicted that the fear-inducing cue in blue crab urine consists of relatively simple, primary metabolites that vary in concentration depending on diet.

A subset of metabolites account for fear-inducing properties of blue crab urine

To provide further evidence of the role of metabolites found in blue crab urine, we applied partial least squares regression (PLS-R) analysis to the ^{1}H NMR spectroscopic data to test for correlation between the measured potency of blue crab urine samples and the chemical variation among urine samples as revealed by PCA. A near-perfect linear fit was observed based on analysis of seven blue crab urine samples, four from blue crabs fed mud crabs and three from blue crabs fed oysters (Figure 2.9A). Upon inspection of the variable importance parameters (VIP, Figure 2.10A) and the PLS-R loadings (Figure 2.10B), trigonelline (**1**) was the only urinary metabolite identified by the PLS-R model that was also a critical component of the loadings via PCA (Table 2.2, Figure 2.10).

In addition to trigonelline being predicted as a constituent of the fear-inducing cue, the VIP and the loadings of the PLS-R model suggested that additional unidentified metabolites were constituents of the cue mixture. Inspection of the aromatic spectral region of the PLS-R loadings (Figure 2.10), coupled with total correlation spectroscopy (TOCSY) data (Figure 2.11), pointed to a second fear-inducing metabolite, differing from trigonelline only in the pattern of substituents around the aromatic ring. Homarine (**14**), a constitutional isomer of trigonelline, was isolated from blue crab urine, characterized by MS and NMR spectroscopy (Figure 2.11), and synthesized to confirm its molecular structure.

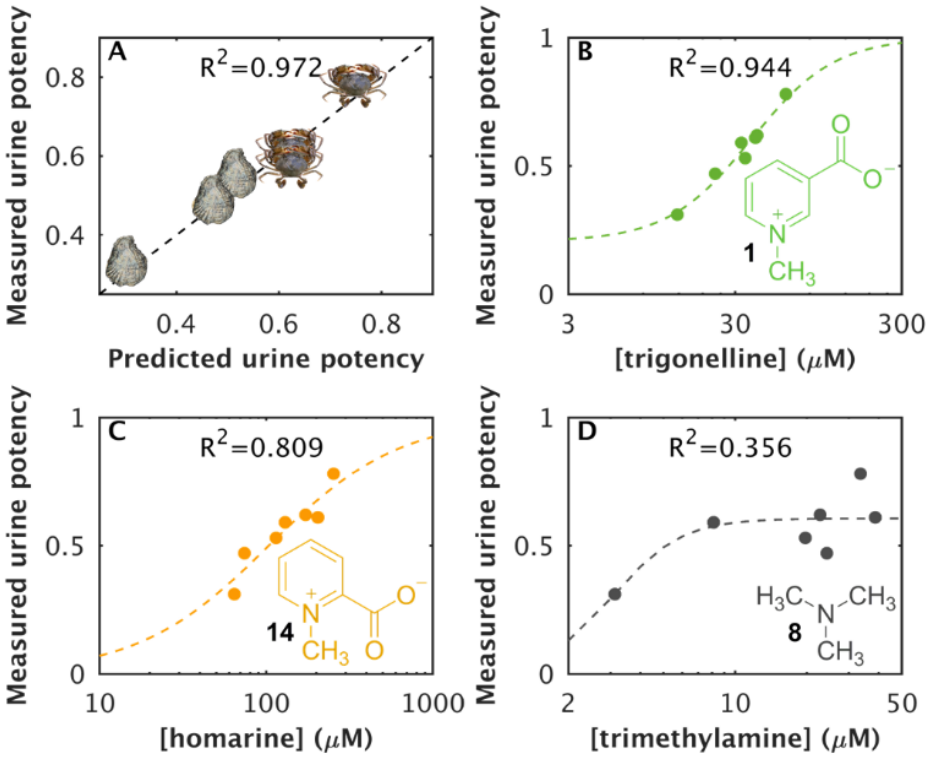

Figure 2.9: Partial least squares regression (PLS-R) model of ^{1}H NMR metabolomics data suggests that trigonelline (**1**) and homarine (**14**), but not trimethylamine (**8**) are components of the fear-inducing cue of blue crab urine. (*A*) PLS-R model highlights the linear relationship between the measured and model-predicted potency of fear-inducing behavior of blue crab urine. A potency value of 1 would indicate complete suppression of mud crab feeding in the presence of the urine sample whereas a potency value of zero represents no feeding suppression. Crab symbols represent data from urine from blue crabs fed mud crabs; oyster symbols represent data from urine from blue crabs fed oysters (N = 4 for urine from blue crabs fed mud crabs, N = 3 for urine from blue crabs fed oysters). Dashed lines represent sigmoidal curve fitted to experimental data using Matlab curve fitting toolbox with adjusted R^2 values for (*B*) Trigonelline (**1**), (*C*) homarine (**14**), and (*D*) trimethylamine (**8**) at the highest possible concentration, as indicated by square brackets around metabolite name (based on all protons resonating at 2.89 ppm belonging to trimethylamine and no other metabolites). N = 7 urine samples.

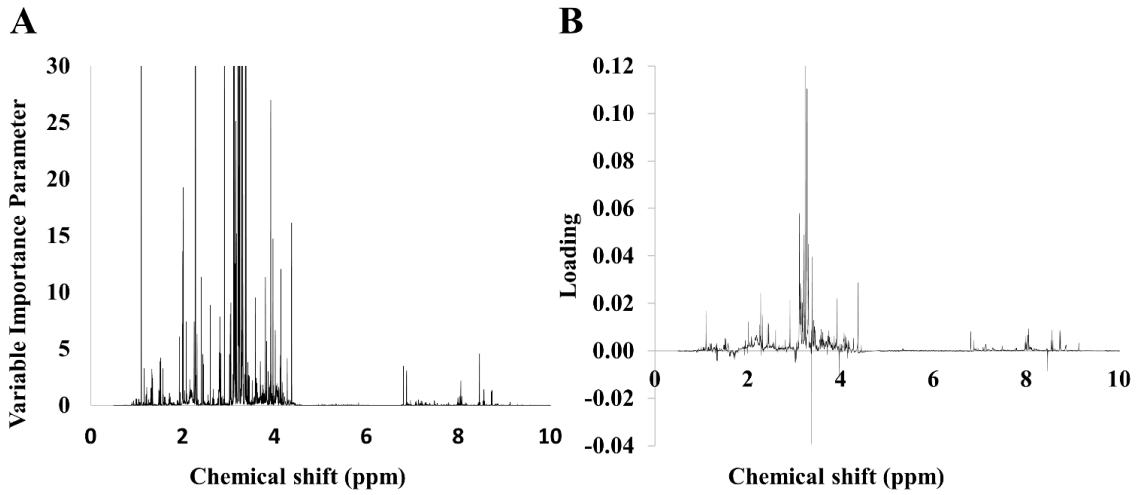

Figure 2.10: PLS-R models for ^{1}H NMR metabolomics highlight metabolites whose concentrations correlate with urine fear-inducing potency. (A) PLS-R variable importance parameters (VIP) and (B) loadings for ^{1}H NMR spectroscopic features in urine from blue crabs. All VIP scores above 30 were truncated to allow for visualization of spectroscopic features with smaller VIP scores.

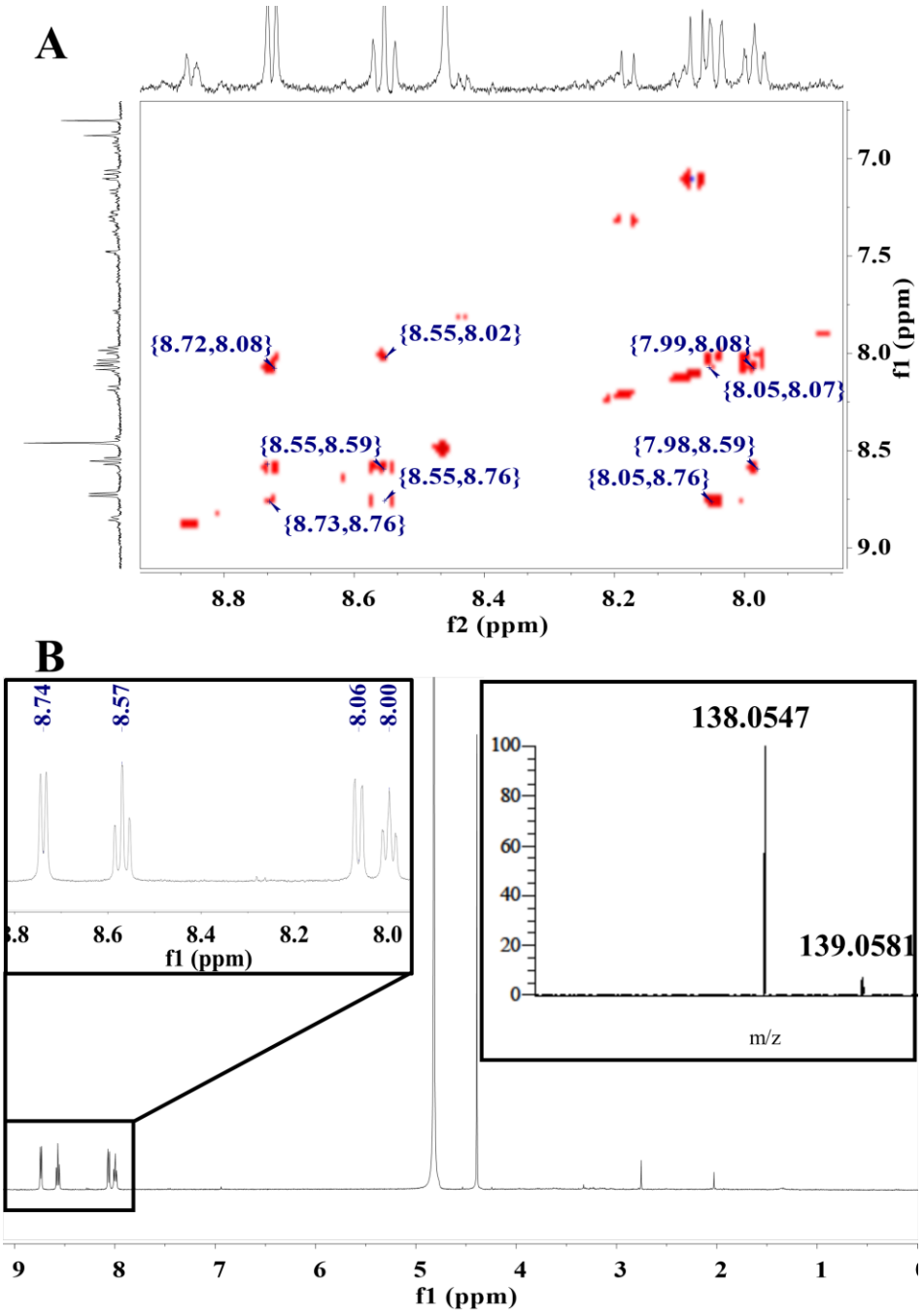

Figure 2.11: NMR spectroscopic and MS-based identification of homarine (**14**) in blue crab urine. A) Expanded total correlated spectroscopy (TOCSY) spectrum of blue crab urine, indicating annotated correlations consistent with data for synthetic **14**. B) ^{1}H NMR spectrum of **14** isolated from blue crab urine. Aromatic proton region is expanded and annotated with chemical shifts to show agreement between urine and isolated **14** (within 0.02 ppm for each signal). Inset shows high-resolution mass spectrum of **14** isolated from blue crab urine, corresponding to the molecular ion predicted for this compound.

The relationship between measured potency of blue crab urine and the measured concentrations of trigonelline and homarine indicated sigmoidal relationships for both, with greater fear-inducing potency for urine samples with greater concentrations of trigonelline and homarine, as expected (Figure 2.9). In contrast, the fear-inducing potency of urine poorly correlated with the concentration of trimethylamine. Although trimethylamine was identified by the PCA model as being significantly more concentrated in urine from blue crabs fed mud crabs vs. oysters (Table 2.2), it did not emerge from the PLS-R model as a likely candidate for the fear-inducing cue, and as such it acted as a further calibrant for our model. Overall, these findings led us to conclude that both trigonelline and homarine are likely constituents of the fear-inducing cue in blue crab urine but that trimethylamine is not.

Trigonelline and homarine induce fear in mud crabs

To explicitly test the functions of trigonelline and homarine as components of the fear-inducing cue in blue crab urine, mud crabs were exposed to each compound, alone and together, at concentrations found naturally in urine of blue crabs fed mud crabs (43 µM for trigonelline and 190 µM for homarine). Trigonelline (purchased commercially and analyzed spectroscopically to confirm its identity) and homarine (synthesized and characterized) suppressed foraging by 60% and 67%, respectively, when each compound was presented to mud crabs. Mud crabs reduced their feeding behavior by 65% when these two compounds were tested as a mixture, similar to the effect of blue crab urine itself (Figure 2.12).

In contrast, and as expected given the poor predictive relationship between trimethylamine (**8**) and urine (Figure 2.9D), trimethylamine did not significantly

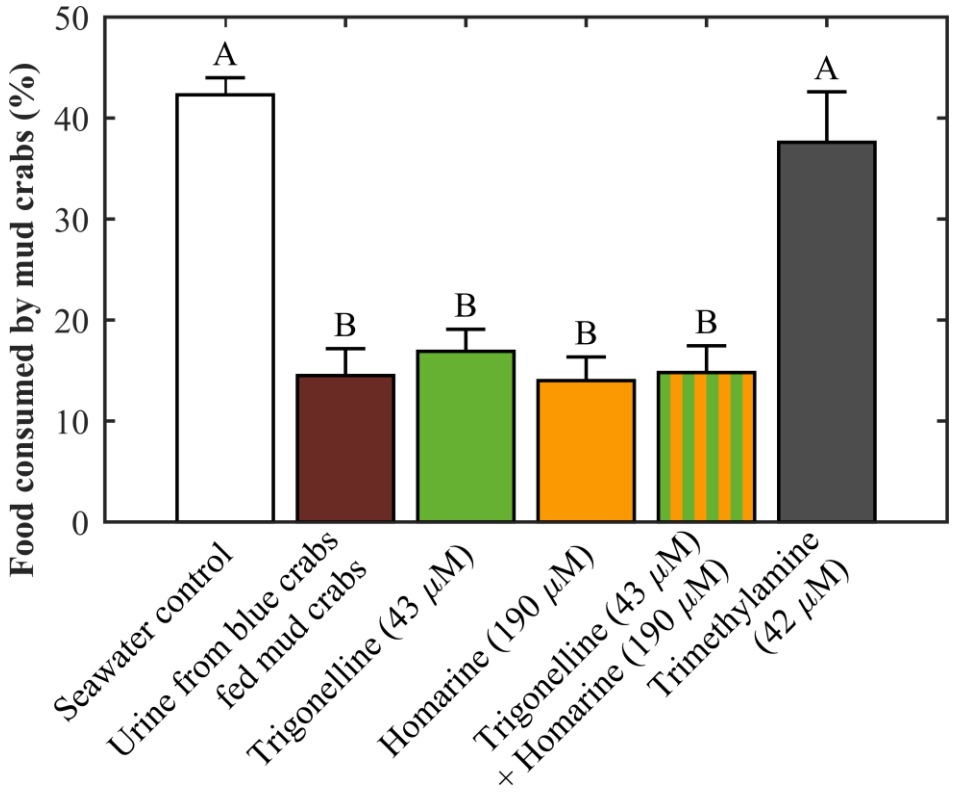

Figure 2.12: At natural concentrations found in blue crab urine, trigonelline (**1**) and homarine (**14**) but not trimethylamine induce fear, evidenced by reduced foraging among mud crabs. Urinary metabolites were formulated to match concentrations observed in blue crab urine (N = 10 for all treatments). Letters indicate significant grouping of treatments (one-way ANOVA with Tukey post-hoc test). Error bars represent ±1 SEM.

affect mud crab behavior (Figure 2.12). The exact concentration of trimethylamine in blue crab urine could not be determined by ^{1}H NMR spectroscopy due to spectral overlap and the non-diagnostic nature of the only unique proton signal associated with trimethylamine. The concentration (42 µM) used in the mud crab behavior assay was the highest possible concentration of trimethylamine (if all protons resonating at 2.89 ppm belonged to trimethylamine and not to other metabolites); yet no significant behavioral response indicative of fear was observed in mud crabs exposed to trimethylamine at this high concentration (Figure 2.12).

Although the PLS-R model predicted that additional unidentified blue crab urine metabolites are likely components of the cue mixture, trigonelline and homarine appear to be the major constituents of the fear-inducing cue. The suppressive effects that these compounds induced on mud crab behavior were statistically indistinguishable from the effects of blue crab urine itself (Figure 2.12), revealing that other compounds were not necessary to recapitulate the activity of whole urine.

To predict the source of the components of the fear-inducing cue, we quantified trigonelline, homarine, and trimethylamine in the flesh of each food source (mud crab, oyster, shrimp; Table 2.6). Trimethylamine and homarine were found in tissues of all three food sources whereas trigonelline was only detected in mud crab and shrimp tissues. The concentrations of all three metabolites were higher in mud crab tissue than other tissues, indicating that it's possible that blue crab urine derives at least a portion of these three metabolites directly from the diets of blue crabs. However, it is unlikely that all of the components of the fear-inducing cue come from blue crab food sources, since trigonelline is present the urine of blue crabs fed oyster but was not detected in oyster tissue.

Table 2.6: Quantification of trigonelline (**1**), trimethylamine (**8**), and homarine (**14**) in the tissue of blue crab dietary sources (N=3 for each diet).

	Metabolite concentration (µg/g tissue)		
Dietary source tissue	Trigonelline (**1**)	Trimethylamine (**8**)	Homarine (**14**)
Shrimp	9 ± 13	16 ± 11	14 ± 19
Oyster	< 0.1	52 ± 26	2 ± 1
Mud crab	19 ± 4	128 ± 112	41 ± 9

Trigonelline and homarine are constitutional isomers with different electron delocalization

The two critical components of the fear-inducing cue in blue crab urine have similar biological activities and appear nearly structurally identical; however, they have different electronic structures. Although each contains a methylated pyridinium ring and a carboxylate group, their connectivity of the ring to the carboxylate differs. Through molecular modeling, the attachment of the carboxylate to carbon three of the pyridinium ring of trigonelline allows for a greater delocalization of electron density, as evidenced by increased electron density around the carboxylate (Figure 2.13). In contrast, homarine does not exhibit such delocalization, since the carboxylate is rotated 64˚ relative to the ring preventing orbital overlap. When similar models were applied to related molecules picolinic acid (**15)** (the demethylated analog of homarine) and *o*-toluic acid (**16**) (the non-nitrogenous analog of homarine), the steric implications on torsional angle of the carboxylate relative to delocalization of electron density became apparent. For picolinic acid, the torsional angle between the carboxylate and the pyridinium ring is 0.0˚, allowing electron density from the aromatic system to be pulled towards the carboxylate (Figure 2.13). However, in *o*-toluic acid, the carboxylate rotates out of the plane of the ring with a torsional angle of 37˚ to decrease steric interactions with the bulkier methyl. This rotation prevents conjugation of the aromatic system with the carboxylate because the *p* orbitals of the carboxylate cannot sufficiently interact with those of the aromatic system, as evidenced by most of the electron density remaining around the aromatic system (Figure 2.13). Thus, connectivity of the carboxylate to the pyridinium ring at carbon 2 in homarine leads to steric interactions with the *N*-methyl, forcing the carboxylate to rotate out of the plane of

the ring, thus preventing further electron delocalization. While not directly tested, the differences in electronic structure could lead to differential interaction with a mud crab receptor, thus possibly explaining the similar levels of potency of trigonelline and homarine at different concentrations (Figure 2.12).

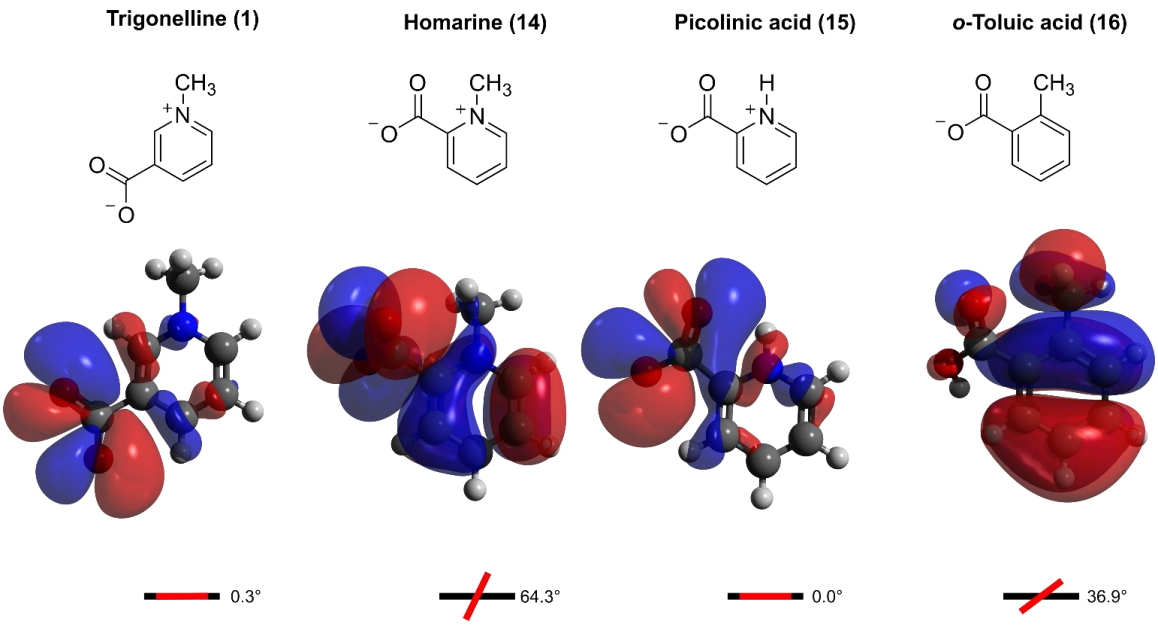

Figure 2.13: Electron delocalization is dependent on carboxylate position for trigonelline, homarine, picolinic acid, and toluic acid. Orbital representations (red and blue shapes, row two) are of the highest occupied molecular orbital (HOMO) for each molecule and were model using Gaussian ’09 and visualized with PyMol. The torsional angle between the pyridinium/aromatic ring (black line) and the carboxylate (red line) are shown in the bottom row.

Discussion

We identified the two major chemical components of a waterborne cue by leveraging the variable fear-inducing potencies of urine from blue crabs fed different diets, resulting in the conclusion that trigonelline and homarine strongly affect risk perception in prey (Figure 2.12). These cues, when released into seawater via the urine of blue crabs, allow mud crab prey to recognize the presence of a predator and adjust their behavior to avoid detection by that predator. The relative concentrations of these metabolites in predator urine reveals whether it has recently consumed mud crabs, which mud crabs then interpret as additional risk. Mud crabs subsequently respond with reduced foraging activity compared to when they are exposed to urine with lower concentrations of trigonelline and homarine (Figure 2.9). Although trigonelline and homarine, when tested alone or in combination, induced fear in prey crabs similarly to intact blue crab urine (Figure 2.12), these two metabolites are not the only components of the fear-inducing cue. Both ^{1}H NMR and MS metabolomics suggested multiple additional components. However, the lack of diagnostic protons with VIP scores greater than those of trigonelline and homarine (Figure 2.10A) and the stand-alone potencies of trigonelline and homarine (Figure 2.12) indicate that while additional metabolites are predicted to act as components of the fear-inducing cue, their importance is limited.

Waterborne cues for predator detection have been infrequently characterized

The current system represents one of the few waterborne cues that has been chemically identified, among those used for predator detection and risk perception by prey. Yet there is significant evidence that such cues are sensed widely in invertebrates (66, 67)

and vertebrates (68, 69). More importantly, the current study is one of the first in which non-consumptive effects of predators, mediated by waterborne predator chemistry, have been revealed at the molecular level. Non-consumptive effects on prey are increasingly predicted to be more important than consumptive effects (removal of prey through consumption) in systems with a top predator, intermediate predator, and basal resource, such as the current system (23). The potential for these interactions to broadly structure communities emphasizes the need to understand the chemical nature of the cues, which would provide insight into what confers cue specificity, and therefore how organisms may respond to in the presence of many cues with different degrees of salience or risk. Since prey in natural communities will be simultaneously exposed to many different cues, developing a framework to predict and understand the effects of multiple cues is essential if we are to progress beyond understanding prey response in single predator-prey pairs.

A rare case of chemically mediated non-consumptive effect in which the chemical cue has been identified involves the copepodamides, a class of taurine-containing polar lipids, released into seawater by copepods leading to an increase in toxicity in their dinoflagellate prey (17). A second example is that of the use of aliphatic sulfates and sulfamates by the freshwater green alga *Scenedesmus* to detect predatory *Daphnia pulex*, inducing colony formation in *Scenedesmus* as a defense mechanism (70). A significant contrast between these two identified cues is that the compounds involved, like many terrestrial cues, appear to be more specific to certain taxonomic groups than the fear-inducing metabolites identified in the current study, trigonelline and homarine; yet many may be waste products. The unavoidable exudation of waste compounds by predators may

therefore be important in many systems enabling prey to recognize predators, sometimes in species-specific or even diet-specific manners.

Trigonelline and homarine are common invertebrate signaling molecules

The two critical components of the fear-inducing cue in blue crab urine, trigonelline and homarine, are well documented in marine invertebrate tissues (71-77). Homarine and trigonelline, present in marine hydroid oocytes at approximately 25 nM and 8 nM respectively, prevent the metamorphosis of larvae to adults as well as limiting formation of the head and stolon in adults (78, 79). Homarine defends an Antarctic gastropod against its sea star predator, which flees from its prey when exposed to high concentrations of the compound (80). Homarine in gorgonian corals repels fouling by a surface-associated diatom (81). When nicotinic acid (the demethylated analog of homarine), picolinic acid (the demethylated analog of trigonelline), and pyridine (neither methylated nor possessing a carboxyl side chain as do trigonelline or homarine) were tested for their antifouling properties, the methylation state of the compound was found to be unimportant, whereas the presence of the carboxyl group at position two of the aromatic ring (as found in homarine) was crucial for the antifouling nature of the compounds (81). These last findings run counter to those of the current study in which trigonelline appears to be slightly more potent than homarine based on the similar fear-inducing effects at lower concentration (Figure 2.12). This suggests different molecular mechanisms of action for these molecules when involved in fear induction in prey compared with fouling deterrence. Additionally, trigonelline and homarine were found to act as waterborne cues in the current study whereas previously reported systems considered the roles of trigonelline and homarine as components in animal tissue, further contrasting the systems.

Trigonelline and homarine appear structurally similar, but differ in electronic properties and biosynthetic origins

The structural similarities of trigonelline and homarine prompted us to further examine the electronic properties of the related molecules. Density functional theory calculations revealed that electron density is differently delocalized in trigonelline and homarine based on the connectivity of the carboxyl group (Figure 2.13). If the fear response in prey is receptor-mediated as we would expect, then broader delocalization of electron density in trigonelline could enhance its interaction with a corresponding receptor in mud crabs, translating into a somewhat greater magnitude of behavioral response.

The multiple biological functions of trigonelline and homarine argue for seeking a better understanding of their biosynthetic origins. Although trigonelline and homarine appear to have very similar molecular structures, their biosynthetic origins differ in organisms for which this has been studied. Homarine biosynthesis in marine invertebrates is predominately known from isotope incorporation experiments of shrimp in which glycine and succinyl CoA form *N*-succinylglycine which, through a series of modifications, is transformed to homarine (82, 83). Tryptophan was not incorporated into homarine in feeding experiments and as such a hypothesized route to homarine through that amino acid was rejected (82); acetate was incorporated to form homarine through quinolinate (84). Although no study has investigated trigonelline biosynthesis in marine invertebrates, it is known that plants produce trigonelline from tryptophan and aspartate via quinolinic acid, which is converted to nicotinic acid and methylated to form trigonelline (85). Despite the incorporation of quinolinic acid into both trigonelline and homarine, the lack of tryptophan incorporation in homarine synthesis suggests that either trigonelline and homarine are

derived from divergent biosynthetic pathways in invertebrates or that invertebrates utilize multiple pathways towards the formation of quinolinic acid.

Metabolomics as a promising tool for chemical ecology

For decades, the principal platform for isolating biologically active compounds in chemical ecology research has been bioassay-guided fractionation. This approach has failed to facilitate the discovery of waterborne cues, despite the obvious importance of such cues in aquatic systems, due in part to the lack of sensitivity and resolution in analytical technologies used to elucidate the molecular structures of compounds accessible only in low quantities. In the current study, we avoided working with a low concentration cue by collecting the cue at its source (urine collection via catheterization) rather than concentrating compounds from seawater after release and dispersal of the cue. Additionally, bioassay-guided fractionation requires a destructive a bioassay after each separation step to pinpoint those fractions containing bioactive molecules in order to proceed to the next step of chemical separation. These separations can lead to loss of biological activity as multicomponent cues are separated into multiple fractions and as protectant molecules, such as antioxidants, are removed from mixtures containing bioactive molecules and degradation processes take over. With increasing NMR sensitivity, MS resolving power, and big data analysis tools, metabolomics has become a useful approach for chemical ecology and natural product discovery (18, 86). The complementary nature of MS metabolomics, which is highly sensitive and allows simultaneous analysis of many compounds, and NMR metabolomics, which is quantitative and can detect compounds with poor MS ionization properties, makes the combination of these two spectroscopic approaches desirable when the identities of relevant molecules are

completely unknown. The advantages of metabolomics for identifying waterborne cues will continue to increase as chemical libraries become more accessible and profiling technologies become more widespread.

Conclusions

A combined NMR-MS metabolomics approach led to the successful characterization of chemical cues in a complex behavioral interaction between predator and prey, in which prey recognize and respond to predators via exuded metabolites. By identifying the major components of this fear-inducing cue, we can now better address important questions about the impacts of non-consumptive effects by predators on prey, the ecological importance of these interactions on community structure, and the possible ubiquity of chemically mediated non-consumptive interactions in the marine environment. More generally, we posit that this study serves as a roadmap for further studies aimed at identifying and understanding the many diverse systems that ecologists hypothesize are mediated by waterborne cues but in which the chemistry is yet unknown. Despite noted examples where metabolomics has previously identified important cues, the cues were either not fully characterized, were terrestrial in origin, or were highly specific pheromones instead of more ubiquitous cues such as in the current study. Only with a more thorough understanding of the chemistry of these systems can we begin to address other important aspects, such as cue dispersal, dose-response relationships, structure-activity relationships, chemoreception and signal transduction, potential effects of climate change on cue longevity in the water column, and potential effects of anthropogenic pollutants in the water.

Ecologists have been long interested in the role of chemical compounds in mediating interactions among species. The natural variation inherent in these systems has often been seen as an inconvenience to be minimized or overcome in order to define the function of individual compounds. This approach misses the opportunity to leverage naturally occurring variation – whether it be in the behavior or chemistry of an organism, or both – towards understanding how chemistry shapes biology. Wherever a correlation between chemical composition and a biological outcome can be gleaned, hypotheses can be constructed to explicitly test the function of such chemistry. In the current study, the chemical fingerprint of blue crab urine was found to be diverse, both in terms of the identity of metabolites and their relative concentrations. Rather than ignoring or minimizing this variation (for example, by pooling urine samples into one large batch), we capitalized on this variation. The fact that urine chemistry could be manipulated by adjusting diet, with concomitant change to the potency of urine in inducing fear among prey, provided the opportunity to determine which urinary metabolites caused fear. The dose dependency of individual metabolites, acting together to enable prey to assess relative risk, confirms that such environmental cues do not act as an on/off switch, but rather produce a subtle range of biological outcomes predictable by compound concentration gradients. This is the great power of metabolomics in chemical ecology: to go beyond a false determination of "yes" (the organism responds) or "no" (the organism does not respond), towards making the most of existing variation and generating a deeper understanding of these responses at the chemical and biological level.

CHAPTER 3. POTENCY OF *KARENIA BREVIS* ALLELOPATHY IS HIGHLY VARIABLE AGAINST CO-OCCURING COMPETITORS (2)

3.1 Abstract

Harmful algae are known to utilize allelopathy, the release of compounds that inhibit competitors, as a form of interference competition. Competitor responses to allelopathy are species-specific and allelopathic potency of producing algae is variable. We mapped the biological variability in allelopathic potency to the underlying chemical variation in the exuded metabolomes of five genetic strains of the red tide dinoflagellate *Karenia brevis* using ^{1}H nuclear magnetic resonance (NMR) spectroscopy. The impacts of *K. brevis* allelopathy on growth of a model competitor, *Asterionellopsis glacialis,* ranged from strongly inhibitory to negligible to strongly stimulatory. *K. brevis* exuded unique metabolomes, visualized as chemical fingerprints, that suggested three distinct metabolic modalities – allelopathic, non-allelopathic, and stimulatory – with each modality distinguished from the others by different concentrations of several metabolites. Allelopathic *K. brevis* was characterized by enhanced concentrations of fatty acid-derived lipids and aromatic compounds, relative to less allelopathic *K. brevis*. These findings point to a previously untapped source of information in the study of allelopathy: the chemical variability of phytoplankton, which has been underutilized in the study of bloom dynamics and plankton chemical ecology.

3.2 Introduction

Allelopathy, or the release of compounds that inhibit competitors, is a form of interference competition that is well documented in terrestrial plants (87, 88), zooplankton (89), and phytoplankton (90, 91). Allelopathy is one of the proposed mechanisms hypothesized to affect harmful algal bloom (HAB) dynamics (29), although the role of allelopathy in the formation of HABs has been disputed (92). While some HAB-forming species produce potent toxins such as brevetoxins (30), domoic acid (31), and saxitoxins (32), none of these toxic compounds have also been identified as an allelopathic agent; one exception is the karlotoxins which have been shown to inhibit competitor growth and immobilize prey with effects depending on sterol composition of target species (93).

Typically, in allelopathy research, scientists have sought to identify allelopathic compounds by applying bioassay-guided fractionation to an extract of a potently allelopathic organism (38, 94, 95). This has left untapped potentially useful biological and chemical variability among samples, whether cultivated or field-collected, of an allelopathic species. Recent advances in metabolic profiling have led to the emergence of chemical fingerprinting as a tool for taxonomic analysis and authentication (96-98), disease diagnosis (99-101), and classification of multi-state systems, such as stressed vs. non-stressed organisms (37, 102). Within-species metabolic variability has also been leveraged to guide identification of mating pheromones in phytoplankton (16), virulence-regulating small molecules in worms (103), and enzymes responsible for the biosynthesis of nematode pheromones (104).

Karenia brevis, a HAB-forming dinoflagellate colloquially known as Florida red tide, produces a family of sodium channel blockers called brevotoxins which do not act as

allelopathic compounds (35, 38). *K. brevis* allelopathy, mediated by unknown compounds exuded by cells during blooms, is understood to negatively impact competing phytoplankton, especially diatoms such as *Amphora* sp., *Skeletonema grethae* (formerly *S. costatum), Thalassiosira* sp., and *Asterionellopsis glacialis* (35, 36). Competitor sensitivity to *K. brevis* allelopathy is variable among competitor species, with some species exhibiting resistance to allelopathic compounds and others suffering reduced growth rates, longer lag before the onset of exponential growth, membrane integrity loss, compromised photosynthesis, inhibited osmoregulation, and increased oxidative stress (36, 37, 105). Previous attempts to identify *K. brevis* compounds responsible for allelopathy have failed; however, chromatographic fractions containing allelopathic compounds exhibited spectroscopic features consistent with aromatic compounds and unsaturated hydrocarbons (38). Due to the substantial variability in allelopathy in this system, we hypothesized that variation in allelopathic potency is also reflected in the exuded metabolome of *K. brevis.* In the current study, nuclear magnetic resonance (NMR) spectroscopy-based comparative metabolomics was used to fingerprint *K. brevis*, correlating allelopathic potency with chemical variability of exuded metabolomes.

3.3 Materials and Methods

Phytoplankton culturing

Five strains of *Karenia brevis* were obtained from the National Center for Marine Algae and Microbiota (CCMP 2228, CCMP 2229, CCMP 2281) or Lisa Campbell at Texas A&M University (TxB3 and TxB4) and cultured in L1 growth media formulated with Instant Ocean at 35 ppt. The model diatom, *Asterionellopsis glacialis* (CCMP 137), a naturally co-occurring competitor known to be moderately vulnerable to *K. brevis*

allelopathy (35, 36), was cultured using the same conditions. Cultures were subjected to a 12:12 light:dark cycle, with irradiance 75-120 μmol m^{-2} s^{-1} at a temperature of 22 °C. Growth of *A. glacialis* was approximated using *in vivo* chlorophyll a fluorescence (Turner Biosystems Trilogy Fluorometer).

Allelopathy assay and generation of extracellular extracts

To determine allelopathic potencies of blocks of each of the five *K. brevis* strains, 12 biological replicates of each strain were cultured in full strength L1 media in paired flasks from the same inoculum: one large 1.8 L culture for the collection of exuded allelochemicals and a second, 250 mL flask that contained a co-culture with *A. glacialis* to assess allelopathic effects. Allelopathy assay flasks consisted of *K. brevis* grown in a 50 mL falcon tube cage (ends removed and capped with 1 μm nylon mesh) placed in a culture of *A. glacialis*. *A. glacialis* grown in dilute L1 medium (90% of typical sodium phosphate levels, 65% of typical nitrate levels, plus typical concentrations of vitamins, and trace metals) in the presence of the same cage acted as a control in the allelopathy assay, to mimic resource consumption by *K. brevis* which we found to deplete macronutrients as described above (37). To make the set-up manageable, the 12 replicate cultures of each strain were split into three block experiments that were performed sequentially, with each block containing four replicates of each strain. Thus, the experiment was designed to assess both strain and block variability in allelopathic compound production.

Growth of the *K. brevis* was monitored every other day (starting on the first day) using samples preserved with Lugol's solution and measured using a FlowCAM autoimager (Fluid Imaging Inc.; 100 μm flow cell, 0.4 mL min^{-1}, autoimage rate of 16

frames per second). *A. glacialis* cell concentrations in the allelopathy assay flasks were monitored daily via *in vivo* fluorescence. Growth was calculated via:

$$\%\ Growth = \frac{final\ fluorescence - initial\ fluorescence}{initial\ fluorescence} \times 100.$$

Strain and block effects of *K. brevis* allelopathy on percent growth of *A. glacialis* were analyzed using two-way analysis of variance (ANOVA) using PRISM version 10.0. Block effect on growth of *A. glacialis* controls were analyzed using one-way analysis of variance (ANOVA) using PRISM version 10.0.

Cultures were grown for 10 days by which time the *K. brevis* had reached mid-exponential growth phase, at which point hydrophobic resins (a 1:1 mixture of Diaion HP20 and Amberlite XAD-7) were added to *K. brevis* monocultures (1.8 L flasks) to extract compounds exuded by *K. brevis*, as described in Prince *et al.* (2008). Resins were incubated for 24 h, gently rinsed with filtered artificial seawater to remove *K. brevis* cells, and rinsed with deionized water to remove salts. Organic compounds were eluted from resins with LC-MS grade methanol and solvent was removed by rotary evaporation. The resulting extracts were triturated three times with ice-cold methanol to remove excess salts and dried again. Extracellular extracts were stored dry at -80 ˚C prior to spectroscopic analysis.

Allelopathic index calculation

To assign strain and block potency of *K. brevis* allelopathy, we used growth of the competitor *A. glacialis* when co-cultured with *K. brevis* as an inverse proxy for *K. brevis* allelopathic potency. More potent *K. brevis* cultures reduced growth of *A. glacialis* and as such we calculated our allelopathic index as:

$$Allelopathic\ index = (1 - \frac{avg\ \%\ growth\ of\ control\ for\ batch - \%\ growth\ of\ A.\ glacialis\ in\ flask}{avg\ \%\ growth\ of\ control\ for\ batch}) \times 100$$

Cultures of *K. brevis* with an allelopathic index within one standard deviation of the mean % growth (mean % growth = 114.7 % relative to *A. glacialis*-only control, standard deviation = 79.4 %) were deemed "non-allelopathic"; those greater than one standard deviation below the mean (% growth below than 35.2 % relative to *A. glacialis*-only control) were deemed "allelopathic"; and those greater than one standard deviation above the mean (% growth greater than 194.1 % relative to *A. glacialis*-only control) were deemed "stimulatory." This assignment allowed a preliminary basis for comparison among strains and blocks, in order to test whether concentrations of some exuded metabolites were associated with a category of allelopathic potency.

NMR spectroscopic data acquisition and processing

To explore the chemical constituents of *K. brevis* exuded metabolomes, extracellular extracts from the *K. brevis* monocultures were profiled using a conventional ^{1}H NMR pulse sequence (zg30) on a Bruker Avance 500 MHz DRX NMR spectrometer equipped with a 5 mm broadband direct detection probe. Extracellular extracts were re-suspended in 90% d_6-DMSO / 10% D_2O (99.9% atom Cambridge Isotope Labs) spiked with the internal standard 3-(trimethylsilyl)propionic-2,2,3,3-d_4 acid (TMSP), gently centrifuged (~2 min) to remove salts, and transferred to NMR tubes. To gather adequate signal, spectra were compiled from 256 scans and processed using NMRLab software (58) version 0.99.0.0 in Matlab version R2013a (8.1.0.604). Spectra were aligned to the chemical shift of 0.00 ppm using TMSP, manually phased, and baseline-corrected to allow for accurate integration of spectral features. Spectral regions corresponding to solvent signals and unoccupied regions were removed to simplify multivariate analysis (TMSP: -5.0 – 0.5 ppm, residual DMSO: 2.46 – 2.53 ppm, methanol: 2.94 – 3.27 ppm, water: 3.40

– 4.40 ppm, and unoccupied low field region: 8.5 – 15.0 ppm). Spectral features were binned into 0.005 ppm bins, filtered to reduce the impact of noise, probabilistic quotient-normalized (59) to remove the effects of differential dilution among samples, and generalized log (glog) transformed to raise sensitivity to low concentration metabolites within each sample with relatively low concentrations (60). Glog optimization was conducted using a set of five quality control extracts separately generated from a single batch of *K. brevis* culture, yielding $\lambda = 1.3879 \times 10^{-7}$.

Multivariate data analysis

To identify the relationship between variation in the exuded metabolome of *K. brevis* and allelopathic potency, a partial least squares regression (PLS-R) model was generated (MATLAB and PLS_Toolbox, version 8.1) using the chemical variation detected via ^{1}H NMR spectroscopy and the calculated allelopathic index for each culture. This multivariate regression approach was used to pinpoint chemical components whose concentrations correlated with allelopathy or whose presence was associated only with allelopathic blocks and strains. Cross-validation was completed using the Venetian blinds method with eight data splits.

To visualize chemical differences among the three metabolic modalities (allelopathic, non-allelopathic, and stimulatory) of *K. brevis* cultures, principal component analysis (PCA) and orthogonalized partial least squares discriminant analysis (OPLS-DA) models were generated (PLS_Toolbox version 8.1). Data were mean centered and cross-validated using Venetian blinds of eight data splits. The first principal component/latent variable was used to identify spectroscopic features differentiating exuded metabolomes of *K. brevis.*

3.4 Results & Discussion

K. brevis allelopathy is variable within and among strains

To exploit previously observed variability in allelopathic potency of *K. brevis*, we first confirmed that different *K. brevis* strains, and different batch cultures of individual strains, have different allelopathic effects on *A. glacialis* growth (Figure 3.1). Rather than invest significant statistical power in large numbers of replicates within a given strain, we chose to sample a smaller number of samples across five strains in three blocks, leading to high diversity in competitive outcome but low statistical power for any single treatment ($p>0.05$ for comparison of *A. glacialis* growth when exposed to each *K. brevis* strain within a block, compared to dilute media controls grown simultaneously). Despite the lack of significant strain effect, a significant block effect was observed ($p<0.0001$; no strain X block interaction, $p = 0.92$; no significant block effect observed for the growth of *A. glacialis*-only controls, $p = 0.15$), which, combined with variation among strains, led to chemically distinct exuded metabolomes (Figure 3.2, Figure 3.3, Figure 3.4). To our surprise, *K. brevis* stimulated the growth of *A. glacialis* in multiple co-cultures (Figure 3.1). Stimulation of growth of a competitor by *K. brevis* has previously been reported, but never to such an extent as observed here and not previously involving *A. glacialis* (105). The variability in allelopathic potency has also been observed in the field between *K. brevis* and another competitor, *Skeletonema grethae*, and is likely ubiquitous among co-occurring phytoplankton (36).

The observed variable response by *A. glacialis* to *K. brevis* exposure suggested three distinct exudate-based metabolic modalities of *K. brevis*: allelopathic,

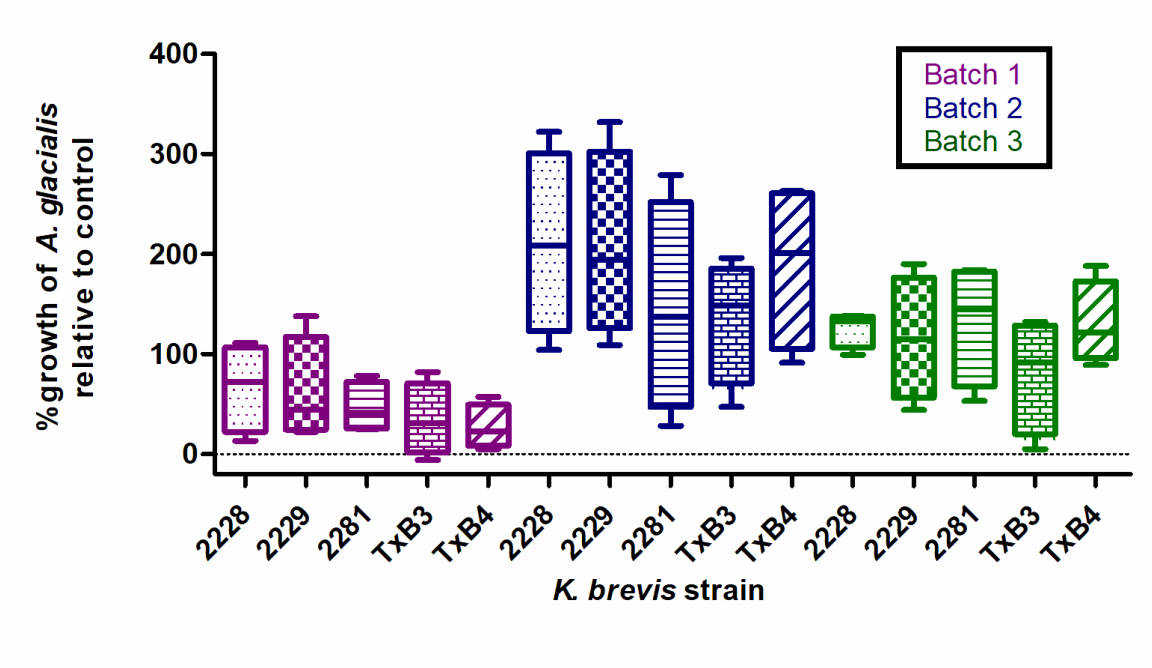

Figure 3.1: Effects of *Karenia brevis* allelopathy on *Asterionellopsis glacialis* are variable among and within block of *K. brevis* strains. *K. brevis* and *A. glacialis* were co-cultured for 10 days separated by a mesh barrier to prevent direct contact between species. Growth of *A. glacialis* was calculated using fluorescence as a proxy for cell concentration, normalized to controls for each strain within a block (N = 4 replicates per strain per block). *K. brevis* strains were CCMP 2228 (small dots), CCMP 2229 (large checkers), CCMP 2281 (horizontal lines), TxB3 (bricks), and TxB4 (diagonal lines). Purple represents *K. brevis* from block one, blue from block two, and green from block 3. A significant block effect existed ($p < 0.0001$ via two-way ANOVA). Boxes represent inter-quartile range of % growth for each strain with the upper edge representing the upper quartile and the bottom edge the lower quartile; the median % growth for each strain is the dividing line of the box. Whiskers represent the full range of % growth.

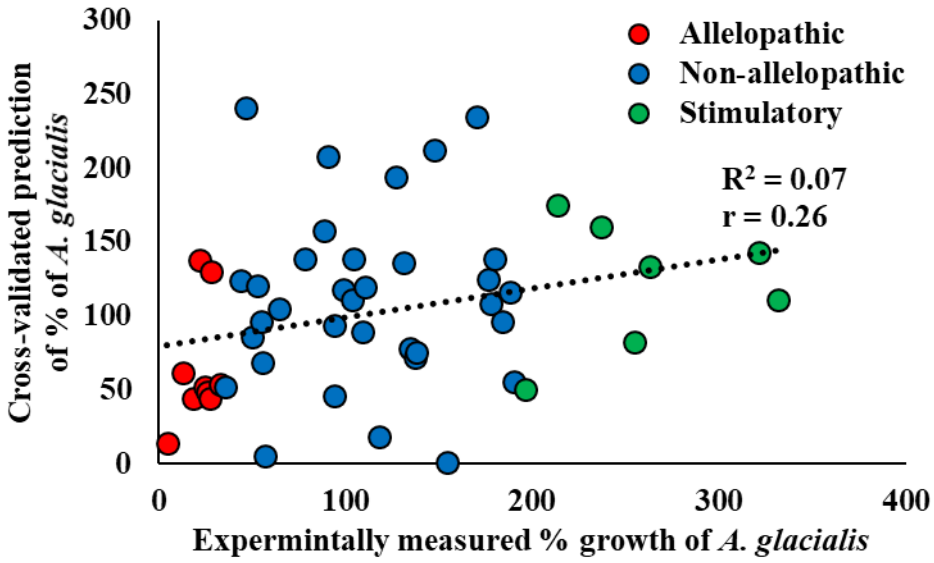

Figure 3.2: Potency of *K. brevis* allelopathy against *A. glacialis* weakly correlates with chemical variation of *K. brevis* exuded metabolome. PLS-R analysis was performed on growth data for *A. glacialis* exposed to allelopathic (red, N = 19), non-allelopathic (blue, N = 10) and stimulatory *K. brevis* (green, N = 21) belonging to five strains, cross-validated using Venetian blinds method.

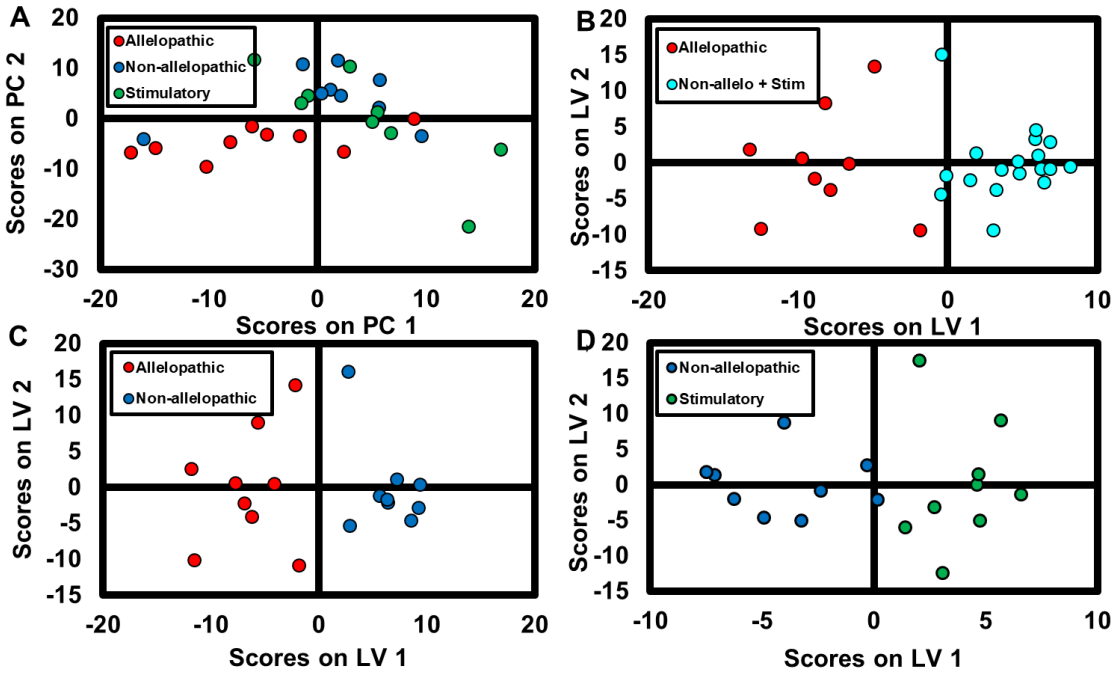

Figure 3.3: PCA and OPLS-DA discriminate among allelopathic effects of *K. brevis* against *A. glaclialis.* A) PCA of allelopathic exuded metabolomes (red) vs. non-allelopathic exuded metabolomes (blue) vs most stimulatory *K. brevis* exuded metabolomes (green). B) OPLS-DA of allelopathic exuded metabolomes (red) vs. combination of non-allelopathic exuded metabolomes and most stimulatory *K. brevis* exuded metabolomes (teal). C) OPLS-DA of allelopathic exuded metabolomes (red) vs non-allelopathic exuded metabolomes (blue) and D) non-allelopathic exuded metabolomes (blue) vs. most stimulatory *K. brevis* exuded metabolomes (green, N = 9 for each class in each model).

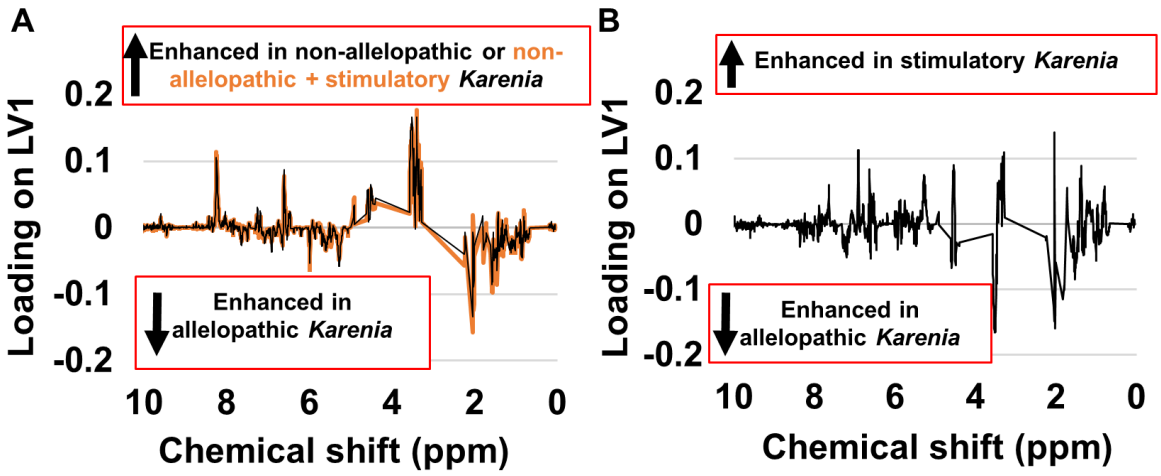

Figure 3.4: Chemical differences of *K. brevis* exuded metabolomes with differing allelopathic potencies, as detected by ^{1}H NMR spectroscopy. A) Overlay of loadings from OPLS-DA of allelopathic exuded metabolomes vs. combination of non-allelopathic exuded metabolomes and most stimulatory *K. brevis* exuded metabolomes (orange line, Figure 3B) and loadings from OPLS-DA of allelopathic exuded metabolomes vs non-allelopathic exuded metabolomes (black line, Figure 3C). B) Loadings from OPLS-DA of non-allelopathic exuded metabolomes vs exuded metabolomes of stimulatory *K. brevis* (Figure 3D). Negative loadings represent metabolites that are enhanced in allelopathic *K. brevis* while positive loadings represent metabolites that are enhanced non-allelopathic or stimulatory *K. brevis*.

non-allelopathic, and stimulatory. When compared across block experiments conducted at different times, no *K. brevis* strain was *always* or *never* allelopathic, despite identical culture conditions: all five *K. brevis* strains trended at different times towards being allelopathic, stimulatory, or neither allelopathic nor stimulatory towards *A. glacialis* in at least one block (Figure 3.1). While this classification of *K. brevis* into three modalities was somewhat arbitrary given that allelopathic potency measurements revealed an uninterrupted spectrum of effects without distinct cut-off between categories (Figure 3.1, Figure 3.2), it provided a useful framework for further exploration of chemical differences between groups of *K. brevis* blocks and strains.

Chemical variability in exuded metabolomes is captured in distinct fingerprints

Leveraging the variability in allelopathic potency among *K. brevis* strains and blocks, we utilized partial least squares regression (PLS-R) analysis to test for correlation between the measured potencies of *K. brevis* blocks and the chemical variation of their exuded metabolomes, as detected by ^{1}H nuclear magnetic resonance (NMR) spectroscopy. We detected a weakly positive correlation ($r = 0.26$) between allelopathic potency and chemical variation among cultures of five *K. brevis* strains (Figure 3.2). When a principal component analysis (PCA) model was generated to complement the regression analysis, a predominance of the exuded metabolomes of non-allelopathic and stimulatory *K. brevis* clustered together, suggesting chemical similarities (Figure 3.3A). An orthogonalized partial least squares discriminant analysis (OPLS-DA) model of allelopathic versus combined non-allelopathic and stimulatory *K. brevis* exuded metabolomes led to successful discrimination among classes (Figure 3.3B). Notably, the variation in chemical composition that discriminated allelopathic from non-allelopathic *K. brevis* (Figure 3.3C)

and that differentiating allelopathic from combined non-allelopathic/stimulatory *K. brevis* (Figure 3.3B) were approximately the same, qualitatively and quantitatively (Figure 3.3A, Figure 3.4A). This suggested that allelopathic *K. brevis* exudes molecules that are absent or exuded at significantly lower concentrations by non-allelopathic and stimulatory *K. brevis*. Furthermore, despite non-allelopathic and stimulatory *K. brevis* metabolomes exhibiting similar features when focusing on contrasts with allelopathic *K. brevis* (Figure 3.4A), OPLS-DA revealed distinct chemistry differentiating non-allelopathic and stimulatory *K. brevis* from each other (Figure 3.3D, Figure 3.4B). The chemical differences between non-allelopathic and stimulatory *K. brevis*, while not accounting for the majority of the observed chemical variation among all strains and blocks, likely confounded the original PLS-R analysis (Figure 3.2) that included all metabolic modalities of *K. brevis* (allelopathic, non-allelopathic, and stimulatory).

Similar to how chemical variation was leveraged in the current study, variation in biological responses to stressors have been used to classify phytoplankton. In Lake Washington, biological responses of 40 phytoplankton species to changes in over 25 environmental factors, such as nutrient chemistry, presence of herbivorous zooplantkton, and other physical variables, were found to cluster into six main modalities of responses to chemical and physical variables across taxa (106). Taxon-specific growth rates in response to each variable were compared to classify similar responses into two main categories, with four additional variations on a category.

Genetic variation has also been used to fingerprint phytoplankton. Inter simple sequence repeats markers were used to fingerprint and taxonomically differentiate among 12 phytoplankton species including members of the genera *Alexandrium*, *Pseudo-*

nitzschia, Skeletonema, and *Tetraselmis* (107). Variation in gene sequences encoding DNA polymerase B and the capsid protein *g23* of viruses from *Phycodnaviridae* and *Myoviridae,* two families of viruses that target phytoplankton and bacteria, were displayed as denaturing gradient gel electrophoresis fingerprints and used to identify family-based changes in genetic composition in response to productivity and hydrological conditions (108).

In addition to interspecies and inter-strain variability, cell to cell variability and intra-strain variability are possible sources of metabolic information. Despite identical culturing conditions in the current study, intra-strain variability was expansive, both physiologically (Figure 3.1, Figure 3.2) as well as chemically (Figure 3.3, Figure 3.4). While the underlying mechanism for this variability is unknown, it could serve as a potential source of untapped information and should be studied further.

Allelopathic *K. brevis* exudes aromatic compounds and lipids

Inspection of NMR spectroscopic data and loadings from the OPLS-DA model distinguishing allelopathic from non-allelopathic *K. brevis* suggested that allelopathic *K. brevis* exudes enhanced concentrations of aromatic compounds and lipids (Figure 3.4A, Figure 3.5). Unsaturated fatty acid-derived lipids are evident from ^{1}H NMR chemical shifts observed at 0.9, 1.2, 1.5, and 5.3 ppm in both the loadings (Figure 3.4A) and ^{1}H NMR spectrum of allelopathic *K. brevis* (Figure 3.5). Characteristic aromatic ^{1}H NMR chemical shifts 6.0-8.0 ppm trended in both positive and negative directions in the loadings (Figure 3.4A), indicating that some aromatic compounds were more abundant in allelopathic *Karenia,* represented by chemical shifts of 6.0, 6.7, 6.9, 7.2, 7.6, and 7.8 ppm, whereas other aromatic compounds were more abundant in less allelopathic and stimulatory *Karenia* (Figure 3.4A, Figure 3.5).

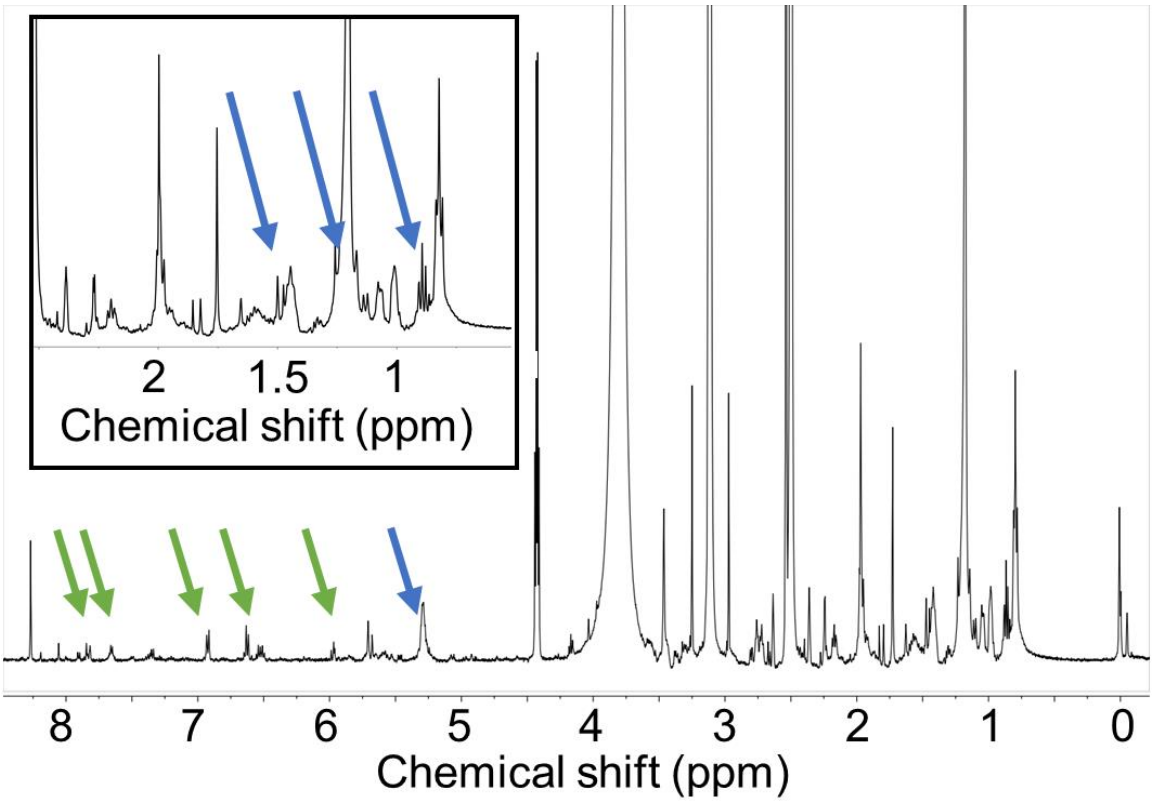

Figure 3.5: Fatty acid-derived lipids and aromatic metabolites are apparent, but not abundant, in exuded metabolomes of allelopathic *Karenia brevis*, as shown in ^{1}H NMR spectrum above. Inset is an expansion of the upfield region of the same ^{1}H NMR spectrum. Blue arrows highlight spectroscopic features indicative of fatty acid-derived lipids and green arrows spectroscopic features indicative of aromatic compounds associated with allelopathy.

Identification of individual lipid and aromatic molecules was not achieved in the current study. Because metabolomic analyses are conducted on complex mixtures without purification of individual compounds, full structure determination is challenging, requiring acquisition of additional data and, typically, access to a public database containing spectroscopic data of relevant metabolites. Metabolomics databases are becoming more useful for environmental studies such as this one, but still suffer from under-representation of rare metabolites; by definition, a previously unknown molecule cannot be expected to be described in an existing database. Karlotoxins, allelopathic polyhydroxy polyketides produced by the dinoflagellate *Karlodinium veneficum* (109, 110), would be expected to share some but not all spectroscopic features with the fatty acid-derived lipid resonances observed in the current study (Figure 3.5). It's also clear from the NMR signals associated with allelopathy (Figure 3.4A) that brevetoxins produced by *K. brevis* (including the strains used in the current study) are not responsible for allelopathy. In previous work conducted by bioassay-guided fractionation, unstable polar aromatic compounds and unsaturated fatty acids (and not brevetoxins) were detected in the active fraction of allelopathic agents of *K. brevis* (38), consistent with the findings of the current study (Figure 3.3C, Figure 3.4A). The findings of the current study can guide further investigation, NMR- and mass spectrometry-based, aimed at identifying individual allelopathic compounds exuded by *K. brevis* and other phytoplankton.

***K. brevis* exudes a variety of metabolites that stimulate competitor**

Inspection of the loadings from the OPLS-DA model distinguishing non-allelopathic from stimulatory *K. brevis* revealed multiple classes of molecules responsible for stimulation of its competitor (Figure 3.4B). Spectroscopic features characteristic of

aromatic compounds were observed trending in both positive and negative directions in the loadings (Figure 3.4B), suggesting that *K. brevis* produces some aromatic compounds that stimulate competitor growth whereas others have little effect. Signals typically associated with unsaturated fatty acid-derived lipids did not trend consistently in one direction or another, indicating their limited role in stimulation of competitor growth. Spectroscopic features characteristic of aromatic compounds exhibited on average loadings of greater intensity compared with features characteristic of other metabolites, which suggested that a variety of aromatic compounds likely contribute a majority of the stimulatory effect of *K. brevis* (Figure 3.4B).

3.5 Conclusions

Using a metabolomics approach, chemical variation in the exuded metabolome of the red tide dinoflagellate *K. brevis* was found to correlate, albeit weakly, with allelopathic potency against a co-occurring competitor, the diatom *A. glacialis*. Variability in *K. brevis* allelopathy was evident both within as well as among strains (Figure 3.1), allowing for the generation of clearly distinct exudate-based fingerprints (Figure 3.3). Multiple *K. brevis* cultures belonging to five genetic strains were classified as exhibiting three distinct metabolic modalities: allelopathic, non-allelopathic, and stimulatory; providing a framework for examining the chemical profiles of *K. brevis* of differing impacts on *A. glacialis* (Figure 3.2, Figure 3.3). More allelopathic *K. brevis cultures* were associated with enhanced exudation of unsaturated fatty acid-derived lipids and aromatic compounds, making these classes of molecules candidates for further investigation as allelopathic agents. The chemically encoded variability in allelopathic potency in this and possibly other plankton systems has likely complicated previous studies aimed at identifying

compounds responsible for allelopathy, including those studies that have sought to measure competitor responses to allelopathy and studies that have addressed the relative importance of allelopathy in the field. These complications could also affect our ability to understand the hypothesized role of allelopathy in bloom ecology. We suggest that further studies aimed at understanding mechanisms and targets of *K. brevis* allelopathy should address the intraspecific variability in allelopathic compound production.

CHAPTER 4. LIPIDOME AND MEMBRANE INTEGRITY OF COMPETITORS COMPROMISED BY *KARENIA BREVIS* ALLELOPATHY (3)

4.1 Abstract

The formation, propagation, and maintenance of harmful algal blooms is of interest due to their negative effects on marine life and human health. Some bloom-forming algae utilize allelopathy, the release of compounds that inhibit competitors, to exclude other species dependent on a common pool of limiting resources. Allelopathy is hypothesized to effect bloom dynamics and is well established in the red tide dinoflagellate *Karenia brevis*. *K. brevis* typically suppresses competitor growth rather than being acutely toxic to other algae. When we investigated the effects of allelopathy on two competitors, *Asterionellopsis glacialis* and *Thalassiosira pseudonana*, using nuclear magnetic resonance (NMR) spectroscopy and mass spectrometry (MS)-based metabolomics, we found that the lipidomes of both species were significantly altered. However, *A. glacialis* maintained a more robust metabolism in response to *K. brevis* allelopathy whereas *T. pseudonana* exhibited significant alterations in lipid synthesis, cell membrane integrity, and photosynthesis. Membrane-associated lipids were significantly suppressed for *T. pseudonana* exposed to allelopathy such that membranes of living cells became permeable. *K. brevis* allelopathy appears to target lipid biosynthesis affecting multiple physiological pathways suggesting that exuded compounds have the ability to significantly alter competitor physiology, giving *K. brevis* an edge over sensitive species.

4.2 Introduction

Harmful algal blooms, dense congregations of marine phytoplankton that often produce noxious compounds, can be toxic to human and marine life and are becoming increasingly more frequent (111). In addition to killing various marine mammals, potent algal toxins exuded by bloom-forming phytoplankton accumulate in predators and filter feeders, eventually entering the human food web through contaminated seafood such as clams, oysters, and fish (33, 34, 112-114). Toxins produced by some algae also persist in ambient waters, affecting human health through exposure to toxin-containing aerosols and cellular debris, leading to respiratory distress (113, 115-117).

Allelopathy, the release of compounds into the surrounding water that negatively affect competitors, is an important manifestation of competition that influences aquatic community structure (118). Allelopathy can significantly alter species composition (119, 120) and species succession (121, 122) through lethal interactions (122, 123), as well as sub-lethal outcomes such as reduced growth (124, 125), induction of cyst formation (126), and suppression of swimming behavior (127, 128). Little is known of the compounds responsible for allelopathy in the marine plankton or the molecular targets of allelopathy despite significant research (45). Typically, toxins produced by these phytoplankton have not been shown to be allelopathic, with the exception of karlotoxins produced by the dinoflagellate *Karlodinium veneficum* (129). A more thorough understanding of the modes of action of allelopathy and of the compounds responsible could enhance our understanding of the roles and ecosystem-wide impacts of allelopathy in algal blooms.

Karenia brevis, a dinoflagellate that blooms in the Gulf of Mexico and Southeastern Atlantic Ocean, produces a suite of neurotoxins called brevetoxins that cause neurotoxic shellfish poisoning in humans and marine life (130). Despite their toxicity, brevetoxins are not responsible for observed allelopathic effects of *K. brevis* on competitors (35, 38, 105). Instead, allelopathic compounds are yet uncharacterized fatty acid-derived lipids and aromatic molecules whose lack of stability has prevented complete characterization (38). Potency of *K. brevis* allelopathy varies among blooms, strains, and cultured blocks and its effects are selective towards certain competitor species in the early stages of growth (35, 36, 94). Reduced growth, membrane integrity, and photosynthetic efficiency have previously been reported for allelopathy-affected competitors; however, the molecular explanation for these physiological responses is yet poorly understood (36, 37). *K. brevis* is a particularly useful model for addressing the metabolic responses of competitors to allelopathy as the effects of *K. brevis* exposure are sub-lethal (35, 37, 94, 105). Metabolomics can provide a snapshot of alterations to the collection of small molecule metabolites in an organism during allelopathic stress, providing broad, system-level insights into possible mechanisms of action and causative agents of physiological responses.

Using proteomics as well as analysis of the polar metabolomes of two competing phytoplankton, *Asterionellopsis glacialis* and *Thalassiosira pseudonana*, we previously showed that energy metabolism, osmoregulation, photosynthesis, and fatty acid synthesis were all disrupted due to *K. brevis* allelopathy (37). Notably, various aspects of lipid metabolism appeared to be disrupted, with enhanced concentrations of enzymes associated with lipid anabolism, such as sulpholipid synthase and UDP-sulfoquinovose synthase, and

decreased concentrations of certain lipids, such as terpene glycosides, when *T. pseudonana* was exposed to allelopathy (37). This previous study, while providing significant insights into the molecular targets and metabolic pathways affected by allelopathy, was biased towards polar metabolites and therefore unable to fully describe the effect of allelopathy on competitor phytoplankton. The disruption of lipid metabolic enzymes and pathways has been shown to drive many human diseases and disorders, including diabetes, many forms of cancer, neurodegenerative disease, and infectious diseases (131, 132). Additionally, changes in lipid concentrations and the use of various lipids as signals is common in plants (133, 134), as well as in phytoplankton during stress (135, 136).

The previously observed complex response of lipid metabolism to allelopathy (37), coupled with the importance of the lipidome in regulating stress responses in many systems, led us to investigate the impacts of *K. brevis* allelopathy on the lipidome of competitors. Using nuclear magnetic resonance (NMR) spectroscopy and mass spectrometry (MS)-based metabolomics we identified the major metabolic effects of *K. brevis* allelopathy on the lipidomes of two competitors, one co-occurring with *K. brevis* during blooms and the other originating from non-bloom areas, in order to achieve a more complete understanding of the physiological responses and mode of action of allelopathy.

4.3 Materials and Methods

Generation and preparation of extracts for lipidomics

Lipids were accessed from intracellular phytoplankton extracts obtained for the experiment described by Poulson-Ellestad et al. (2014) (37). Briefly, diatoms *Thalassiosira pseudonana* strain CCMP 1335 and *Asterionellopsis glacialis* strain CCMP 137 were

grown in silicate-amended L1 media in artificial seawater (Instant Ocean, 35 ppt). *Karenia brevis* strain CCMP 2228 was cultured in similar conditions above with L1 media-amended artificial seawater. All cultures were maintained at 21 ˚C with a 12:12 light/dark cycle and an irradiance of 100-145 µmol/m^2s in a Percival incubator (Biospherical Instrument QSL2100). Diatom cell concentrations were quantified via *in vivo* fluorescence as a proxy for cell concentration or by visual counts under microscope. A Fluid Imaging Technologies FlowCam was used to determine *K. brevis* cell concentrations.

To expose competitors to allelopathic *K. brevis, K. brevis* was co-cultured with each of the two diatom species (n=14 per species). *K. brevis* was grown inside a permeable dialysis membrane to allow for exchange of exuded allelopathic compounds without direct interaction of *K. brevis* and diatom cells, which were grown in flasks in which the dialysis tubes were placed. Control cultures consisted of dialysis membranes (molecular weight cutoff, 50 kDa) filled with L1 media diluted to conditions similar to that of exponential growth phase *K. brevis* (n = 15 per diatom species) in place of diatom species. This co-culture experiment was halted once competitor cultures reached exponential growth stage, which was 6 d for *T. pseudonana* and 8 d for *A. glacialis,* after which diatom cells were filtered onto GF/C filters (Whatman #1922-110, muffled at 450 ˚C for 3 h) and dipped into liquid nitrogen to quench intracellular metabolism. Filtered cells were stored at -80 ˚C until extraction. Cells were ground with a liquid nitrogen-cooled mortar and pestle, and extracted with 30 mL of an ice-cold mixture of 3:1:2 methanol/acetone/acetonitrile. Particulate matter was removed via centrifugation (5 min at 0 ˚C, 1,460 x g) and the supernatant was removed. Cell pellets were rinsed twice with 10 mL of fresh solvent

mixture and a final 3 mL rinse. Rinses were added to the supernatant and solvent was removed *in vacuo*.

To separate polar and lipid intracellular metabolites, dried extracts were dissolved in a biphasic mixture of 9:10:15 water/methanol/chloroform. The more lipophilic layer was removed and washed twice with 9:10 water/methanol. Polar metabolites of diatoms undergoing stress from competition with *K. brevis* were previously reported by Poulson-Ellestad *et al. (*2014) (37). For the current work, the lipid-soluble chloroform-methanol fractions were analyzed by ^{1}H NMR spectroscopy and ultrahigh performance liquid chromatography mass spectrometry (UHPLC/MS) metabolomics.

NMR sample preparation and data acquisition

To compare equivalent metabolomes, each lipid extract was prepared from a total of 1.52 x 10^{6} *A. glacialis* cells or 2.56 x 10^{6} *T. pseudonana* cells. ^{1}H NMR spectra were collected for all samples on a Bruker Avance 500 MHz AVIIIHD NMR spectrometer equipped with a 5 mm broadband direct detection probe using an excitation-sculpting gradient pulse (37). Extracts were reconstituted in 250 µL d_6-DMSO (99.9% atom d_6-DMSO; Cambridge Isotope Labs) containing 0.1% trimethylsilane (TMS) as an internal standard in 3 mm NMR tubes. Spectra of each extract were compiled from 256 scans.

Spectra were preprocessed in NMRLab version 3.5.0.0 (58) in MATLAB R2013a version 8.1.0.604. TMS was used to align spectra at 0.00 ppm. All spectra were manually phased and baseline corrected prior to the spectral regions around TMS (-2.00 to 0.50), DMSO (2.35 to 2.70), water (3.30 to 3.50), and unoccupied downfield region (7.75 to 8.50) being removed in spectra of *A. glacialis* lipid extracts. The spectral regions around TMS (-

2.00 to 0.50), DMSO (2.45 to 2.57), water (3.14 to 3.19), a contaminant peak (4.00 to 4.20), and unoccupied downfield region (7.75 to 8.50) were removed in spectra of *T. pseudonana* lipid extracts. All spectra were binned (0.005 ppm), probabilistic quotient normalized (59) to correct for minute differential dilution among samples, and generalized log (glog) transformed to reduce bias toward higher concentration metabolites. A single batch of culture of each diatom species was used to generate a set of five quality control extracts using the above methods. Quality control samples were used to obtain glog optimized lambda values of 1.3093×10^{-8} for *A. glacialis* extracts and 8.4010×10^{-9} for *T. pseudonana* extracts.

Spectral features with discriminatory power in NMR-based models were annotated using the Human Metabolome Database and Chenomx Profiler. Pooled extracts of each species were used to collect 2D NMR spectral data including: correlation spectroscopy (COSY), heteronuclear single quantum coherence (HSQC), and heteronuclear multiple bond correlation spectroscopy (HMBC) to aid in annotation.

UHPLC/MS data collection

Lipid extracts were reconstituted in 200 μL 2-propanol. Quantitative metabolomics data were acquired using a Waters Xevo G2 QTOF mass spectrometer. The instrument was operated in negative electrospray ionization mode with a capillary voltage of -2.0 kV and a sampling cone voltage of 30 V. The source temperature of 90 °C was maintained throughout the experiment. Nitrogen was used as a desolvation gas at 250 °C with a flow rate of 600 L/h. The mass spectrometer was calibrated across the 50-1200 Da mass range using a sodium formate solution. Leucine Enkephalin was infused at a flow rate of 2

μL/min and acquired as a lockmass correction. Run order was randomized and samples were acquired in duplicate. Pooled quality control samples were acquired after every twelfth sample injection to monitor instrumental drift and minimize block effects.

Chromatographic separation was accomplished using a Waters Acquity UPLC quaternary solvent manager system fitted with a Waters ACQUITY UPLC BEH C18 column (1.7-μm particle size, 2.1 × 50 mm), with an injection volume of 10 μL. The column was operated at 60 °C, while the autosampler tray was maintained at 5 °C. Mobile phase A contained water: acetonitrile (40:60) and mobile phase B contained 10% acetonitrile in 2-propanol. A flow rate of 300 μL/min was used with the following gradient: 0-1 min, 70% B; 1-3 min, 75% B; 3-6 min, 80% B; 6-10 min, 90% B; 10-14 min, 100% B. Both mobile phases included 10 mM ammonium formate (Sigma Aldrich, >99.995%) and 0.1% formic acid (Fluka Analytical) additives to improve peak shape and ionization efficiency. All solvents used were of LCMS grade and provided by OmniSolv (water, acetonitrile) or Honeywell (2-propanol).

UHPLC/MS Data Processing

Data were imported into Progenesis QI for chromatographic alignment, de-isotoping, adduct deconvolution, normalization, and peak picking. Peaks detected in the sample blanks at greater than 10% of the average sample intensity were removed as potential contaminants. The corresponding normalized intensities across each sample for every feature (m/z, retention time pair) were imported into Matlab for multivariate analysis.

MS Metabolomics Statistical Analyses

PCA and oPLS-DA plots were constructed using PLS toolbox version 8.1 in Matlab. PCA plots are provided for both cell types to assess PCA scores of treatment vs. controls. PCA is an unsupervised analysis technique that reduces dimensionality in the data in order to visualize multivariate matrices in a linear space. It can be helpful in observing clustering patterns in the data without potential overfitting imposed by imparting class information.

For oPLSDA, plots were orthogonalized such that the maximum variance between classes is produced across the first latent variable (LV), with all other LVs explaining within class variance. Data were autoscaled and the model containing the fewest LVs that produced the lowest cross-validated error was selected. Venetian blinds cross validation was employed with six data splits for analysis of treatment/control effects of each cell type, while eight data splits were used when comparing all samples (n=61) including pooled quality controls. Significant peaks, defined as $p<0.05/n$ (number of features, n = 322 for *A. glacialis,* n = 360 for *T. pseudonana*) were identified using a 2-tailed t-test with unequal variance following Bonferroni correction for multiple comparisons. To normalize the significance cutoff for both competitor species at $\alpha = 0.05$ (Figure 4.3), p-values were adjusted by multiplying p-values by n instead of dividing α by n.

MS Metabolite Annotation

Tandem MS experiments were performed on Thermo Q-Exactive HF quadrupole-Orbitrap mass spectrometer using the top 10 Data Dependent Analysis (DDA) method to select and fragment all ions of interest with resolution=30,000, automatic gain control

(AGC) = 1e5, max injection time (IT) = 30 ms, and a stepped normalized collision energy (NCE) ranging from 10 to 50.

All features with significant differences between control and treatment groups for either cell type were analyzed by MS/MS to elucidate structure. Following adduct analysis, elemental formulae were determined based on exact mass and isotopic distribution. Features with exact masses corresponding to matches in the LOBSTAHS database were tentatively identified, with identities confirmed by matching headgroup fragments and fatty acid chains from the MS/MS spectra to tentative identities (137). For those features without LOBSTAHS matches, identifications were performed by hand using known lipid fragmentation patterns and cross-checked against other the KEGG, Metlin and LIPID MAPS databases (138-140).

Membrane permeability assay

To detect differences in membrane permeability between *T. pseudonana* grown in the presence vs. absence of *K. brevis*, 250 mL media bottle containing L1 media were inoculated with *T. pseudonana* to a concentration of ~1.0 x 10^4 cells mL^{-1}. Cages made of 50 mL falcon tubes with 1 μm mesh bottoms containing 25 mL of either media (control) or *K. brevis* (~1.0 x 10^4 cells mL^{-1}) (treatment) were added to the *T. pseudonana* cultures. Cultures were rearranged daily and cages were gently moved up and down twice per day to maximize exposure of *T. pseudonana* to the allelopathic compounds of *K. brevis*. After five days, two 500 μL samples of *T. pseudonana* were removed from experimental flasks. The first sample was preserved with an acidified Lugol's solution for measurement of total cell concentration. The second sample was stained with 20 μL Neutral Red solution (0.05%

w:v in deionized water, Mallinckrodt Chemical) and 10 μL SYTOX Green solution (50 μM in DMSO, Invitrogen Molecular Probes, detected with excitation at 504 nm and emission at 523 nm), to test for live and permeable cells, respectively. Stained *T. pseudonana* cells were counted using fluorescence microscopy on an Olympus IX-50 inverted microscope with a Palmer-Maloney settling chamber to determine the ratio of living cells with permeable membranes (red and fluorescent green) compared to the total number of living cells (red but not fluorescent green). T-test of unequal variances were conducted using Prism graphpad version 4.0.

4.4 Results

Allelopathy affects the lipidomes of competing phytoplankton

In the current study, *K. brevis* allelopathy significantly affected the lipidomes of both competitor species *T. pseudonana* and *A. glacialis* (Figure 4.1), even more dramatically than was observed for polar metabolites (37). When we employed a multi-platform metabolomics approach combining NMR spectroscopy and MS, algae exposed to *K. brevis* allelopathy were distinguished from algae grown alone based on chemical dissimilarities in their lipidomes (Figure 4.1). Orthogonal partial least squares discriminant analysis (oPLS-DA) identified a subset of spectral features corresponding to putatively identified metabolites that differentiated algae exposed to *K. brevis* allelopathy from controls. The concentration of any individual molecule alone could not comprehensively describe the differences in plankton lipidomes, but when combined as part of a discriminating panel they accurately differentiated the treatment effects of exposure to *K. brevis* allelopathy. Principal component analysis (PCA) models were also generated;

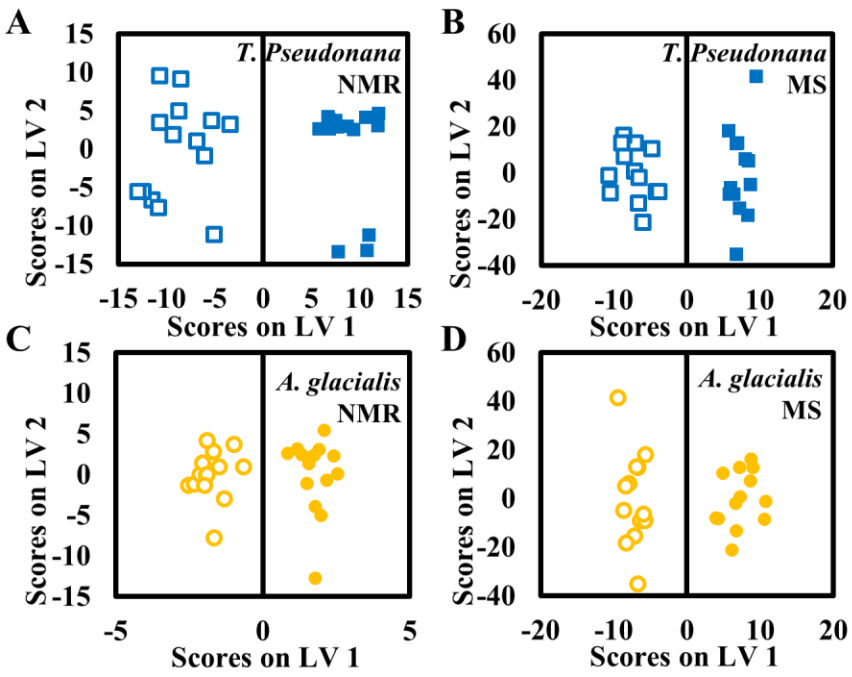

Figure 4.1: oPLS-DA models reveal that lipidomes of *Thalassiosira pseudonana* and *Asterionellopsis glacialis* are disrupted by *Karenia brevis* allelopathy. Filled symbols represent lipidomes of algae exposed to *K. brevis* through molecule-permeable but cell impermeable membranes, empty symbols represent lipidomes from unexposed algae (controls). oPLS-DA model generated from (*A*) ^{1}H NMR spectral data and (*B*) from UHPLC-MS metabolic features from lipidomes of *T. pseudonana* (blue squares). oPLS-DA model generated from (*C*) ^{1}H NMR spectral data and (*D*) from UHPLC/MS metabolic features from lipidomes of *A. glacialis* (yellow circles).

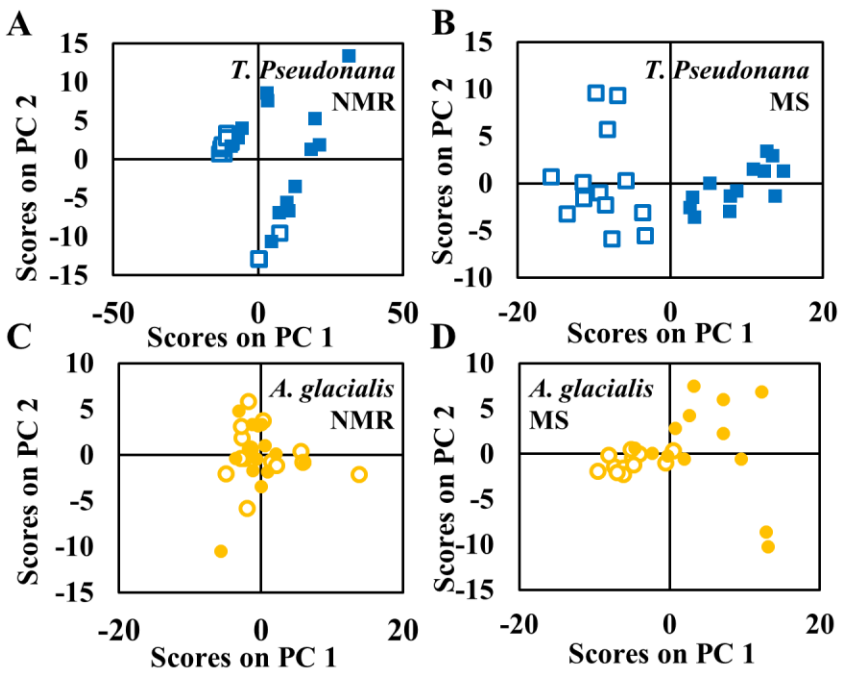

Figure 4.2: PCA models fail to fully differentiate between cellular extracts of *Thalassiosira pseudonana* and *Asterionellopsis glacialis* exposed or not exposed to *Karenia brevis* allelopathy. Filled symbols represent lipidomes of algae exposed to *K. brevis* through molecule-permeable but cell impermeable membranes, empty symbols represent lipidomes from unexposed algae (controls). oPLS-DA model generated from (*A*) ^{1}H NMR spectral data and (*B*) from UHPLC/MS metabolic features from extracts of *T. pseudonana* (blue squares). oPLS-DA model generated from (*C*) ^{1}H NMR spectral data and (*D*) from UHPLC/MS metabolic features from extracts of *A. glacialis* (yellow circles).

however, the discriminating power of most of these models was insufficient to identify algae based on their exposure to *K. brevis* allelopathy (Figure 4.2). Despite this lack of discriminatory power, PCA of *T. pseudonana* metabolome profiles obtained via ultra-high performance liquid chromatography mass spectrometry (UHPLC-MS) accurately classified algae as having been exposed or unexposed to *K. brevis* (Figure 4.2B). However, the rest of these PCA scores plots thus suggested the need for supervised multivariate classification tools to describe differences in the lipidomes, as well as to determine which variables or features were most critical in distinguishing between exposed and unexposed algae. Because MS is significantly more sensitive than NMR spectroscopy and therefore allowed detection of differences in lower abundance metabolite concentrations, the ability of the MS-based PCA model to successfully differentiate between *T. pseudonana* exposed or not exposed to *K. brevis* was not surprising, and consistent with previous findings (37).

Metabolic responses to allelopathy are conserved among competitors, despite differential sensitivities

MS-based metabolomics analysis of lipidomes led to identification of 80 lipid metabolites whose concentrations differed significantly in *T. pseudonana* depending on exposure to *K. brevis* allelopathy (Table 4.1, Table 4.2). Of these metabolites, 33 were significantly more abundant whereas 47 were significantly less abundant when *T. pseudonana* experienced *K. brevis* allelopathy (Figure 4.3), with many of the metabolites exhibiting considerable fold differences due to *K. brevis* exposure (Table 4.3, Figure 4.3). These 80

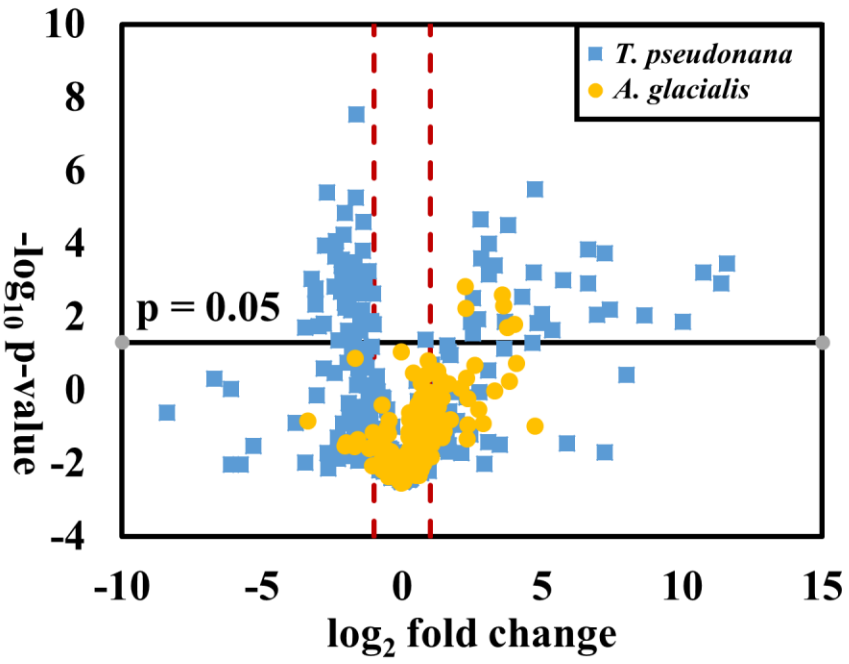

Figure 4.3: Volcano plot summarizes the differences in the lipdome of *T. pseudonana* (blue squares) and *A. glacialis* (yellow circles) when exposed vs. not exposed to *K. brevis* allelopathy. The relative abundances of 80 metabolites were significantly different ($p < 0.05$ after Bonferroni correction, see materials and methods – Section 3.3) in *T. pseudonana* upon exposure to *K. brevis* allelopathy. Red lines indicate $\log_2$ fold difference of ±1. Six metabolites with concentrations that were significantly different in *A. glacialis* when exposed to *K. brevis* were also significantly different in concentration when *T. pseudonana* was exposed to *K. brevis.*

Table 4.1: Identification of metabolites via MS metabolomics analysis whose concentrations were significantly different when *T. pseudonana* was exposed to *K. brevis* vs. controls. Observed *m/z* and parts-per-million mass error (PPM), adduct, elemental formula, and molecular composition (full fatty acid chain information) are provided where possible. Fold change values are shown as positive when relative abundance of metabolite increased when *T. pseduaona* was exposed to allelopathy and negative when abundances decreased. Annotation confidence ranges from 1-3. Confidence level 1: observed MS/MS data consistent with predicted spectrum and LOBSTAHS exact mass match to corresponding lipid class; 2: observed MS/MS data consistent with predicted spectrum; 3: observed exact mass match to LOBSTAHS database and/or partial MS/MS structural determination (137).

* Fold change value uncertain due to extremely low concentration of metabolites in control samples

***m/z* error (PPM)**	**Adduct**	**Elemental formula**	**Identity**	**Fold change**	**p value**	**Conf.**	**Lipid Class**
563.3986 0.71	$[M-H]^-$	$C_{30}H_{60}O_7S$	Tetradecanoyl sulfohexadecanoic acid	>25*	2.39E-05	2	Other (sulfur containing)
577.4146 1.39	$[M-H]^-$	$C_{31}H_{62}O_7S$	Pentadecenoyl sulfohexadecanoic acid	>25*	3.83E-06	2	Other (sulfur containing)
591.4308 2.20	$[M-H]^-$	$C_{32}H_{64}SO_7$	Pentadecenoyl sulfoheptadecanoic acid	>25*	1.88E-06	2	Other (sulfur containing)
379.2148 7.12	$[M-H]^-$	$C_{21}H_{32}O_6$	FFA(21:5 + 4 O)	>25*	4.25E-5	3	Free fatty acid
607.4243 1.81	$[M-H]^-$	$C_{32}H_{64}O_8S$	Hydroxypentadecanoyl sulfoheptadecanoic acid	>25*	2.77E-5	2	Other (sulfur containing)
619.4249 0.81	$[M-H]^-$	$C_{33}H_{64}SO_8$	Hydroxypentadecanoyl sulfooctadecenoic acid	>25*	1.96E-05	2	Other (sulfur containing)
572.4354 0.87	$[M-H]^-$	$C_{32}H_{63}NO_5S$	Hydroxyhexadecyl sulfohexadecenamide	>25*	5.77E-07	2	Other (sulfur containing)
367.2127 1.63	$[M-H]^-$	$C_{20}H_{32}O_6$	FFA(20:4 + 4 O)	>25*	2.75E-05	3	Free fatty acid
575.4356 1.91	$[M-H]^-$	$C_{32}H_{64}O_6S$	Pentadecenoyl sulfohexadecenoic acid	>25*	4.38E-07	2	Other (sulfur containing)
592.4942 0.17	$[M-H]^-$	$C_{36}H_{67}NO_5$	Heptadecenoyl octadecanamide	>25*	3.82E-06	2	Fatty acid amide
665.5117 3.31	$[M-H]^-$	$C_{35}H_{74}N_2O_7S$	Not – identified	>25*	3.04E-06	2	Other (sulfur containing)
257.2125 3.11	$[M-H]^-$	$C_{15}H_{30}O_3$	FFA(15:0 + 1 O)	>25*	7.05E-05	3	Free fatty acid
616.4615 0.65	$[M-H]^-$	$C_{34}H_{67}NO_6S$	Pentadecenoyl sulfononadecenamide	>25*	1E-08	2	Other (sulfur containing)
561.4194 0.89	$[M-H]^-$	$C_{31}H_{62}O_6S$	Tetradecanoyl sulfohexadecenoic acid	>25*	1.9E-06	2	Other (sulfur containing)
787.5583 0.76	$[M+HCOO]^-$	$C_{42}H_{78}O_{10}$	MGDG(33:1)	20.	8.84E-06	3	Mono-galactosyl diacylglycerol
574.4516 1.91	$[M-H]^-$	$C_{32}H_{65}NO_5S$	Hydroxyhexadecyl sulfohexadecanamide	14	9.71E-08	2	Other (sulfur containing)
578.4790 1.04	$[M-H]^-$	$C_{35}H_{65}NO_5$	Hexadecenoyl octadecanamide	8.5	2.14E-06	2	Fatty acid amide
564.4639 1.95	$[M-H]^-$	$C_{34}H_{63}NO_5$	Pentadecenoyl octadecanamide	7.1	7.94E-07	2	Fatty acid amide
566.4792 1.41	$[M-H]^-$	$C_{34}H_{65}NO_5$	Pentadecenoyl octadecanamide	7.0	6.79E-08	2	Fatty acid amide
686.4778 1.75	$[M-H]^-$	$C_{37}H_{70}NO_8P$	PE(16:1_16:1)	6.5	3.54E-05	1	Phosphatidyl-ethanolamine
550.4480 1.64	$[M-H]^-$	$C_{33}H_{61}NO_5$	Pentadecenoyl heptadecenamide	5.8	9.45E-06	2	Fatty acid amide

Table 4.1 continued

682.5090 1.47	$[M-H]^-$	$C_{39}H_{73}NO_6S$	Octadecenoyl sulfoheneicosadienamide	5.5	4.23E-05	2	Other (sulfur containing)
651.4958 3.68	$[M-H]^-$	$C_{34}H_{72}N_2O_7S$	Not – identified	3.3	3.48E-04	2	Other (sulfur containing)
793.5113 3.53	$[M-H]^-$	$C_{41}H_{78}O_{12}S$	SQDG(16:0_16:0)	-2.0	5.05E-05	1	Sulfo-quinovosyl-diacylglycerol
763.4646 1.83	$[M+HCOO]^-$	$C_{41}H_{66}O_{10}$	MGDG(16:3_16:3)	-2.1	4.05E-05	1	Mono-galactosyl-diacylglycerol
791.4988 0.38	$[M-H]^-$	$C_{41}H_{76}O_{12}S$	SQDG(16:0_16:1)	-2.2	4.52E-05	1	Sulfo-quinovosyl-diacylglycerol
771.5272 1.04	$[M+HCOO]^-$	$C_{41}H_{74}O_{10}$	MGDG(16:1_16:1)	-2.5	2.6E-06	1	Mono-galactosyl-diacylglycerol
719.4879 1.39	$[M-H]^-$	$C_{38}H_{73}O_{10}P$	PG(16:0_16:1)	-2.6	4.89E-07	1	Phosphatidyl-glycerol
737.4527 1.63	$[M-H]^-$	$C_{37}H_{70}O_{12}S$	SQDG(14:0_14:0)	-2.6	7.99E-08	1	Sulfo-quinovosyl-diacylglycerol
779.4988 0.38	$[M-H]^-$	$C_{40}H_{76}O_{12}S$	SQDG(15:0_16:0)	-2.6	7.16E-06	1	Sulfo-quinovosyl-diacylglycerol
813.4798 3.07	$[M-H]^-$	$C_{43}H_{74}O_{12}S$	SQDG(16:0_18:4)	-2.7	1.79E-06	1	Sulfo-quinovosyl-diacylglycerol
765.4723 1.44	$[M-H]^-$	$C_{42}H_{71}O_{10}P$	PG(16:1_20:5)	-2.8	2.33E-02	1	Phosphatidyl-glycerol
769.5111 0.39	$[M+HCOO]^-$	$C_{41}H_{72}O_{10}$	MGDG(16:0_16:3)	-2.8	1.30E-03	1	Mono-galactosyl-diacylglycerol
977.5477 0.20	$[M+HCOO]^-$	$C_{51}H_{80}O_{15}$	DGDG(16:3_20:5)	-2.8	1.07E-02	1	Digalactosyl-diacylglycerol
759.4368 1.19	$[M-H]^-$	$C_{39}H_{68}O_{12}S$	SQDG(14:0_16:3)	-2.9	1.42E-02	1	Sulfo-quinovosyl-diacylglycerol
751.4681 1.20	$[M-H]^-$	$C_{38}H_{72}O_{12}S$	SQDG(14:0_15:0)	-3.1	2.93E-08	1	Sulfo-quinovosyl-diacylglycerol
765.4796 3.53	$[M-H]^-$	$C_{39}H_{74}O_{12}S$	SQDG(14:0_16:0)	-3.2	1.69E-08	1	Sulfo-quinovosyl-diacylglycerol
691.4565 1.30	$[M-H]^-$	$C_{36}H_{69}O_{10}P$	PG(14:0_16:1)	-3.2	9.85E-07	1	Phosphatidyl-glycerol
819.5268 0.49	$[M+HCOO]^-$	$C_{45}H_{74}O_{10}$	MGDG(16:1_20:5)	-3.3	9.7E-05	1	Mono-galactosyl-diacylglycerol
791.4989 0.51	$[M-H]^-$	$C_{41}H_{76}O_{12}S$	SQDG(14:0_18:1)	-2.2	4.52E-05	1	Sulfo-quinovosyl-diacylglycerol
745.5114 1.61	$[M+HCOO]^-$	$C_{39}H_{72}O_{10}$	MGDG(14:0_16:1)	-3.6	2.05E-06	1	Mono-galactosyl-diacylglycerol
748.5145 2.14	$[M+HCOO]^-$	$C_{38}H_{74}NO_8P$	PC(14:0_16:1)	-3.7	2.59E-06	1	Phosphatidyl-choline
761.4489 3.41	$[M-H]^-$	$C_{39}H_{70}O_{12}S$	SQDG(14:0_16:2)	-3.9	9.06E-06	1	Sulfo-quinovosyl-diacylglycerol
799.4681 1.13	$[M-H]^-$	$C_{42}H_{72}O_{12}S$	SQDG(15:0_18:4)	-3.9	7.44E-05	1	Sulfo-quinovosyl-diacylglycerol
743.4965 2.69	$[M+HCOO]^-$	$C_{39}H_{70}O_{10}$	MGDG(14:0_16:2)	-4.0	1.75E-05	1	Mono-galactosyl-diacylglycerol
802.5609 1.37	$[M+HCOO]^-$	$C_{42}H_{80}NO_8P$	PC(16:1_18:1) / PC(16:0_18:2)	-4.0	9.41E-06	1	Phosphatidyl-choline

Table 4.1 continued

907.5639 0.33	$[M+HCOO]^-$	$C_{45}H_{82}O_{15}$	DGDG(14:0_16:1)	-4.0	4.9E-06	1	Digalactosyl-diacylglycerol
762.5017 35.1	$[M+HCOO]^-$	$C_{39}H_{76}NO_8P$	PC(15:0_16:1)	-4.0	8.47E-06	1	Phosphatidyl-choline
822.5293 0.24	$[M+HCOO]^-$	$C_{44}H_{76}NO_8P$	PC(16:1_20:5)	-4.1	4.57E-08	1	Phosphatidyl-choline
841.5108 3.92	$[M-H]^-$	$C_{45}H_{78}O_{12}S$	SQDG(36:4)	-4.2	1.24E-05	3	Sulfo-quinovosyl-diacylglycerol
935.5961 1.28	$[M+HCOO]^-$	$C_{47}H_{86}O_{15}$	DGDG(16:0_16:1)	-4.2	1.8E-07	1	Digalactosyl-diacylglycerol
757.4210 1.06	$[M-H]^-$	$C_{39}H_{66}O_{12}S$	SQDG(14:0_16:4)	-4.4	5.19E-06	1	Sulfo-quinovosyl-diacylglycerol
820.5129 0.61	$[M+HCOO]^-$	$C_{44}H_{74}NO_8P$	PC(16:2_20:5)	-4.4	3.36E-06	1	Phosphatidyl-choline
583.3129 1.89	$[M-H]^-$	$C_{30}H_{48}O_{11}$	MGDG(21:4+1 O)	-4.5	1.23E-06	3	Mono-galactosyl-diacylglycerol
773.5427 0.78	$[M+HCOO]^-$	$C_{41}H_{76}O_{10}$	MGDG(16:0_16:1)	-4.5	8.48E-07	1	Mono-galactosyl-diacylglycerol
795.5265 0.13	$[M+HCOO]^-$	$C_{43}H_{74}O_{10}$	MGDG(16:0_18:4)	-4.5	6.45E-06	1	Mono-galactosyl-diacylglycerol
829.4763 1.09	$[M-H]^-$	$C_{43}H_{74}O_{13}S$	SQDG(34:4 + 1O)	-4.8	0.000138	3	Sulfo-quinovosyl-diacylglycerol
818.4976 0.24	$[M+HCOO]^-$	$C_{44}H_{72}NO_8P$	PC(16:3_20:5) / PC(18:4_18:4)	-5.1	2.69E-07	1	Phosphatidyl-choline
850.5604 0.00	$[M+HCOO]^-$	$C_{46}H_{80}NO_8P$	PC(18:1_20:5)	-5.3	4.66E-06	1	Phosphatidyl-choline
870.5292 0.11	$[M+HCOO]^-$	$C_{48}H_{76}NO_8P$	PC(20:5_20:5)	-5.3	6.87E-07	1	Phosphatidyl-choline
796.5138 1.13	$[M+HCOO]^-$	$C_{42}H_{74}NO_8P$	PC(14:0_20:5) / PC(16:1_18:4)	-6.3	3.49E-07	1	Phosphatidyl-choline
824.5454 0.85	$[M+HCOO]^-$	$C_{44}H_{78}NO_8P$	PC(16:0_20:5)	-6.4	1.25E-08	1	Phosphatidyl-choline
896.5448 0.11	$[M+HCOO]^-$	$C_{50}H_{78}NO_8P$	PC(20:5_22:6)	-6.7	3.46E-07	1	Phosphatidyl-choline
800.5449 0.25	$[M+HCOO]^-$	$C_{42}H_{78}NO_8P$	PC(16:0_18:3)	-6.9	4.77E-05	1	Phosphatidyl-choline
798.5286 0.63	$[M+HCOO]^-$	$C_{42}H_{76}NO_8P$	PC(16:0_18:4)	-7.8	5.7E-05	1	Phosphatidyl-choline
844.5135 0.12	$[M+HCOO]^-$	$C_{46}H_{74}NO_8P$	PC(18:4_20:5)	-8.5	1.41E-05	1	Phosphatidyl-choline
848.5448 0.12	$[M+HCOO]^-$	$C_{46}H_{78}NO_8P$	PC(18:2_20:5) / PC(16:1_22:6)	-8.5	5.3E-06	1	Phosphatidyl-choline
821.5427 1.46	$[M+HCOO]^-$	$C_{45}H_{76}O_{10}$	MGDG(36:5)	-9.3	2.82E-06	3	Mono-galactosyl-diacylglycerol
843.5266 0.24	$[M+HCOO]^-$	$C_{47}H_{74}O_{10}$	MGDG(18:3_20:5)	-11	6E-05	1	Mono-galactosyl-diacylglycerol

Table 4.2: Identification of metabolites via MS metabolomics analysis whose concentrations are significantly different when *A. glacialis* was exposed to *K. brevis*. Observed m/z and parts-per-million mass error (PPM), adduct, elemental formula, and molecular composition (full fatty acid chain information) are provided where possible. Fold change values are positive when relative abundance of metabolite increased when *A. glacialis* was exposed to allelopathy. Annotation confidence ranges from 1-3. Confidence level 1: observed MS/MS data consistent with predicted spectrum and LOBSTAHS exact mass match to corresponding lipid class; 2: observed MS/MS data consistent with predicted spectrum; 3: observed exact mass match to LOBSTAHS database and/or partial MS/MS structural determination (137).
* Fold change value uncertain due to extremely low concentration of metabolites in control samples

***m/z* error (PPM)**	**Adduct**	**Elemental formula**	**Identity**	**Fold change**	**p value**	**Conf.**	**Lipid Class**
591.4308 2.37	$[M-H]^-$	$C_{32}H_{64}SO_7$	Pentadecanoyl sulfohydroxyheptadecanoic acid	4.9	4.24E-06	2	Other (sulfur containing)
607.4243 1.81	$[M-H]^-$	$C_{32}H_{64}O_8S$	Pentadecanoyl sulfohydroxyheptadecanoic acid	4.9	1.66E-05	2	Other (sulfur containing)
616.4615 0.65	$[M-H]^-$	$C_{34}H_{67}NO_6S$	*N*-sulfo,*N*-pentadecanoyl nonadecanamide	13.8	5.55E-05	2	Other (sulfur containing)
578.4790 1.04	$[M-H]^-$	$C_{35}H_{65}NO_5$	*N*-palmitoleic acid oleamide	12.2	7.2E-06	2	Fatty acid amide
651.4958 3.68	$[M-H]^-$	$C_{34}H_{72}N_2O_7S$	Pentadecenoyl *N*-sulfanediol dihydroxynonadecane-diamide	12.5	1.42E-05	2	Other (sulfur containing)
653.5117 3.37	$[M-H]^-$	$C_{34}H_{74}N_2O_7S$	Pentadecanoyl *N*-sulfanediol dihydroxynonadecane-diamide	16.4	4.57E-05	2	Other (sulfur containing)

Table 4.3: Lipid classes identified by MS-based oPLS-DA model as having significantly different concentrations in *T. pseudonana* based upon exposure to *K. brevis* allelopathy. Common adducts used to identify class of compound, the number of compounds in each class of lipids, and the average fold change is included for each class. The average fold change is an average of the individual fold changes each lipid identified in a class. Classes of lipids identified include: phosphatidylcholines (PCs), sulfoquinovosyldiacylglycerides (SQDGs), digalactosyldiacylglycerides (DGDGs), phosphatidylglycerols (PGs), monogalatoyldiacylglycerides (MGDGs), phosphatidylethanolamines (PEs), primary fatty acid amides (PFAAs), free fatty acids (FFAs), and non-SQDG sulfonated lipids (SULF).

Lipid Class	Adduct Detected	# Chemical Species	Average Fold Change
PC	$[M+HCOO]^-$	15	-5.8
SQDG	$[M-H]^-$	14	-3.3
DGDG	$[M+HCOO]^-$	3	-3.3
PG	$[M-H]^-$	3	-2.9
MGDG	$[M+HCOO]^-$	12	-2.8
PE	$[M+HCOO]^-$	1	6.5
PFAA	$[M-H]^-$	5	25
FFA	$[M-H]^-$	3	>25*
SULF	$[M-H]^-$	14	>25*

*Fold change value uncertain due to extremely low concentration of metabolites in control samples

metabolites represent nine major lipid classes, of which members of five (phosphatidylcholines [PCs], sulfoquinovosyldiacylglycerides [SQDGs], monogalatosyldiacylglycerides [MGDGs], digalactosyldiacylglycerides [DGDGs], and phosphatidylglycerols [PGs]) were generally less abundant when *T. pseudonana* was subjected to *K. brevis* allelopathy, whereas members of four classes (non-SQDG sulfonated lipids [SULF], free fatty acids [FFAs], primary fatty acid amides [PFAAs], and phosphatidylethanolamines [PEs]) were generally more abundant due to allelopathy (Table 4.3). In contrast, for the other competitor, *A. glacialis*, concentrations of only six metabolites were significantly affected by allelopathy, reinforcing that *A. glacialis* maintains a more robust metabolism in response to *K. brevis* allelopathy (Figure 4.3, Table 4.1, Table 4.2). All six *A. glacialis* lipid metabolites whose concentrations varied with exposure to allelopathy were also modulated in *T. pseudonana*, all experiencing enhanced concentrations in both competitor species due to *K. brevis* exposure.

In addition to observing mass spectral features that represent SGQDs, MGDGs, DGDGs, PCs, and PGs (Table 4.3) as major lipid classes affected by allelopathy, five additional metabolites analysis whose concentrations in *T. pseudonana* were suppressed by *K. brevis* allelopathy were revealed only by NMR spectroscopic analysis. There were identified as aconitic acid, malonic acid, methyl guanidine, *N*-acetyl cysteine, and *N*-acetyl glutamine.

Cell membrane integrity is weakened by *K. brevis* allelopathy

Upon inspection of the identities of disrupted lipids in the current study, two major classes of lipids common to cell and thylakoid membranes were noted as being significantly affected by allelopathy: SQDGs and MGDGs. Prince *et al.* had previously

found cell membranes of some competing algae to be disrupted upon exposure to *K. brevis* allelopathy (36); however, *T. pseudonana* was not tested in that study. In the current study, following exposure to *K. brevis* for six days, the proportion of living *T. pseudonana* cells with permeable and therefore damaged cell membranes was significantly greater than for unexposed *T. pseudonana* (Figure 4.4). In this experiment, *T. pseudonana* growth was statistically indistinguishable for exposed and unexposed treatments indicating that even at sub-lethal doses, *K. brevis* allelopathy causes substantial alterations to competitor physiology, prior to changes being evident at the population level. This confirms that one of the major mechanisms or outcomes of allelopathy is via cell membrane disruption, possibly due to a decreased concentration of membrane lipids such as SQDGs and MGDGs.

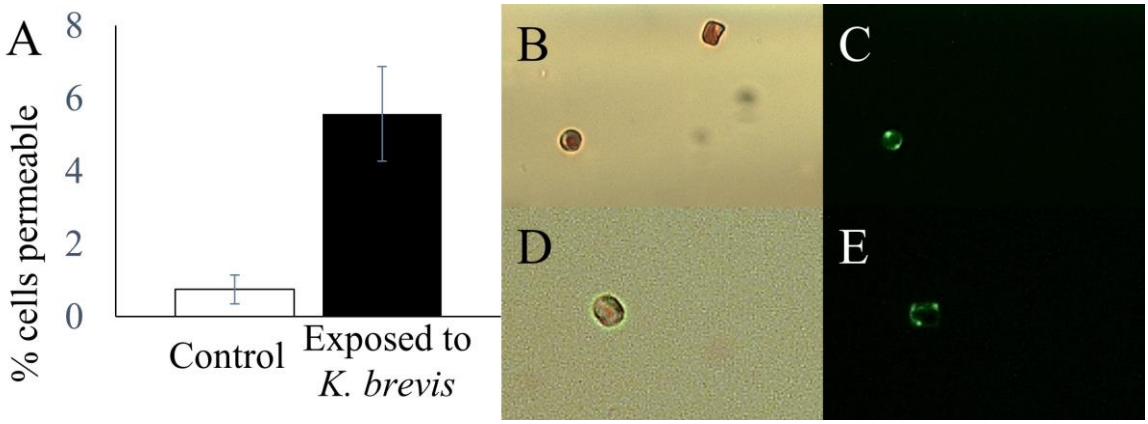

Figure 4.4: Exposure of *K. brevis* to *T. pseudonana* led to cell membrane damage. (*A*) Allelopathy significantly led to decreased *T. pseudonana* membrane integrity as indicated by membrane permeability of live cells measured by SYTOX Green and Neutral Red staining (N = 5; p = 0.0006). (*B* and *D*) Brightfield imaging of *T. pseudonana* stained with Neutral Red indicate living cells. (*C* and *E*) Fluorescence imaging of *T. pseudonana* stained with SYTOX Green indicate cells with permeable membranes. Simultaneous red and fluorescent green staining signify living *T. pseudonana* with permeable, damaged cell membranes.

4.5 Discussion

Dominant impact of allelopathy on competitor lipidome

The major metabolic responses of two model algae indicate that a dominant consequence of *K. brevis* allelopathy is increased membrane permeability and decreased photosynthetic capability, both likely due to decreases in the concentrations of membrane- and thylakoid-associated lipids (Figure 4.1, Figure 4.4, Table 4.3). Decreases in the concentrations of cell membrane associated PCs, SQDGs, and PGs (Table 4.1, Table 4.3) and permeabilization of the cell wall (Figure 4.4) suggested that allelopathy significantly disrupts membrane integrity by altering the lipid content without directly killing cells (Figure 4.4). Similarly, previously observed reduction in photosynthetic efficiency, as evidenced by decreases in the maximum quantum yield of photosystem II (36) and in expression of 12 photosynthesis-related proteins (37) could be due to damage to the thylakoid membrane and significant suppression of MGDGs, DGDGs, and SQDGs (Table 4.1, Table 4.3).

K. brevis allelopathy damages competitor cell membranes

Allelopathy-induced cell membrane permeabilization and depolarization is common in terrestrial plants (141-143); however, it does not appear to be well known in phytoplankton (but see ref. 36). Fluorescent staining of *T. pseudonana* showed that *K. brevis* allelopathy significantly reduced cell membrane integrity in living *T. pseudonana* cells (Figure 4.4). This increased permeability could have been caused by decreased abundance of membrane-associated lipids (Table 4.3). This trend was also identified in the polar metabolome of *T. pseudonana* when exposed to *K. brevis* allelopathy suggesting that

one of the major outcomes of allelopathy prior to cell death is cell membrane destabilization (37). Despite this prior report, no molecular mechanism of action for *K. brevis* allelopathy has been described to account for the observed phenotypic response. The current work implicates that decreases in PCs, SQDGs, and PGs are molecular underpinnings of cell membrane destabilization (Table 4.1, Table 4.3).

Thylakoid-associated lipids are significantly disrupted by allelopathy

A second likely mechanism by which allelopathy affects competitor physiology is via reduction of photosynthetic efficiency, which has been previously reported for competitors exposed to *K. brevis*.(36) Previously, we showed that the concentrations of 12 photosynthesis-related proteins decreased in response to *K. brevis* allelopathy (37). Here we show that MGDGs, DGDGs, and SQDGs are also less abundant when competing algae are exposed to allelopathy (Table 4.1, Table 4.2, Table 4.3). MGDGs and DGDGs are the most abundant lipids in chloroplasts, constituting up to 80% of total plastidic lipid content (144). In *Arabidopsis* leaves, higher MGDG content in the chloroplast led to maintenance of photosynthetic activity when subjected to ethylene-promoted senescence (145). Additionally, plastids have been shown to elongate in mustard seedlings when exposed to high enough concentrations of the known allelochemical benzoic acid (146). In general, the current findings suggest that an explanation for the observed loss in photosynthetic efficiency (36) is destabilization of plastid membranes. While no direct experimental evidence exists in the current study that the number of plastids decreased or that thylakoid membranes became permeable, the downregulation of thylakoid-associated lipids and known consequences of allelopathy on plastids warrant additional tests of this hypothesis.

Competitors display different responses to *K. brevis* allelopathy

Previous research showed that competing algae exhibit differential sensitivities to *K. brevis* allelopathy (35-37, 105). Herein we report that both competitor species studied, *A. glacialis* and *T. pseudonana,* are affected by allelopathy, although *T. pseudonana* was significantly more sensitive (Figure 4.1, Table 4.1, Table 4.2, Table 4.3). These findings support the previously posited hypothesis that *A. glacialis* possesses a resistance mechanism to mitigate the effects of allelopathy (37). The long-term geographic and seasonal co-occurrence of *A. glacialis* and *K. brevis* may have provided the selection pressure for *A. glacialis* to evolve resistance, which *T. pseudonana* has not yet acquired (37).

Consideration of the specific classes of lipids most affected in *T. pseudonana* by allelopathy (PC, SQDG, PFAA, FFA, and taurolipids) suggests that a majority of lipids induced (PFAA, FFA, and SULF) by allelopathic exposure are either metabolic breakdown products or metabolic precursors of PCs and SQDGs, whose pools shrunk in *T. pseudonana* upon exposure to allelopathy. These findings allow for two possible mechanisms: the stress of allelopathic exposure leads to the degradation of complex lipids, such as SQDGs and PCs, to their less complex components; or, allelopathic compounds exuded by *K. brevis* inhibit the biosynthetic enzymes within *T. pseudonana* that are responsible for the anabolic synthesis of complex lipids from more simple building blocks, resulting in a build-up of biosynthetic precursors (PFAA, FFA) and a loss of more complex lipids (SQDG, PC). Breakdown of more complex lipids to smaller products has been observed in the green alga *Dunaliella salina,* where the degradation of MGDGs to DGDGs was observed using radiolabeled carbon precursors (147). In the current case of *K. brevis* allelopathy affecting

T. pseudonana, the observed increase in concentrations, rather than decrease, of lipid biosynthetic enzymes such as sulpholipid synthase and UDP-sulfoquinovose synthase (37), favors the hypothesis that complex lipids are degraded in response to allelopathy.

Complementing the MS lipidomic analysis, NMR spectroscopic profiling revealed that additional essential metabolites in *T. pseudonana* were disrupted by *K. brevis* allelopathy. Aconitic acid, an intermediate in the TCA cycle, and malonic acid, intermediate building block for fatty acid synthesis, were both less abundant due to allelopathy, which could be explained by the degradation of these acids, an enhanced production of some fatty acids thus reducing cellular stocks of starting materials and intermediates, or the slowdown in anabolism of these acids (148, 149). Three methylated and acetylated amino acids were also suppressed which point to alterations in amino acid metabolism as a consequence of allelopathic exposure. None of the five compounds identified via NMR spectroscopic profiling were identified as components of the MS-based model, highlighting the complementary nature of NMR and MS profiling.

K. brevis' sub-lethal allelopathy provides a unique study system

K. brevis allelopathy is relatively mild among algae, some of which release compounds that are acutely toxic to other algae (150-154). *K. brevis* allelopathy acts slowly on competitors, affecting cell viability and population growth over days by weakening cell membranes, impeding photosynthesis, and disrupting osmoregulation (37). In contrast, *Alexandrium* dinoflagellates can cause lysis of competitor cells in minutes to hours (150, 154). The freshwater dinoflagellate *Peridinium aciculiferum* produces bubbles that later burst leading to cell death in its competitor *Rhodomonas lacustris* (153). Due to the slow

acting allelopathic effects of *K. brevis*, we were able to observe the disruption of lipid metabolism, which ultimately leads to catastrophic effects on membrane integrity and photosynthesis in some competing phytoplankton (Figure 4.4, Table 4.3).

Lipidomics provides essential knowledge on how competitors respond to allelopathy

In the current study focused on lipidomics, we show that the major effects of *K. brevis* allelopathy on *T. pseudonana* are the permeabilization of the cell membrane and significant decreases in the concentrations of membrane-associated lipids, including those associated with the thylakoid and cell membranes (Figure 4.4, Table 4.1, Table 4.2, Table 4.3). This complements previous findings regarding the polar metabolome and proteome in which we showed that *T. pseudonana* suffered significantly increased glycolysis activity, suppressed osmoregulation, enhanced enzymatic capabilities related to oxidative stress, as well as an increase in proteins associated with the pentose phosphate pathway and anti-trypsin protease inhibitors, when exposed to *K. brevis* allelopathy (37). The integration of metabolomics involving both polar and non-polar classes with proteomics analysis suggests that *K. brevis* allelopathy significantly alters *T. pseudonana* cellular functions on many levels. Cell membrane permeability, significantly altered metabolism, and decreased photosynthesis together paint a dreary picture for *T. pseudonana* that leads to decreased growth. The current lipidomics work offers a glimpse into the robust metabolome of a more resistant competitor, *A. glacialis*, providing unique opportunities for exploring mechanisms of resistance to allelopathy.

CHAPTER 5. CONCLUSIONS AND FUTURE DIRECTIONS

Chemically mediated interactions are diverse and numerous, ranging from finding mates and food, to detecting predators and defending oneself. Waterborne cues are commonly utilized by organisms in the marine environment since visual, auditory, and mechanosensory stimuli can be complicated. Despite decades of research suggesting the presence and importance of waterborne cues, little is known of the compounds that make up these cues. The current body of work investigates the chemical nature of waterborne cues utilized for predator detection and of waterborne cues involved in chemically mediated competition among marine phytoplankton. In addition, the studies herein describe the catastrophic effects of allelopathy on phytoplankton metabolism and cellular integrity.

Ecologically important waterborne cues have historically been difficult to isolate and characterize due to their lability, polarity, and low abundance in nature (18). Additionally, biological activity of multicomponent cues is likely to be lost during chromatographic separation using traditional bioassay-guided fractionation, since essential components of a mixture are likely to be isolated into different fractions (155). Metabolomics paired with multivariate statistical modeling enables prediction of the functions of individual compounds within a complex mixture without labor-intensive separation or successive rounds of assays after each separation step to determine which fraction contains bioactive molecules. Compounds predicted to illicit biological responses following metabolomics analysis are then tested in a small number of assays as single components or in combination to test model-based predictions. Using this approach as

reported in Chapter 2 (1) of this dissertation, we identified trigonelline and homarine as the major constituents of a waterborne fear-inducing cue, released in the urine of the predatory blue crab, that prey crabs perceive, resulting in altered prey behavior to avoid being consumed by blue crabs. The fear-inducing effects of each compound as a single component as well as in a mixture, at their natural concentrations, were confirmed via bioassay without having fully purified either compound from blue crab urine. Bypassing compound isolation from natural mixtures saved time, resources, and likely deconvoluted the characterization of constitutional isomers that are difficult to separate. This study serves as a roadmap for future studies aimed at characterizing waterborne cues, specifically those that have been shown to involve multicomponent, labile, or low abundance cues.

In addition to characterizing the fear-inducing cue, we also described the concentration- and diet-dependent risk perception of mud crabs by quantifying trigonelline and homarine in urine of varying potencies. Trigonelline and homarine occurred at highest concentration in urine that also caused the greatest behavioral disturbance to prey. To our knowledge, this is the first fully characterized system of chemically mediated risk perception that promotes a behavioral response by prey in the marine environment. With the identities of the components of the fear-inducing cue now known, we can begin to address the relative strength of their community-structuring effects in estuarine environments. Non-consumptive effects of predators have been predicted to be strong compared to the direct effects of predators consuming individual prey and therefore warrant significant future study (23). Scientists may also now assess the potential role of this fear-inducing cue as a management tool for oyster fisheries and coastal management.

Chapters 3 (2) and 4 (3) of this dissertation report chemical profiling of allelopathic compounds and the metabolic consequences of allelopathy to competing phytoplankton. Harmful algal blooms such as those formed by *K. brevis* have disastrous effects on marine ecosystems through the poisoning of wildlife (33, 34). A significant number of these ecosystem-structuring interactions are mediated by well-described toxins that are not known to be allelopathic (35, 38). Allelopathy is, however, hypothesized to play a significant role in bloom dynamics allowing these blooms to persist and out-compete co-occurring phytoplankton (29). Previous efforts to isolate and characterize the compounds responsible for allelopathy have failed (38) due to reasons discussed previously. Without knowledge of the exact identities of compounds responsible for allelopathy, we cannot determine structure-activity relationships of allelopathic compounds, impacts of biotic and abiotic factors on their production rates, metabolic pathways that lead to their production and release into the environment, or the selective pressures that have led to their evolution.

In Chapter 4 (3) of this dissertation we identified and utilized previously untapped variation in allelopathic potency to chemically fingerprint *K. brevis*. Metabolomics and multivariate statistical modeling provided a unique tool set for working with these ecologically important waterborne cues that mediate interspecific interactions between *K. brevis* and competitors. Spectroscopic fingerprinting led to the identification of three distinct metabolic modalities of *K. brevis*: allelopathic, non-allelopathic, and stimulatory towards one important competitor, *Asterionellopsis glacialis*. Additionally, multivariate models predicted that allelopathic compounds contain aromatic moieties, unsaturated fatty-acid derived moieties, or both. While the individual compounds responsible for allelopathy were not identified, the chemical variability in the exuded metabolome of *K. brevis* was

established as a source of untapped information that was utilized to elucidate chemical properties of allelopathic compounds. Utilizing the variability in allelopathic potency, future studies can now assess the relative proportion of each metabolic modality in bloom and non-bloom conditions in the field, the relative ecological importance of each metabolic modality in bloom dynamics, and investigate the conditions that promote one metabolic modality over another, possibly with the hopes of managing/affecting bloom patterns in areas commonly afflicted with red tide blooms.

In Chapter 3 (2) of this dissertation we described the physiological effects of allelopathy on competitor metabolism. Significant alterations to the lipidome of competitor *T. pseudonana* were observed in the cell membrane, where decreases in membrane-associated lipids led to visible perforations in living cells when exposed to *K. brevis* allelopathy. Decreases in thylakoid membrane-associated lipids were also measured, likely explaining disruption of photosynthesis that has been previously reported for *K. brevis* allelopathy (36, 37). The catastrophic effects of allelopathy on competitor lipidomes coupled with previously reported effects on polar metabolomes such as increased oxidative stress and inhibited osmoregulation (37), paint a picture of cells doomed to die with multiple failing systems apparent. Future research could be aimed at understanding the molecular targets of allelopathic compounds that lead to the observed alterations in the lipidome. A thorough understanding of the pathways, enzymes, and systems affected is possible through multi-platform studies combining guided metabolomics, proteomics, and genomics analyses of this sub-lethal allelopathy.

This dissertation describes three significant advances in understanding the chemical nature of waterborne cues and the metabolic effects they have on other species.

Metabolomics analyses paired with multivariate statistical modeling provide an effective alternative to traditional bioassay-guided fractionation which has particular weaknesses when applied to identifying waterborne cues as previously discussed. As more such cues are characterized we can address numerous additional questions including: What are the biosynthetic origins of these cues? What biosynthetic machinery is required to synthesize them? How do cues disperse? How long do these cues persist in the water column? Are responses to the cues learned or innate? Are responses to the cues in the field equivalent to responses in the lab? How strong are the community structuring effects? What mechanisms are there for cue degradation in the water column? Answers to these questions will provide significant insight into the roles and mechanisms of chemically mediated interactions.

REFERENCES

1. Poulin RX, *et al.* (2017) Chemical encoding of risk perception and predator detection among estuarine invertebrates. *Proc Natl Acad Sci U S A* **In Revision**
2. Poulin RX, Poulson-Ellestad KL, Roy J, & Kubanek J (2017) Variable allelopathy among phytoplankton reflected in red tide metabolome. *Harmful Algae*. **In Review**
3. Poulin RX, *et al.* (2017) *Karenia brevis* allelopathy compromises the lipidome, membrane integrity, and photosynthetic efficiency of competitors. *Sci Rep*. **In Review**
4. Courchamp F, *et al.* (2015) Fundamental ecology is fundamental. *Trends Ecol Evol* 30(1):9-16.
5. Barlow RB, Hitt JM, & Dodge FA (2001) Limulus vision in the marine environment. *Biol Bull* 200(2):169-176.
6. R J Prokopy a & Owens ED (1983) Visual detection of plants by herbivorous insects. *Annu Rev Entomol* 28(1):337-364.
7. Atema J (1995) Chemical signals in the marine environment: dispersal, detection, and temporal signal analysis. *Proc Nat Acad Sci U S A* 92(1):62-66.
8. Thomas ML (2011) Detection of female mating status using chemical signals and cues. *Biol Rev* 86(1):1-13.
9. Griffin DR, Webster FA, & Michael CR (1960) The echolocation of flying insects by bats. *Anim Behav* 8(3):141-154.
10. Ketten DR (1992) The Marine mammal ear: specializations for aquatic audition and echolocation. *The Evolutionary Biology of Hearing*, eds Webster DB, Popper AN, & Fay RR (Springer New York, New York, NY), pp 717-750.
11. Montgomery J, Coombs S, & Halstead M (1995) Biology of the mechanosensory lateral line in fishes. *Rev Fish Biol Fish* 5(4):399-416.
12. Yen J, Lenz PH, Gassie DV, & Hartline DK (1992) Mechanoreception in marine copepods: electrophysiological studies on the first antennae. *J Plankton Res* 14(4):495-512.
13. Buskey EJ (1984) Swimming pattern as an indicator of the roles of copepod sensory systems in the recognition of food. *Mar Biol* 79(2):165-175.
14. Dixson DL, Abrego D, & Hay ME (2014) Chemically mediated behavior of recruiting corals and fishes: A tipping point that may limit reef recovery. *Science* 345(6199):892-897.
15. Rehnberg BG & Schreck CB (1987) Chemosensory detection of predators by coho salmon (*Oncorhynchus kisutch*): behavioural reaction and the physiological stress response. *Can J Zool* 65(3):481-485.
16. Gillard J, *et al.* (2013) Metabolomics Enables the Structure Elucidation of a Diatom Sex Pheromone. *Angew Chem Int Edit* 52(3):854-857.
17. Selander E, Jakobsen HH, Lombard F, & Kiørboe T (2011) Grazer cues induce stealth behavior in marine dinoflagellates. *Proc Nat Acad Sci U S A* 108(10):4030-4034.

18. Prince EK & Pohnert G (2010) Searching for signals in the noise: metabolomics in chemical ecology. *Anal Bioanal Chem* 396(1):193-197.
19. Guajardo E, Correa JA, & Contreras-Porcia L (2016) Role of abscisic acid (ABA) in activating antioxidant tolerance responses to desiccation stress in intertidal seaweed species. *Planta* 243(3):767-781.
20. Reese ES (1969) Behavioral adaptations of intertidal hermit crabs. *Am Zool* 9(2):343-355.
21. Trussell GC, Ewanchuk PJ, & Bertness MD (2003) Trait-mediated effects in rocky intertidal food chains: Predator risk cues alter prey feeding rates. *Ecology* 84(3):629-640.
22. Hill JM (2011) Predator biomass and habitat characteristics affect the magnitude of consumptive and non-consumptive effects (NCEs): experiments between blue crabs, mud crabs, and oyster prey. Doctor of Philosophy in Biology Doctoral (Georgia Institute of Technology).
23. Preisser EL, Bolnick DI, & Benard MF (2005) Scared to death? The effects of intimidation and consumption in predator–prey interactions. *Ecology* 86(2):501-509.
24. Creel S, Christianson D, Liley S, & Winnie JA (2007) Predation risk affects reproductive physiology and demography of Elk. *Science* 315(5814):960-960.
25. Creel S, Winnie J, Maxwell B, Hamlin K, & Creel M (2005) Elk alter habitat selection as an antipredator response to wolves. *Ecology* 86(12):3387-3397.
26. Winnie J, Christianson D, Creel S, & Maxwell B (2006) Elk decision-making rules are simplified in the presence of wolves. *Behav Ecol Sociobiol* 61(2):277.
27. Ripple WJ & Beschta RL (2012) Trophic cascades in Yellowstone: The first 15years after wolf reintroduction. *Biological Conservation* 145(1):205-213.
28. Baril LM, Hansen AJ, Renkin R, & Lawrence R (2011) Songbird response to increased willow (*Salix* spp.) growth in Yellowstone's northern range. *Ecol Appl* 21(6):2283-2296.
29. Smayda TJ (1997) Harmful algal blooms: Their ecophysiology and general relevance to phytoplankton blooms in the sea. *Limnol Oceanogr* 42:1137-1153.
30. Baden DG (1989) Brevetoxins: unique polyether dinoflagellate toxins. *FASEB J* 3(7):1807-1817.
31. Bates SS, *et al.* (1989) Pennate diatom *Nitzschia pungensas* the primary source of domoic acid, a toxin in shellfish from Eastern Prince Edward Island, Canada. *Can J Fish Aquat Sci* 46(7):1203-1215.
32. Maranda L, Anderson DM, & Shimizu Y (1985) Comparison of toxicity between populations of *Gonyaulax tamarensis* of eastern North American waters. *Estuar Coast Shelf Sci* 21(3):401-410.
33. Flewelling LJ, *et al.* (2005) Brevetoxicosis: red tides and marine mammal mortalities. *Nature* 435(7043):755-756.
34. Scholin CA, *et al.* (2000) Mortality of sea lions along the central California coast linked to a toxic diatom bloom. *Nature* 403(6765):80-84.
35. Kubanek J, Hicks MK, Naar J, & Villareal TA (2005) Does the red tide dinoflagellate *Karenia brevis* use allelopathy to outcompete other phytoplankton? *Limnol Oceanogr* 50(3):883-895.

36. Prince EK, Myers TL, & Kubanek J (2008) Effects of harmful algal blooms on competitors: Allelopathic mechanisms of the red tide dinoflagellate *Karenia brevis*. *Limnol Oceanogr* 53(2):531-541.
37. Poulson-Ellestad KL, *et al.* (2014) Metabolomics and proteomics reveal impacts of chemically mediated competition on marine plankton. *Pro Nat Acad Sci U S A* 111(24):9009-9014.
38. Prince EK, Poulson KL, Myers TL, Sieg RD, & Kubanek J (2010) Characterization of allelopathic compounds from the red tide dinoflagellate *Karenia brevis*. *Harmful Algae* 10(1):39-48.
39. Dobretsov S, Teplitski M, & Paul V (2009) Mini-review: quorum sensing in the marine environment and its relationship to biofouling. *Biofouling* 25(5):413-427.
40. Kats LB & Dill LM (1998) The scent of death: Chemosensory assessment of predation risk by prey animals. *Écoscience* 5(3):361-394.
41. Zimmer RK & Butman CA (2000) Chemical signaling processes in the marine environment. *The Biol Bull* 198(2):168-187.
42. Blunt JW, Copp BR, Keyzers RA, Munro MHG, & Prinsep MR (2013) Marine natural products. *Nat Prod Rep* 30(2):237-323.
43. M E Hay a & Fenical W (1988) Marine Plant-Herbivore Interactions: The Ecology of Chemical Defense. *Annu Rev Ecol Syst* 19(1):111-145.
44. Paul VJ, Puglisi MP, & Ritson-Williams R (2006) Marine chemical ecology. *Nat Prod Rep* 23(2):153-180.
45. Schwartz ER, Poulin RX, Mojib N, & Kubanek J (2016) Chemical ecology of marine plankton. *Nat Prod Rep* 33(7):843-860.
46. Cragg GM & Newman DJ (2013) Natural products: A continuing source of novel drug leads. *Biochimica et Biophysica Acta (BBA) - General Subjects* 1830(6):3670-3695.
47. Harvey AL, Edrada-Ebel R, & Quinn RJ (2015) The re-emergence of natural products for drug discovery in the genomics era. *Nat Rev Drug Discov* 14(2):111-129.
48. Lane AL, *et al.* (2009) Desorption electrospray ionization mass spectrometry reveals surface-mediated antifungal chemical defense of a tropical seaweed. *Proc Nat Acad Sci U S A* 106(18):7314-7319.
49. Lima SL (1998) Nonlethal effects in the ecology of predator-prey interactions. *BioScience* 48(1):25-34.
50. Bjærke O, Andersen T, & Titelman J (2014) Predator chemical cues increase growth and alter development in nauplii of a marine copepod. *Mar Ecol Prog Ser* 510:15-24.
51. Castorani MCN & Hovel KA (2016) Native predator chemical cues induce anti-predation behaviors in an invasive marine bivalve. *Biol Invasions* 18(1):169-181.
52. Chivers DP & Smith RJF (1998) Chemical alarm signalling in aquatic predator-prey systems: A review and prospectus. *Écoscience* 5(3):338-352.
53. Grabowski JH & Powers SP (2004) Habitat complexity mitigates trophic transfer on oyster reefs. *Mar Ecol Prog Ser* 277:291-295.
54. Turner AM & Montgomery SL (2003) Spatial and temporal scales of predator avoidance: Experiments with fish and snails. *Ecology* 84(3):616-622.

55. Peckarsky BL, *et al.* (2008) Revisiting the classics: considering nonconsumptive effects in textbook examples of predator-prey interactions. *Ecology* 89(9):2416-2425.
56. Agelopoulos NG, Hooper AM, Maniar SP, Pickett JA, & Wadhams LJ (1999) A Novel approach for isolation of volatile chemicals released by individual leaves of a plant in situ. *J Chem Ecol* 25(6):1411-1425.
57. Weissburg M, Poulin RX, & Kubanek J (2016) You are what you eat: a metabolomics approach to understanding prey responses to diet-dependent chemical cues released by predators. *J Chem Ecol* 42(10):1037-1046.
58. Gunther UL, Ludwig C, & Ruterjans H (2000) NMRLAB-Advanced NMR data processing in matlab. *J Magn Reson* 145(2):201-208.
59. Dieterle F, Ross A, Schlotterbeck G, & Senn H (2006) Probabilistic quotient normalization as robust method to account for dilution of complex biological mixtures. Application in 1H NMR metabonomics. *Anal Chem* 78(13):4281-4290.
60. Parsons HM, Ludwig C, Günther UL, & Viant MR (2007) Improved classification accuracy in 1- and 2-dimensional NMR metabolomics data using the variance stabilising generalised logarithm transformation. *BMC Bioinformatics* 8.
61. Sumner LW, *et al.* (2007) Proposed minimum reporting standards for chemical analysis. *Metabolomics* 3(3):211-221.
62. Wang X-B, *et al.* (2003) Photodetachment of zwitterions: probing intramolecular coulomb repulsion and attraction in the gas phase using pyridinium dicarboxylate Anions. *J Am Chem Soc* 125(1):296-304.
63. Frisc E, Frisch M, Clemente F, & Trucks G (2013) Gaussian 09, Revision D. 01, Gaussian. *Inc., Wallingford CT*.
64. Schrödinger L (2015) The PyMOL molecular graphics system, version 1.8.
65. Wishart DS, *et al.* (2013) HMDB 3.0-The Human Metabolome Database in 2013. *Nucleic Acids Research* 41(D1):D801-D807.
66. Keppel E & Scrosati R (2004) Chemically mediated avoidance of *Hemigrapsus nudus* (Crustacea) by *Littorina scutulata* (Gastropoda): effects of species coexistence and variable cues. *Anim Behav* 68(4):915-920.
67. Smee DL & Weissburg MJ (2006) Hard clams (*Mercenaria mercenaria*) evaluate predation risk using chemical signals from predators and injured conspecifics. *J Chem Ecol* 32(3):605-619.
68. Laurila A, Kujasalo J, & Ranta E (1997) Different antipredator behaviour in two anuran tadpoles: effects of predator diet. *Behav Ecol Sociobiol* 40(5):329-336.
69. Martel G & Dill LM (1993) Feeding and aggressive behaviours in juvenile coho salmon (*Oncorhynchus kisutch*) under chemically-mediated risk of predation. *Behav Ecol Sociobiol* 32(6):365-370.
70. Yasumoto K, *et al.* (2008) Isolation of new aliphatic sulfates and sulfamate as the *Daphnia* kairomones inducing morphological change of a phytoplankton *Scenedesmus gutwinskii*. *Chem Pharm Bull* 56(1):133-136.
71. Gasteiger EL, Haake PC, & Gergen JA (1960) An investigation of the distribution and fucntion of homarine (*N*-methyl picolinic acid). *Ann N Y Acad Sci* 90(3):622-636.
72. Hayashi T & Konosu S (1977) Quaternary ammonium bases in the adductor muscle of fan-mussel. *Nippon Suisan Gakk* 43(3):343-348.

73. Hiltz DF (1970) Occurrence of trigonelline (*N*-methyl nicotinic cid) in the adductor muscle of a Lamellibranch, the sea scallop (*Placopecten magellanicus*). *J Fish Res Board Can* 27(3):604-606.
74. Hirano T (1975) On the Distribution and seasonal variation of homarine in some marine invertebrates. *Nippon Suisan Gakki* 41(10):1047-1051.
75. Núñez-Pons L & Avila C (2015) Natural products mediating ecological interactions in Antarctic benthic communities: a mini-review of the known molecules. *Nat Prod Rep* 32(7):1114-1130.
76. Suwetja IK, Hori K, Miyazawa K, & Ito K (1989) Changes in content of ATP-related compounds, homarine, and trigonelline in marine-invertebrates during ice storage. *Nippon Suisan Gakk* 55(3):559-566.
77. Yasumoto T, Kawagishi N, & Asano H (1978) Identification of *N*-methyl-alpha-picolinium and other quaternary ammonium compounds from the oyster. *Nippon Suisan Gakk* 44(5):529-529.
78. Berking S (1986) Is homarine a morphogen in the marine hydroid Hydractinia? *Roux's Arch Dev Biol* 195(1):33-38.
79. Berking S (1987) Homarine (N-methylpicolinic acid) and trigonelline (N-methylnicotinic acid) appear to be involved in pattern control in a marine hydroid. *Development* 99(2):211-220.
80. McClintock JB, *et al.* (1994) Homarine as a feeding deterrent in common shallow-water antarctic lamellarian gastropod *Marseniopsis mollis*: A rare example of chemical defense in a marine prosobranch. *J Chem Ecol* 20(10):2539-2549.
81. Targett NM, Bishop SS, McConnell OJ, & Yoder JA (1983) Antifouling agents against the benthic marine diatom, *Navicula salinicola* homarine from the gorgonians *Leptogorgia virgulata* and *L. setacea* and analogs. *J Chem Ecol* 9(7):817-829.
82. Netherton JC & Gurin S (1980) Biosynthesis in vitro of homarine and pyridine carboxylic acids in marine shrimp. *J Biol Chem* 255(20):9549-9551.
83. Netherton JC & Gurin S (1982) Biosynthesis and physiological role of homarine in marine shrimp. *J Biol Chem* 257(20):11971-11975.
84. Hall ER & Gurin S (1975) Experiments in marine biochemistry. Homarine metabolism in *Penaeus duorarum*. *J Biol Chem* 250(17):6943-6946.
85. Ashihara H (2006) Metabolism of alkaloids in coffee plants. *Brazil J Plant Physiol* 18:1-8.
86. Kuhlisch C & Pohnert G (2015) Metabolomics in chemical ecology. *Nat Prod Rep* 32(7):937-955.
87. Nilsson MC (1994) Separation of allelopathy and resource competition by the boreal dwarf shrub *Empetrum hermaphroditum* Hagerup. *Oecologia* 98(1):1-7.
88. Ridenour WM & Callaway RM (2001) The relative importance of allelopathy in interference: the effects of an invasive weed on a native bunchgrass. *Oecologia* 126(3):444-450.
89. Folt C & Goldman CR (1981) Allelopathy between zooplankton: a mechanism for interference competition. *Science* 213(4512):1133-1135.
90. Fistarol GO, *et al.* (2004) Allelopathy in *Alexandrium* spp.: effect on a natural plankton community and on algal monocultures. *Aquat Microb Ecol* 35(1):45-56.

91. van Donk E & van de Bund WJ (2002) Impact of submerged macrophytes including charophytes on phyto- and zooplankton communities: allelopathy versus other mechanisms. *Aquat Bot* 72(3-4):261-274.
92. Jonsson PR, Pavia H, & Toth G (2009) Formation of harmful algal blooms cannot be explained by allelopathic interactions. *Proc Natl Acad Sci U S A* 106(27):11177-11182.
93. Sheng J, Malkiel E, Katz J, Adolf JE, & Place AR (2010) A dinoflagellate exploits toxins to immobilize prey prior to ingestion. *Proc Natl Acad Sci U S A* 107(5):2082-2087.
94. Poulson KL, Sieg RD, Prince EK, & Kubanek J (2010) Allelopathic compounds of a red tide dinoflagellate have species-specific and context-dependent impacts on phytoplankton. *Mar Ecol Prog Ser* 416:69-78.
95. Ma H, Krock B, Tillmann U, & Cembella A (2009) Preliminary characterization of extracellular allelochemicals of the toxic marine dinoflagellate *Alexandrium tamarense* using a *Rhodomonas salina* bioassay. *Marine Drugs* 7(4):497.
96. Choi YH, *et al.* (2005) Classification of Ilex species based on metabolomic fingerprinting using nuclear magnetic resonance and multivariate data analysis. *J Agric Food Chem* 53(4):1237-1245.
97. Kim HJ, Baek WS, & Jang YP (2011) Identification of ambiguous cubeb fruit by DART-MS-based fingerprinting combined with principal component analysis. *Food Chem* 129(3):1305-1310.
98. Kim HK, Choi YH, Erkelens C, Lefeber AWM, & Verpoorte R (2005) Metabolic fingerprinting of *Ephedra* species using 1H-NMR spectroscopy and principal component analysis. *Chem Pharm Bull* 53(1):105-109.
99. Ellis DI, Dunn WB, Griffin JL, Allwood JW, & Goodacre R (2007) Metabolic fingerprinting as a diagnostic tool. *Pharmacogenomics* 8(9):1243-1266.
100. Ellis DI & Goodacre R (2006) Metabolic fingerprinting in disease diagnosis: biomedical applications of infrared and Raman spectroscopy. *Analyst* 131(8):875-885.
101. Lamers RJ, *et al.* (2003) Identification of disease- and nutrient-related metabolic fingerprints in osteoarthritic Guinea pigs. *J Nutr* 133(6):1776-1780.
102. Johnson HE, Broadhurst D, Goodacre R, & Smith AR (2003) Metabolic fingerprinting of salt-stressed tomatoes. *Phytochemistry* 62(6):919-928.
103. Bommarius B, *et al.* (2013) A family of indoles regulate virulence and Shiga toxin production in pathogenic *E. coli*. *PLoS One* 8(1).
104. von Reuss SH, *et al.* (2012) Comparative metabolomics reveals biogenesis of ascarosides, a modular library of small-molecule signals in *C. elegans*. *J Am Chem Soc* 134(3):1817-1824.
105. Prince EK, Myers TL, Naar J, & Kubanek J (2008) Competing phytoplankton undermines allelopathy of a bloom-forming dinoflagellate. *Proc Biol Sci* 275(1652):2733-2741.
106. Lehman JT, Abella SEB, Litt AH, & Edmondson WT (2004) Fingerprints of biocomplexity: Taxon-specific growth of phytoplankton in relation to environmental factors. *Limnol Oceanogr* 49:1446-1456.

107. Bornet B, Antoine E, Bardouil M, & Baut CM-L (2004) ISSR as new markers for genetic characterization and evaluation of relationships among phytoplankton. *J Appl Phyco* 16(4):285-290.
108. Payet JP & Suttle CA (2014) Viral infection of bacteria and phytoplankton in the Arctic Ocean as viewed through the lens of fingerprint analysis. *Aquat Microb Ecol* 72(1):47-61.
109. Cai P, *et al.* (2016) Two new karlotoxins found in *Karlodinium veneficum* (strain GM2) from the East China Sea. *Harmful Algae* 58:66-73.
110. Van Wagoner RM, *et al.* (2010) Structure and relative potency of several karlotoxins from *Karlodinium veneficum*. *J Nat Prod* 73(8):1360-1365.
111. Glibert PM, Anderson DM, Gentien P, Granéli E, & Sellner KG (2005) The global, complex phenomena of harmful algal blooms.
112. Backer LC, *et al.* (2003) Recreational exposure to aerosolized brevetoxins during Florida red tide events. *Harmful Algae* 2(1):19-28.
113. Backer LC, *et al.* (2005) Occupational exposure to aerosolized brevetoxins during Florida red tide events: effects on a healthy worker population. *Environ Health Perspect* 113(5):644-649.
114. Fleming LE, *et al.* (2011) Review of Florida red tide and human health effects. *Harmful Algae* 10(2):224-233.
115. Fleming LE, Backer LC, & Baden DG (2005) Overview of aerosolized Florida red tide toxins: exposures and effects. *Environ Health Perspect* 113(5):618-620.
116. Fleming LE, *et al.* (2005) Initial evaluation of the effects of aerosolized Florida red tide toxins (brevetoxins) in persons with asthma. *Environ Health Perspect* 113(5):650-657.
117. Music SI, Howell JT, & Brumback CL (1973) Red tide. Its public health implications. *JFMA* 60(11):27-29.
118. Wardle DA, Karban R, & Callaway RM (2011) The ecosystem and evolutionary contexts of allelopathy. *Trends Ecol Evol* 26(12):655-662.
119. Fistarol GO, Legrand C, & Granéli E (2003) Allelopathic effect of *Prymnesium parvum* on a natural plankton community. *Mar Ecol Prog Ser* 255:115-125.
120. Uronen P, Kuuppo P, Legrand C, & Tamminen T (2007) Allelopathic effects of toxic haptophyte *Prymnesium parvum* lead to release of dissolved organic carbon and increase in bacterial biomass. *Microb Ecol* 54(1):183-193.
121. Keating KI (1977) Allelopathic influence on blue-green bloom sequence in a eutrophic lake. *Science* 196(4292):885-887.
122. Vardi A, *et al.* (2002) Dinoflagellate-cyanobacterium communication may determine the composition of phytoplankton assemblage in a mesotrophic lake. *Curr Biol* 12(20):1767-1772.
123. Ma H, Krock B, Tillmann U, & Cembella A (2009) Preliminary characterization of extracellular allelochemicals of the toxic marine dinoflagellate *Alexandrium tamarense* using a *Rhodomonas salina* bioassay. *Marine drugs* 7(4):497-522.
124. Ribalet F, Berges JA, Ianora A, & Casotti R (2007) Growth inhibition of cultured marine phytoplankton by toxic algal-derived polyunsaturated aldehydes. *Aquat Toxicol* 85(3):219-227.

125. Suikkanen S, Engström-Öst J, Jokela J, Sivonen K, & Viitasalo M (2006) Allelopathy of Baltic Sea cyanobacteria: no evidence for the role of nodularin. *J Plankton Res* 28(6):543-550.
126. Fistarol GO, Legrand C, Rengefors K, & Granéli E (2004) Temporary cyst formation in phytoplankton: a response to allelopathic competitors? *Environ Microbiol* 6(8):791-798.
127. Tillmann U & John U (2002) Toxic effects of *Alexandrium* spp. on heterotrophic dinoflagellates: an allelochemical defence mechanism independent of PSP-toxin content. *Mar Ecol Prog Ser* 230:47-58.
128. Tillmann U, John U, & Cembella A (2007) On the allelochemical potency of the marine dinoflagellate *Alexandrium ostenfeldii* against heterotrophic and autotrophic protists. *J Plankton Res* 29(6):527-543.
129. Sheng J, Malkiel E, Katz J, Adolf JE, & Place AR (2010) A dinoflagellate exploits toxins to immobilize prey prior to ingestion. *Proc Nat Acad Sci U S A* 107(5):2082-2087.
130. Landsberg J, Flewelling L, & Naar J (2009) *Karenia brevis* red tides, brevetoxins in the food web, and impacts on natural resources: Decadal advancements. *Harmful Algae* 8(4):598-607.
131. Vance JE (2006) Lipid imbalance in the neurological disorder, Niemann-Pick C disease. *FEBS letters* 580(23):5518-5524.
132. Wenk MR (2005) The emerging field of lipidomics. *Nat Rev Drug Discov* 4(7):594.
133. Testerink C & Munnik T (2005) Phosphatidic acid: a multifunctional stress signaling lipid in plants. *Trends Plant Sci* 10(8):368-375.
134. Welti R, *et al.* (2002) Profiling membrane lipids in plant stress responses role of phospholipase Dα in freezing-induced lipid changes in *Arabidopsis*. *J Biol Chem* 277(35):31994-32002.
135. Hessen D, Lange, H, & van Donk E (1997) UV-induced changes in phytoplankton cells and its effects on grazers. *Freshw Biol* 38(3):513-524.
136. Van Mooy BA, *et al.* (2009) Phytoplankton in the ocean use non-phosphorus lipids in response to phosphorus scarcity. *Nature* 458(7234):69.
137. Collins JR, Edwards BR, Fredricks HF, & Van Mooy BA (2016) LOBSTAHS: An adduct-based lipidomics strategy for discovery and identification of oxidative stress biomarkers. *Anal Chem* 88(14):7154-7162.
138. Smith CA, *et al.* (2005) METLIN: a metabolite mass spectral database. *Ther Drug Monit* 27(6):747-751.
139. Kanehisa M (2002) The KEGG Database. *'In Silico' Simulation of Biological Processes*, Novartis Foundation Symposia, (John Wiley & Sons, Ltd), pp 91-103.
140. Fahy E, *et al.* (2009) Update of the LIPID MAPS comprehensive classification system for lipids. *J Lipid Res* 50(Supplement):S9-S14.
141. Bates GW & Goldsmith MHM (1983) Rapid response of the plasma-membrane potential in oat coleoptiles to auxin and other weak acids. *Planta* 159(3):231-237.
142. Dakshini K & Einhellig FA (1994) *Allelopathy: organisms, processes, and applications* (ACS Publications).
143. Glass AD & Dunlop J (1974) Influence of phenolic acids on ion uptake. *Plant Physiol* 54(6):855-858.

144. Devaiah SP, *et al.* (2006) Quantitative profiling of polar glycerolipid species from organs of wild-type Arabidopsis and a phospholipase Dα1 knockout mutant. *Phytochemistry* 67(17):1907-1924.
145. Jia Y & Li W (2015) Characterisation of lipid changes in ethylene-promoted senescence and its retardation by suppression of phospholipase Dδ in Arabidopsis leaves. *Front Plant Sci* 6.
146. Kaur H & Kaushik S (2005) Cellular evidence of allelopathic interference of benzoic acid to mustard (*Brassica juncea* L.) seedling growth. *Plant Physiol Biochem* 43(1):77-81.
147. Cho SH & Thompson G (1987) On the metabolic relationships between monogalactosyldiacylglycerol and digalactosyldiacylglycerol molecular species in *Dunaliella salina*. *J Biol Chem* 262(16):7586-7593.
148. Krebs H & Eggleston L (1944) Metabolism of acetoacetic acid in animal tissues. *Nature* 154:209-210.
149. Wakil SJ (1958) A malonic acid derivative as an intermediate in fatty acid synthesis. *J Am Chem Soc* 80(23):6465-6465.
150. Hansen PJ (1989) The red tide dinoflagellate *Alexandrium tamarense*: effects on behaviour and growth of a tintinnid ciliate. *Mar Ecol Prog Ser*:105-116.
151. Granéli E, Edvardsen B, Roelke DL, & Hagström JA (2012) The ecophysiology and bloom dynamics of *Prymnesium spp*. *Harmful Algae* 14(Supplement C):260-270.
152. Ribalet F, *et al.* (2014) Phytoplankton cell lysis associated with polyunsaturated aldehyde release in the Northern Adriatic Sea. *PLOS ONE* 9(1):e85947.
153. Rengefors K & Legrand C (2001) Toxicity in *Peridinium aciculiferum*—an adaptive strategy to outcompete other winter phytoplankton? *Limnol Oceanogr* 46(8):1990-1997.
154. Tillmann U & Hansen PJ (2009) Allelopathic effects of *Alexandrium tamarense* on other algae: evidence from mixed growth experiments. *Aquat Microb Ecol* 57(1):101-112.
155. Wyatt TD (2011) Pheromones and Behavior. *Chem Comm Crustaceans*, eds Breithaupt T & Thiel M (Springer New York, New York, NY), pp 23-38.